Biological Uncertainties in Proton Radiation Therapy

María Marteinsdóttir

Faculty of Physical Sciences
University of Iceland
2021

Biological Uncertainties in Proton Radiation Therapy

María Marteinsdóttir

Dissertation submitted in partial fulfillment of a
Philosophiae Doctor degree in Physics

Advisor
Harald Paganetti

PhD Committee
Harald Paganetti
Snorri Þorgeir Ingvarsson
Garðar Mýrdal

Opponents
Ludvig Muren
Iuliana Toma-Dasu

Faculty of Physical Sciences
School of Engineering and Natural Sciences
University of Iceland
Reykjavik, April 2021

Biological Uncertainties in Proton Radiation Therapy

Dissertation submitted in partial fulfillment of a *Philosophiae Doctor* degree in Physics

Faculty of Physical Sciences
School of Engineering and Natural Sciences
University of Iceland
Dunhagi 5
107, Reykjavik
Iceland

Telephone: 525-4000

Bibliographic information:
María Marteinsdóttir, 2021, *Biological Uncertainties in Proton Radiation Therapy*, PhD dissertation, Faculty of Physical Sciences, University of Iceland, 117 pp.

ISBN 978-9935-9564-3-9

Printing: Háskólaprent
Reykjavik, Iceland, April 2021

Abstract

Application of external beam radiation therapy (EBRT) to localized cancer has long been regarded as a standard treatment option with its purpose being to deliver a homogeneous high-dose distribution within the tumor volume while protecting organs at risk. Advanced EBRT techniques are used to reduce normal tissue complications by creating a sharp dose fall-off towards the healthy tissue; the most commonly used is the photon based intensity modulated radiation therapy (IMRT). Another application is proton beam therapy (PBT) which, due to the physical characteristics of the protons, reduces the volume of the normal tissue exposed to radiation.

In order to benefit from decades-long clinical experience and a large cohort of patients in photon radiation therapy, prescription doses in photon therapy are used as the basis for proton therapy. Current treatment planning methods for proton radiotherapy rely on applying a constant relative biological effectiveness (RBE) of 1.1 in clinical practice as protons are assumed to be 10% more biologically effective than photons. However, this is in contrast to substantial experimental evidence suggesting that RBE varies as a function of dose, tissue type, linear energy transfer (LET) and endpoint, among other parameters. For the proton energy range used in the clinic, the RBE increases at the distal end of proton fields. This may influence decisions such as beam configurations for certain proton treatments, e.g. if critical organs are situated downstream of the patient's tumor.

The work presented in this thesis consists of evaluating the clinical impact of RBE variations in proton radiotherapy and comparing it to the assumption of a fixed RBE of 1.1. Four cohorts of patients have been studied. The first study assessed the clinical impact of applying a variable RBE in proton therapy for prostate cancer due to the uncertainty in the $(\alpha/\beta)_x$ ratio. Patients treated with passive scattered proton therapy (PSPT) or intensity modulated proton therapy (IMPT) were compared to patients receiving IMRT. For proton beam therapy, phenomenological and biophysical RBE models were used to predict the variable RBE. Furthermore, tumor control probabilities (TCP) and normal tissue complication probabilities (NTCP) for the rectum and the bladder were estimated. The second study assessed the uncertainties in proton therapy due to the RBE variations for small fields as they are subject to elevated LET values throughout the field. A phenomenological RBE model was used to calculate the variable RBE. Additionally, the clinically used range uncertainty margin of 3.5% + 1 mm was reduced to assess the effect on RBE in the target volume. In the third study, the clinical impact of using a variable RBE for patients receiving proton beam scanning treatment (PBS) for left-sided breast cancer was examined, and compared with patients treated with either the photon-based three-dimensional conformal radiotherapy (3DCRT) or volumetric modulated arc therapy (VMAT). Furthermore, eight 3DCRT patients were re-planned

for PBS to allow for a one-to-one comparison. The variable RBE was calculated using a phenomenological RBE model. Normal tissue toxicity probabilities for the heart, left anterior descending artery (LAD) and left lung were evaluated for different endpoints. In the final study, three different phenomenological RBE models were used to evaluate the variable RBE effect in patients receiving proton therapy for soft tissue sarcoma.

In conclusion, while calculating RBE using the phenomenological RBE models, the choice of the $(\alpha/\beta)_x$ ratio has the largest impact on the uncertainty in RBE. The biophysical RBE model did not vary much with the $(\alpha/\beta)_x$ ratio. Furthermore, the range uncertainty margin reduction did not significantly affect the RBE in the target. The work in this thesis demonstrated that disregarding variations in the proton RBE may limit the interpretation of results from clinical trials while comparing photon and proton radiotherapy treatments.

Útdráttur

Geislameðferð staðbundinna æxla (*external beam ratiation therapy* - EBRT) er þaulreynd aðferð við krabbameinslækningar með það að markmiði að skila háum jafndreifðum geislaskammti inn í æxlið sjálft án þess að skaða aðliggjandi líkamsvef. Við nútíma geislameðferð eru notaðar háþróaðar aðferðir til að draga úr aukaverkunum með því að stilla meðferðargeislann þannig að geislaskammturinn falli hratt þegar út úr æxlinu kemur og inn í heilbrigðan vef. Algengast er að nota styrkmótaða ljóseindageisla (*intensity modulated radiation therapy* - IMRT) en annar valkostur er meðferð með róteindabunu (*proton beam therapy* - PBT) sem veldur minna geislaálagi á heilbrigðan vef vegna hagfelldra eðliseiginleika róteinda.

Læknavísindin búa að áratuga reynslu af geislalækningum með ljóseindum sem reynt er að nýta við róteindameðferð. Hefðbundnir geislaskammtar ljóseinda eru hafðir til hliðsjónar þegar skipuleggja á meðferð með róteindabunu. Að jafnaði er miðað við fast hlutfall líffræðilegrar virkni (*relative biological effectiveness* - RBE) upp á 1,1 sem gerir ráð fyrir að róteindir hafi 10% meiri lífræn áhrif en ljóseindir. Þessi einfalda nálgun gengur hinsvegar í berhögg við niðurstöður fjölda rannsókna sem sýna að RBE stuðullinn er breytilegur eftir stærð geislaskammts, eðli líkamsvefs, orkuskilum á lengdareiningu (*linear energy transfer* - LET) og endapunkts, auk fleiri atriða. Til að mynda hækkar RBE stuðulinn nærri endastöð róteindanna á meðferðarsvæðinu þegar orka róteindabununnar er á því bili sem notast er við í geislalækningum. Þetta þarf að hafa í huga þegar beina á róteindabunu að æxlum sem liggja þétt upp við mikilvæg líffæri.

Í ritgerðinni eru metin klínísk áhrif þess að gera ráð fyrir breytilegum RBE stuðli í róteindameðferð í samanburði við meðferð þar sem gengið er út frá föstum RBE stuðli upp á 1,1. Stuðst var við fjögur þýði krabbameinssjúklinga og rannsókninni skipt í jafn marga þætti. Í fyrsta þættinum voru skoðuð klínisk áhrif þess að nota breytilegan RBE stuðul við meðferð blöðruhálskrabbameins sökum óvissu í hlutfalli $(\alpha/\beta)_x$. Róteindameðferð, sem byggir á kyrrstæðri dreifingu róteindageislans (*passive scattered proton therapy* - PSPT) annars vegar og styrkmótun róteindageisla (*intensity modulation proton therapy* - IMPT) hins vegar, var borin saman við hefðbundna IMRT geislameðferð með ljóseindum. Mátunar- (*phenomenological*) og lífeðlisfræðileg (*biophysical*) RBE líkön voru notuð til að meta líffræðilega virkni (RBE) róteindastraumsins. Einnig voru áætlaðar árangurslíkur á eyðingu æxlisins (*tumor control probabilities* - TCP) og líkur á skaðlegum áhrifum á nærliggjandi heilbrigðan líkamsvef (*normal tissue complication probabilities* - NTCP). Annar þáttur rannsóknarinnar fólst í mati á óvissuþáttum í róteindameðferð á litlu meðferðarsvæði, sem rekja má til breytilegs RBE stuðuls vegna hækkunar á orkuskilun á lengdareiningu (LET) innan meðferðarsvæðisins. RBE mátunarlíkan var notað til að segja fyrir um gildi RBE stuðulsins. Auk þess var kannað

hvaða áhrif það hefur á mat á RBE stuðulinn á meðferðarsvæðinu með því að draga úr umframslaglengd róteindageislans en við klíníska róteindameðferð er venja að bæta 3,5% + 1 mm við slaglengdina. Þriðji þáttur rannsóknarinnar beindist að sjúklingum sem fengu róteindameðferð með mjóbunustraumi (*pencil beam scanning* - PBS) til að meðhöndla æxli í vinstra brjósti og klínískur árangur borinn saman við meðhöndlun með þrívíðri hnitmiðaðri ljóseindageislun (*three-dimensional conformal radiotherapy* - 3DCRT) og mótaðri snúnings ljóseindageislun (*volumetric modulated arc therapy* - VMAT). Að auki voru gerð ný PBS geislaplön fyrir átta sjúklinga sem höfðu áður fengið 3DCRT meðferð, sem gaf færi á beinum samanburði á meðferðum. RBE mátunarlíkan var notað til að segja fyrir um gildi RBE stuðulsins og líkur á skaðlegum áhrifum á nærliggjandi heilbrigðan líkamsvef voru metnar í hjarta, fremri millisleglakvísl vinstri kransæðar og vinstra lunga, fyrir breytilega endapunkta. Í fjórða og lokaþætti rannsóknarinnar voru þrjú mismunandi RBE mátunarlíkön notuð til að meta áhrif breytilegs RBE stuðuls á meðferð sjúklinga með sarkmein í mjúkvef með róteindageislun.

Að lokum, þegar RBE stuðullinn er reiknaður út frá þeim mátunarlíkönum sem hér var stuðst við er það valið á $(\alpha/\beta)_x$ hlutfalli sem veldur mestri óvissu í RBE stuðlinum meðan $(\alpha/\beta)_x$ hlutfallið hefur ekki teljandi áhrif í lífeðlisfræðilega RBE líkaninu. Ennfremur hefur styttri umframslaglengd ekki veruleg áhrif á RBE stuðulinn. Að samanlögðu sýna þessar rannsóknir að hafa þarf breytilegan RBE stuðul róteindageislunar í huga þegar gera á samanburð á geislameðferð með róteindum og ljóseindum.

Table of Contents

List of Figures

List of Tables

Abbreviations

3DCRT	Three-Dimensional Conformal Radiotherapy
ADC	Analytical Dose Calculation
CAR	Carabe
CERR	Computational Environment for Radiation therapy Research
CPE	Charged Particle Equilibrium
CT	Computed Tomography
CTV	Clinical Target Volume
DVH	Dose-Volume Histogram
DNA	Deoxyribonucleic Acid
DSB	Double-Strand Break
EBRT	External Beam Radiation Therapy
FSU	Functional Subunit
IAEA	International Atomic Energy Agency
ICRU	International Commission on Radiation Units and Measurements
IMRT	Intensity Modulated Radiation Therapy
IMPT	Intensity Modulated Proton Therapy
gEUD	generalized Equivalent Uniform Dose
GTV	Gross Tumor Volume
HR	Homologous Recombination
LAD	Left Anterior Descending Artery
LENT	Late Effects Normal Tissue Task Force
LET	Linear Energy Transfer
LKB	Lyman-Kutcher-Burman
LQ	Linear-Quadratic
MC	Monte Carlo
MCDS	Monte Carlo Damage Simulation
McN	McNamara
MCS	Multiple Coulomb Scattering
MFUD	Multiple Field Uniform Dose
MLC	Multileaf Collimator
MRI	Magnetic Resonance Imaging

NCI	National Cancer Institute
NHEJ	Non-Homologous End Joining
NIH	National Institutes of Health
NTCP	Normal Tissue Complication Probability
OAR	Organ at Risk
PBS	Proton Beam Scanning
PBT	Proton Beam Therapy
PET	Positron Emission Tomography
PSPT	Passive Scattered Proton Therapy
PTV	Planning Target Volume
RBE	Relative Biological Effectiveness
RTOG	Radiation Therapy Oncology Group
RMF	Repair-Misrepair-Fixation
SFUD	Single Field Uniform Dose
SOBP	Spead-Out Bragg Peak
SOMA	Subjective, Objective, Management, Analytic
SSB	Single-Strand Break
TERMA	Total Energy Released per unit Mass
TCP	Tumor Control Probability
VMAT	Volumetric Modulated Arc Therapy
WED	Wedenberg
WHO	World Health Organization

Acknowledgments

First and foremost I would like to thank Dr. Harald Paganetti for his supervision, and who generously shared his valuable time. Without his expert scientific guidance and helpful suggestions this PhD would not have been possible.

I would also like to thank Dr. Snorri Ingvarsson for his advice and suggestions, and for always being there to discuss any problems, scientific or otherwise. My gratitude to Gardar Myrdal for having introduced me to the field of Medical Radiation Physics and his ongoing support.

To my co-authors; I am extremely grateful for Dr. Aimee McNamara for her invaluable help, encouragement and suggestions. It has been a great privilege to get to know her as a scientist and as a friend. I would further like to thank Dr. Jan Schuemann for the many valuable discussions, and useful suggestions that have resulted in improvements to this work. I am truly thankful to Dr. Jungwook Shin for his support and endless availability. My sincere gratitude to Dr. Chia-Chun Wang and Dr. Nicolas Depauw, for their commitment, co-operation and advice.

A warm thanks to Dr. Clemens Grassberger for all his encouragement, and for all of the intriguing discussions we shared. I am grateful to Dr. Maryam Moteabbed and to Dr. Tracy Underwood for their valuable support and help throughout this work. I would also like to thank Dr. Andrzej Niemierko for his helpful suggestions. My further gratitude to Grímur Björnsson and Dr. Lárus Thorlacius for their invaluable input.

This work was carried at the Department of Radiation Oncology, Massachusetts General Hospital in Boston. Special thanks go to the Enterprise Research Infrastructure and Services (ERIS) group at Partners Healthcare for their computer support.

Finally, I want to thank my mother, her partner and my siblings, for their endless encouragement and support. I am also deeply grateful to my in-laws for allowing me to stay at their home during my time in Boston. Last, but not least, I am eternally thankful to my husband for his support, patience, understanding and love.

1 Introduction

At the end of 1895, a German physics professor, Wilhelm Conrad Roentgen, discovered a new and different kind of ray when investigating cathode rays from a Crookes tube. The new ray could penetrate through black cardboard as well as books and papers. He called the new ray X-rays where the "X" represented an unknown quantity. Further experiments revealed that the X-rays passed through a wide range of matter, including the soft tissue of the body, but not through everything, such as bones and metal. The first X-ray photograph was taken of his wife Bertha's hand with the bone and the wedding ring clearly visible. The medical community quickly shared a wide interest in the discovery and within months, X-rays were used for both diagnosis and for therapeutic use in cancer; the fields of radiology and radiation oncology were born. In 1901, Roentgen received the first Nobel Prize awarded in physics for his discovery.

The first case of X-rays being applied therapeutically was done by E. G. Grubbé, a manufacturer of incandescent lamps, Geissler and Crookes tubes and a medical student. As a manufacturer he tested the tubes several times daily on his left hand, resulting in a dermatitis on the back of his hand. By cause of the dermatitis, the question rose whether X-rays could be used as a treatment for lupus and cancer. On January 29th 1896, Grubbé treated a patient with X-rays for carcinoma of the breast. The X-ray tube was placed close to the lesion for an exposure of almost an hour. Due to his own dermatitis, Grubbé protected the healthy tissue surrounding the lesion by a sheet of lead, thus being the first case of using lead as a protective material. Yet, the physical properties of X-rays and their biological effects, along with the hazards of radiation, were unknown at first. For example, the calibration of the X-ray machines was performed by analyzing the skin reddening (erythema) produced when radiologists placed their hands directly in the X-ray beam. The lack of knowledge resulted in numerous injuries to physicians, scientists, and patients. In 1903, animal studies revealed that X-rays could kill living tissue and induce cancer.

An important scientific development was achieved in 1922 when it was discovered that fractionated dose delivery for laryngeal cancer treatment showed better results regarding cancer control and side effects than a singular treatment session. The discovery, made by Henri Coutard, a French radiologist working with the Institut Curie, was based on a study revealing that a single dose of X-rays sufficient to sterilize a rabbit's testicle produced severe skin damage, but if administered in fractions over a course of days, sterilization was achieved without significant effect on the skin. In 1934, Coutard proposed a fractionation scheme of 200 Rontgen per fraction and 5 fractions per week, which remains the basis for current radiation therapy. A number of other important developments were technological. In 1932, the ionizing chamber was introduced which allowed for the determination of the radiation dose delivered. Furthermore, the intro-

duction of the Cobalt machine in the 1950s, which produced high-energy γ-rays, along with the linear accelerators in the 1960s, which delivered megavoltage X-rays, allowed for deeper tissue penetration compared to the prior X-ray tubes which were able to deliver energy only up to hundreds of kV. A revolutionary development was the use of computer technology in radiation treatment, e.g. in dose calculation and treatment optimization as well as the introduction of computed tomography (CT) in the 1970s, making it possible to obtain three-dimensional images of the patient anatomy.

In 1946, an American physicist at the Harvard University, Robert R. Wilson, wrote a seminal paper proposing the idea of using protons in radiation treatment for cancer. Six years later, the first paper on biological studies in mice using protons, deuterons, and helium beams was published. The first patients to receive proton therapy were treated in 1954 at Lawrence Berkeley Laboratory in Berkeley, USA. Three years later, in 1957, the Gustaf Werner Institute at the University of Uppsala, Sweden became the second facility to treat cancer with protons. In the years following, a few facilities began proton therapy treatment, such as the Harvard University in Boston, USA and the Institute for Theoretical and Experimental Physics in Moscow, Russia. However, the cost to build the necessary particle accelerators and the space needed to house them kept the numbers down. Today, the number of proton therapy centers operating worldwide is rapidly increasing as the accelerators are getting more affordable and require less space.

According to estimates from the World Health Organization (WHO) in 2018, cancer is a leading cause of death worldwide, accounting for an estimated 9.6 million deaths in 2018. Radiation therapy, combined with surgery and chemotherapy, is the standard and worldwide adopted treatment for most cancer patients. Approximately 2/3 of cancer patients receive radiotherapy, where over 80% of the patients are treated with high energy X-rays (referred to as photons from here on) produced in linear accelerators. Only 0.8% of patients are irradiated with high-energy charged particles, such as protons, but that number is steadily increasing. As proton therapy is a much more expensive technique than photon therapy, it is essential to accurately estimate its overall benefit.

The outline of this thesis is as follows: In sections 2 to 4, the general principles of radiotherapy are described. The specific aims of the thesis can be found in section 5. Section 6 outlines the methods used in the studies and section 7 summarizes the results. Concluding remarks of the presented work are provided in section 8.

2 Interaction of Radiation with Matter

2.1 Photon Interactions

Photons are considered to deposit their energy indirectly, i.e. their kinetic energy is transferred to orbital electrons of atoms which then deposit their kinetic energy in the target matter. Photon interactions with matter can be classified either as absorption or scattering processes. The main absorption processes are photoelectric effect (pe), pair production (pp) and triplet production (tp) whereas coherent scattering (Rayleigh, Ry) and incoherent scattering (Compton scattering, cs) are the main scattering processes. All these mechanisms, with the exception of Rayleigh scattering, lead to partial or complete transfer of the photon kinetic energy to electron energy.

The probability of a photon interacting with a nucleus, an atom or an electron can be described in terms of atomic interaction cross-section, ${}_a\sigma$, expressed in cm^2/atom. The total atomic cross section at a given photon energy $h\nu$, in which h is Planck's constant and ν is the photon's frequency, is determined by adding up the atomic cross sections of all possible interactions, ${}_a\sigma_i$, in the matter (ICRU, 2011)

$$ {}_a\sigma_{\mathrm{tot}}(h\nu) = \sum_{\mathrm{i}=1}^{n} {}_a\sigma_i(h\nu) \tag{2.1} $$

2.1.1 Photoelectric Effect

Photoelectric effect is a process where a photon interacts with a tightly bound atomic electron and is completely absorbed. This results in the ejection of the electron from its shell. The kinetic energy of the electron[1] is given by

$$ E = h\nu - E_b \tag{2.2} $$

where $h\nu$ is the energy of the incident photon and E_b represents the binding energy of the electron. The resulting vacancy in the inner atomic shell is filled by an electron from an outer shell. The energy liberated is carried away either in the form of a characteristic X-ray or in the form of an Auger electron.

Photoelectric effect is dependent on the energy of the incoming photon as well as on the atomic number of the absorbing matter, Z. It is the most important interaction for

[1] Kinetic energy is often denoted as E in radiotherapy physics, whereas E usually stands for total energy in particle physics.

low energy photons. The cross-section per atom is approximately given by (Attix, 1986)

$$ {}_a\sigma_{\text{pe}} \propto \frac{Z^4}{(h\nu)^3} \tag{2.3} $$

2.1.2 Compton Scattering

Compton scattering is an incoherent scattering process in which a photon collides with an electron assumed to be unbound and stationary. The photon, with initial energy $h\nu$, is deflected through an angle θ. Its energy after the collision is given by (Attix, 1986)

$$ h\nu' = \frac{h\nu}{1 + \frac{h\nu}{m_0c^2}(1-\cos\theta)} \tag{2.4} $$

where m_0c^2 is the rest energy of the electron. The electron is ejected from its shell at an angle ϕ from the incident photon direction with kinetic energy of

$$ E = h\nu - h\nu' \tag{2.5} $$

For photon energies larger than 10 keV, the cross-section per electron depends inversely on the incident photon energy (Attix, 1986)

$$ {}_e\sigma_{\text{cs}} \propto \frac{1}{h\nu} \tag{2.6} $$

However, the cross-section per electron for a Compton interaction can be approximated to the Thomson cross-section for low energies, representing a coherent scattering process between the incoming photon and the unbound atomic electron. The cross-section becomes ${}_e\sigma_{\text{cs}} \approx \frac{8}{3}\pi r_e^2$ where r_e is the the classical electron radius (Attix, 1986).

Due to the assumption of an unbound electron, the electron binding energy is considered to be zero. Therefore, ${}_e\sigma_{\text{cs}}$ is independent of the atomic number Z of the absorbing matter. Multiplying the cross-section per electron with the atomic number Z results in the atomic Compton cross-section (Attix, 1986)

$$ {}_a\sigma_{\text{cs}} = Z \cdot {}_e\sigma_{\text{cs}} \propto \frac{Z}{h\nu} \tag{2.7} $$

2.1.3 Rayleigh Scattering

Rayleigh scattering is a coherent scattering process. The photon is scattered by tightly bound atomic electrons, the photon loses essentially no energy and the scattering angle θ is small. The atomic cross-section for Rayleigh scattering is approximately given by (Attix, 1986)

$$ {}_a\sigma_{\text{Ry}} \propto \frac{Z^2}{(h\nu)^2} \tag{2.8} $$

for photon energies of the order of 0.5 Z MeV. For low photon energies, the atomic cross-section can be reduced to the Thomson cross-section, see previous section.

2.1.4 Pair Production

In pair production the photon is absorbed in the Coulomb force field of the nucleus, resulting in the creation of an electron-positron pair. For this process to be possible, the photon's energy has to exceed twice the rest energy of an electron, i.e. $2m_0c^2$. The kinetic energy of the electron-positron pair is given by

$$E^- + E^+ = h\nu - 2m_0c^2 \tag{2.9}$$

This process can also occur, with lower probability, in the field of an atomic electron. The atomic electron will acquire sufficient kinetic energy to be ejected from its shell, resulting in creation of two electrons and one positron. The process is called triplet production. The minimum photon energy required for this process to occur is $4m_0c^2$.

The positron will rapidly lose all its kinetic energy and subsequently annihilate with an electron in the absorbing matter. The annihilation results in creating two oppositely directed photons, each of energy 511 keV.

The atomic cross-section for pair production above $2m_0c^2$ increases rapidly with photon energy $h\nu$, the relation with the atomic number is (Attix, 1986)

$$_a\sigma_{\text{pp}} \propto Z^2 \tag{2.10}$$

whereas for triplet production the relation is (Attix, 1986)

$$_a\sigma_{\text{tp}} \propto Z \tag{2.11}$$

2.1.5 Linear Attenuation Coefficient

The attenuation of a monoenergetic photon beam penetrating matter with thickness t through a narrow-beam geometry can be described as (Attix, 1986)

$$N = N_0 e^{-\mu t} \tag{2.12}$$

where N_0 is number of the primary photons, N is the number of the transmitted photons and μ is the so-called linear attenuation coefficient, typically expressed in units cm^{-1}. When divided with the density of the matter, ρ, the mass attenuation coefficient is obtained, μ/ρ, in units cm^2/g. The mass attenuation coefficient is related to the total atomic cross-section, $_a\sigma_{\text{tot}}$, through (ICRU, 2011)

$$\frac{\mu}{\rho} = \frac{N_A}{A}{}_a\sigma_{\text{tot}} = \frac{N_A}{A}\left({}_a\sigma_{\text{pe}} + {}_a\sigma_{\text{cs}} + {}_a\sigma_{\text{pp}} + {}_a\sigma_{\text{tp}} + {}_a\sigma_{\text{Ry}}\right) \tag{2.13}$$

where N_A is the Avogadro's constant and A is the atomic mass of the element.

2.2 Proton Interactions

Unlike photons, protons deposit their energy directly. Proton interactions can be classified as either electromagnetic or nuclear interactions. Upon entering matter, incident protons mainly interact with the atomic electrons via inelastic Coulomb interactions. In each interaction, a small fraction of the kinetic energy of the protons is transferred to the electrons. This results in the protons continuously losing energy and slowing down, leaving ionized and excited atoms behind. Due to the small mass of the electrons, proton trajectories are nearly straight lines. In contrast, the protons are scattered when passing close to the atomic nucleus as they experience repulsive elastic Coulomb interactions. Finally, protons can experience elastic and non-elastic nuclear interactions with the atomic nucleus. In elastic collision, the nucleus is left intact whereas the incoming proton is deflected. However, in non-elastic nuclear collision, the protons will be absorbed (around 1% of protons are lost per cm of range in water) and the characteristics of the nucleus are changed. This results in secondary particle production. Possible proton-induced secondary particles include protons, neutrons, deuterons, alphas, tritons, ^{3}He and ^{4}He.

2.2.1 Energy Loss

Mass stopping power is defined as the average energy loss, dE, per unit path length, dx, along a path of a charged particle while traversing matter with a density ρ (ICRU, 2011)

$$\frac{1}{\rho}S = -\frac{1}{\rho}\frac{\mathrm{d}E}{\mathrm{d}x} \tag{2.14}$$

For protons, the mass stopping power is subdivided into three components; mass electronic stopping power, mass nuclear stopping power and mass radiative stopping power. The total mass stopping power is the sum of these contributions (ICRU, 2011)

$$\frac{S_{\mathrm{tot}}}{\rho} = \frac{S_{\mathrm{el}}}{\rho} + \frac{S_{\mathrm{nuc}}}{\rho} + \frac{S_{\mathrm{rad}}}{\rho} \tag{2.15}$$

The predominant contribution comes from the mass electronic stopping power describing inelastic Coulomb interactions between protons and atomic electrons. The nuclear term arises from elastic Coulomb interactions between the incoming protons and the atomic nuclei and is important only at low energies, <20 keV (Janni, 1982). The radiative term represents Bremsstrahlung emission of photons due to Coulomb interaction between the incident proton and the atomic nuclei or the atomic electrons. For therapeutic proton beam energies, the mass nuclear stopping power and the radiative stopping power are negligible.

Following the International Commission on Radiation Units and Measurements (ICRU) Report No. 42 (ICRU, 1993b), the mass electronic stopping power is defined as

$$\frac{1}{\rho}S_{\mathrm{el}} = 4\pi N_{\mathrm{A}} r_e^2 m_0 c^2 \frac{Z}{A}\frac{z^2}{\beta^2}\left[\ln\frac{2m_0c^2\gamma^2\beta^2}{I} - \beta^2 - \frac{\delta(\beta)}{2} - \frac{C(\beta)}{Z}\right] \tag{2.16}$$

where N_A is Avogadro's number, r_e is the classical electron radius and m_0c^2 is the rest energy of the electron. The parameters Z and A represent the atomic number and atomic mass of the absorbing matter, respectively, z is the charge of the incident particle (with $z = 1$ for protons), $\beta = v/c$ where v is the velocity of the proton and c is the velocity of light in vacuum, and $\gamma = (1-\beta^2)^{1/2}$. Furthermore, I is the mean excitation energy of the absorbing matter, δ is the density-effect correction and C is the shell correction term, described below. The equation reveals that the energy loss is proportional to the inverse square of the proton's velocity. Therefore, the rate at which the proton loses energy increases as the proton slows down.

The mean excitation energy, I, is a measure of the ability of a target to absorb kinetic energy from an incident particle and is independent on the the type of the incoming particle. In general, the mean excitation energy is determined from experimental data (ICRU, 1993b). The density-effect correction $\delta(\beta)$ is important in condensed matter and at very high energies, as it accounts for the reduction of the stopping power due to the polarization of the matter caused by the passage of the incident particle. Equation (2.16) assumes that the velocity of the incoming particle is much larger than the velocity of the atomic electrons in the matter. The shell correction $C(\beta)$ is intended to account for this assumption and is therefore important only for low energies where the particle velocity is near the velocity of the electrons. For protons at energies of interest in radiation therapy, the two correction terms are negligible.

2.2.2 Multiple Coulomb Scattering

As described above, the protons can be deflected through Coulomb interactions with the atomic electrons. However, the tracks of the protons are essentially straight as their rest mass is 1832 times greater than that of an electron. A more significant scattering process is the Coulomb interaction between a proton and an atomic nucleus. A proton passing close to the nucleus can be elastically scattered by the repulsive force from the positive charge of the nucleus, resulting in a small change in its trajectory. In clinical proton therapy, most targets are thick enough for each proton in a proton beam to experience myriad scattering events. This results in a lateral spread of the beam with increasing depth. The lateral spread is classified according to the multiple Coulomb scattering (MCS) approach, which can be described by the Moliere's theory (Bethe 1953). Assuming a small angle approximation in which $\sin\theta \approx \theta$, the probability distribution function is defined as

$$f(\theta) = \frac{1}{4\pi\theta_M^2}\sum_k \frac{f^k(\theta')}{B^k} \tag{2.17}$$

where

$$\theta_M = \frac{1}{\sqrt{2}}(\chi_s\sqrt{B}) \tag{2.18}$$

is the characteristic scattering angle and

$$\theta' = \frac{1}{\sqrt{2}\,\theta_{\mathrm{M}}} \tag{2.19}$$

is the reduced scattering angle. The parameter χ_c is the angle such that there is only one collision on average with $\theta > \chi_c$ for a particle traversing a path length t. It can be written as

$$\chi_c = \sqrt{\frac{4\pi\, t\, N_A}{A}}\frac{zZ}{p\,v}(\hbar c)\left(\frac{e^2}{\hbar c}\right) \tag{2.20}$$

where N_A is Avogadro's number, Z and A are the atomic number and atomic mass of the matter, respectively, $\hbar = h/2\pi$ where h is the Plank constant, c is the speed of light, $e^2/\hbar c$ is the fine structure constant, p is the momentum and v the velocity of the scattered proton of charge $z = 1$. The factor B in equation (2.18) is the logarithm of the effective number of collisions on the target. The functions $f^k(\theta')$ in equation (2.17) are defined as

$$f^k(\theta') = \frac{1}{n!}\int_0^\infty y J_0(\theta' y) e^{y^2/4}\left(\frac{y^2}{4}\ln\frac{y^2}{4}\right)^k \mathrm{d}y \tag{2.21}$$

where $J_0(\theta' y)$ is the Bessel function of order 0.

For a first order approximation with $k = 0$, equation (2.17) becomes a Gaussian distribution

$$f^k(\theta') = 2e^{-\theta'^2} \tag{2.22}$$

with a standard deviation of (Highland 1975)

$$\sigma_\theta = \frac{14.1\mathrm{MeV}}{\beta pc} z\sqrt{\frac{L}{L_{\mathrm{rad}}}}\left[1 + 0.038\cdot\ln\left(\frac{L}{L_{\mathrm{rad}}}\right)\right] \tag{2.23}$$

in which L is the target thickness and L_{rad} is the radiation length of the target matter, $L_{\mathrm{rad}} \approx Z^{-2}$. The lateral scattering increases with increasing target thickness and with increasing atomic number Z. Furthermore, the scattering increases with decreasing energy of the particle.

2.2.3 Range

The continuous slowing down range approximation of an individual proton, R_{CSDA}, is defined as the average path-length traveled by the proton while slowing down from an initial energy E_0 to a final energy E_f, close to zero. As the energy loss is considered to be continuous, R_{CSDA} can be evaluated from the mass stopping power (ICRU, 1993b)

$$R_{\mathrm{CSDA}} = \int_{E_f}^{E_0}\left(\frac{S_{\mathrm{tot}}}{\rho}\right)^{-1}\mathrm{d}E \tag{2.24}$$

R_{CSDA} is expressed in units g/cm^2. As the path of most protons in matter is a nearly straight line, the actual range of a proton is considered to be only up to 0.2% larger than R_{CSDA} (Attix, 1986). However, due to the stochastic variation of energy losses, the energy lost by protons in the course of slowing down will fluctuate around its average value. Consequently, all monoenergetic protons will not stop at exactly the same depth. This effect is called energy straggling or range straggling. Therefore, for a proton beam, the range can be described in terms of the mean projected range, R_0, which is defined as the depth at which half of incoming protons incident on an absorbing matter have come to rest (Paganetti, 2012; Newhauser and Zhang, 2015). The definition excludes protons that undergo non-elastic nuclear collisions with the atomic nuclei.

2.2.4 Linear Energy Transfer

Linear energy transfer (LET) of charged particles is defined as the quotient of dE by dl (ICRU, 2011)

$$\mathrm{LET}_{\Delta} = \left(\frac{\mathrm{d}E}{\mathrm{d}l} \right)_{\Delta} \tag{2.25}$$

where dE is the mean energy lost by charged particles due to electronic interactions in traversing a distance dl in matter, minus the sum of all kinetic energies greater than Δ of secondary electrons released by the interactions. The unit for LET_{Δ} is usually presented as keV $(\mu\mathrm{m})^{-1}$.

The use of Monte Carlo (MC) simulations (see section 3.5.2) allows for accurate estimation of LET distributions in patients. In the MC environment, the LET can be calculated as either a dose-averaged $\mathrm{LET}_{\mathrm{d}}$ or a track-averaged $\mathrm{LET}_{\mathrm{t}}$. Throughout this work, the dose-averaged $\mathrm{LET}_{\mathrm{d}}$ will be used. In a patient CT geometry, $\mathrm{LET}_{\mathrm{d}}$ is scored on a voxel-by-voxel basis[2] and is described as (Grassberger et al., 2011)

$$\mathrm{LET}_{\mathrm{d}}(v) = \frac{1}{\rho} \frac{\sum_{\mathrm{events}} \mathrm{d}E \, (\mathrm{d}E/\mathrm{d}x)}{\sum_{\mathrm{events}} \mathrm{d}E} \tag{2.26}$$

where dE is the energy loss of a particle, dx is the length of the particle step and ρ is the density in voxel v. The contribution from N overlapping radiation beams to the $\mathrm{LET}_{\mathrm{d}}$ in voxel v is defined as (Grassberger et al., 2011)

$$\mathrm{LET}_{\mathrm{d}}(v) = \frac{\sum_{i=1}^{N} \mathrm{LET}_{\mathrm{d},i}(v) \, D_i(v)}{\sum_{i=1}^{N} D_i(v)} \tag{2.27}$$

where $D_i(v)$ is the dose distribution from beam i in voxel v.

[2] In treatment planning, the patient geometry is discretized into small volume elements called voxels.

3 Radiotherapy

3.1 Fluence and Absorbed Dose

Particle fluence, Φ, characterizes the number of protons in a beam of radiation. The ICRU (ICRU, 2011) defines it as the number of particles dN incident on a sphere of cross-sectional area da perpendicular to the direction of the particles

$$\Phi = \frac{\mathrm{d}N}{\mathrm{d}a} \tag{3.1}$$

Fluence is measured in units of 1/cm^2. The physical absorbed dose is a dosimetric quantity which determines the energy deposited in a given matter through directly or indirectly ionizing radiation. Following the ICRU definition (ICRU, 2011), the absorbed dose is defined as the mean energy, d$\bar{\varepsilon}$, imparted by ionizing radiation to a mass dm of matter

$$D = \frac{\mathrm{d}\bar{\varepsilon}}{\mathrm{d}m} \tag{3.2}$$

The absorbed dose is expressed in units of Gray (Gy) where 1 Gy = 1 J/kg.

Charged particle equilibrium (CPE) occurs for a volume if for every secondary charged particle of a given energy leaving the volume is replaced with an identical particle of the same energy. In conditions of CPE, the absorbed dose for monoenergetic photons can be given by (Attix, 1986)

$$D = \Phi E \left(\frac{\mu_{\mathrm{en}}(E)}{\rho} \right) \tag{3.3}$$

where Φ is the photon fluence, E is the energy of the photons and μ_{en}/ρ is the mass energy-absorption coefficient. For monoenergetic charged particles under CPE, the absorbed dose can be defined as (Attix, 1986)

$$D = \Phi \left(\frac{S_{\mathrm{col}}(E)}{\rho} \right) \tag{3.4}$$

where Φ denotes the charged particle fluence of energy E and $S_{\mathrm{el}}(E)/\rho$ is the mass electronic stopping power.

3.2 Depth Dose Distributions

Comparison of absorbed dose distributions as a function of depth in water for photon and proton beams can be seen in figure 3.1. A broad 6 MV photon beam is shown in figure 3.1(a). The dose is delivered by secondary electrons set in motion by the primary photons. The beam enters the water where it delivers a certain surface dose. Near the surface the dose rises rapidly due to a relatively long range of energetic secondary electrons being released. The dose increases with depth until it reaches a maximum value. It then decreases almost exponentially until the beam reaches it's exit point.

Figure 3.1(b) shows the depth dose distribution for a broad, unmodulated (pristine) proton beam with an incident energy of 212 MeV. As the proton slows down, its rate of energy loss increases due to the inverse-square dependence between the electronic stopping power of a proton and its velocity, see equation (2.16). Consequently, the dose increases with depth and a sharp maximum at the end of the range, where the particle comes to rest, is formed. The sharp maximum is called Bragg peak. In addition, the dose increase results from the liberation of secondary particles from nuclear reactions. The location of the Bragg peak is determined by the initial energy of the incoming

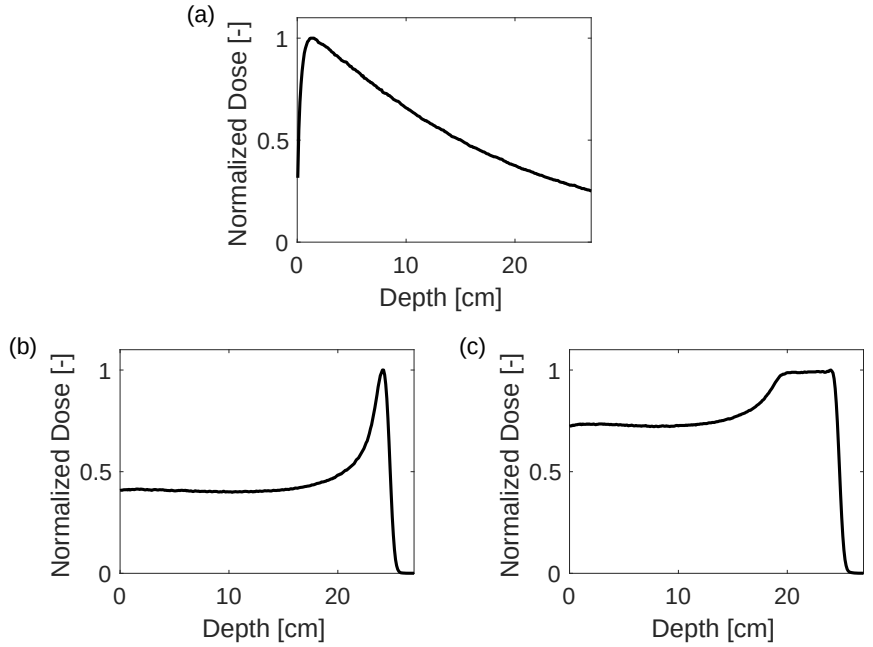

Figure 3.1. Comparisons of absorbed dose as a function of depth in water from (a) a broad beam of 6 MV photons, (b) an unmodulated (pristine) proton Bragg peak produced by a broad proton beam with an initial energy of 212 MeV and (c) SOBP with initial energy of 212 MeV. The distributions are normalized to 100% at depth dose maximum.

proton. The sigmoid shape of the distal falloff is caused by range straggling. The Bragg peak tends to broaden with increasing depth, due to range straggling.

A spread-out Bragg peak (SOBP) is obtained by combining multiple pristine Bragg curves. For each Bragg peak, the initial energy and the fluence are modulated. Figure 3.1(c) shows an example of SOBP proton beam in water.

3.3 Photon Therapy

Photons in photon radiation therapy are generally produced in linear accelerators. Electrons originating in an electron gun are accelerated to the desired kinetic energy and subsequently collided into a target of an optimal atomic number. The incident electrons experience Coulomb interactions with the nuclei of the target; they decelerate and lose kinetic energy in the form of Bremsstrahlung photons. The emitted photons have energies ranging from zero to the kinetic energy of the incident electron.

The photon beam produced is typically passed through a flattening filter to obtain a flat absorbed dose profile at a given depth in water. The beam is further shaped laterally by shielding blocks and multileaf collimators (MLCs) for radiation treatment delivery. MLCs consist of two blocks, each carrying a large numbers of movable leaves with matter of high atomic number. The leaves can move independently, and consequently block some fraction of the beam. For a three-dimentional conformal radiation therapy (3DCRT), the leaf positions in the MLCs are used as apertures, i.e. they change with the shape of the tumor volume according to the incidence direction of the beam. Consequently, multiple beams from different angles create overlapping fields where a high dose area is conformed closely to the tumor volume. Another type of photon therapy is the intensity modulated radiation therapy (IMRT). IMRT typically utilizes higher number of beams compared to 3DCRT. Furthermore, multiple small fields, or segments, of irregular shapes are formed for each beam by moving the MLC leaves. Consequently, a field with modulated fluence is created to give a complex and conformal radiation dose distribution. The IMRT technique is referred to as a static "step and shoot" technique, i.e. the radiation is on only when the MLC leaves are stationary. The intensity modulated fields can also be delivered while the gantry is rotating with the MLC leaves moving continuously during the irradiation of the patient. This technique is called volumetric-modulated arc therapy (VMAT). For both IMRT and VMAT, greater conformity may be be achieved compared to 3DCRT. However, this comes with the cost of increased treatment time. Furthermore, larger volumes of normal tissue are typically exposed to low doses compared to 3DCRT, raising concern over secondary cancer (Kry et al., 2017; Newhauser and Durante, 2011). Tomotherapy is a rotational therapy technique in which the radiation treatment system is combined with a computed tomography (CT) scanner. Before treatment, 3D multivoltage CT images are acquired, allowing for a fine adjustment of the patient's position. A linear accelerator located within the CT gantry rotates around the patient, in which MLC leaves are rapidly moved in and out of the beam to modulate the fluence intensity. Simultaneously, the table moves the patient through the gantry. A highly conformal dose distribution may be achieved.

The 3DCRT represents a conventional forward planning approach, where the treatment parameters (such as number of beams, beam positions and MLC configuration) are chosen at the beginning, and the resulting dose distribution is calculated. This is opposed to an inverse planning approach, where different dose constraints (see section 3.5) on the target and organs at risk are determined at the beginning of the planning process. Subsequently, the treatment parameters are estimated using iterative optimization algorithms to reach the desired dose distribution. Photon therapies typically using the inverse planning approach are IMRT, VMAT and tomography.

3.4 Proton Therapy

A proton beam is usually produced in an accelerator and directed to a treatment room through a beam-line. The leading accelerator types for proton therapy are cyclotrons and synchrotons. The proton beam is transported in a vacuum within the beam-line where multiple magnets are used for focusing and centering, to insure highest beam quality possible. The beam will enter the treatment room in a fixed horizontal direction. For conformal radiation therapy, multiple beams are usually required to be delivered from different directions. This is achieved by using a large gantry, having a diameter of around 10 m, which deflects the beam around the patient using magnetic fields. Just upstream of the patient, the deflected beam will enter a treatment head or a nozzle. The nozzle contains the beam delivery system, see sections 3.4.1 and 3.4.2. Another treatment alternative is a fixed beam delivery, in which the patient must be rotated around the beam. The system consists of the fixed beam and the nozzle.

As the proton beam reaches the treatment room, it is monoenergetic with a Gaussian shaped cross section. The beam's absorbed dose distribution as a function of depth is the so-called Bragg curve, see section 3.2, which is too sharp to cover a tumor of a reasonable size. Therefore, the beam must be spread both laterally and with depth. To change the depth of the Bragg-peak, the energy of the proton beam leaving the accelerator must be modified. Cyclotrons produce nearly continuous proton beams of fixed energy and consequently the energy of the beams can only be reduced. To obtain lower energies, energy degraders are used. The degraders are of tissue equivalent materials of variable thicknesses and are located either outside the treatment room or in the treatment head. In synchrotrons, spills of protons of variable energies are produced, where each spill is several seconds long. Usually, one proton energy is delivered per spill. Consequently, no energy degrader is required. Both cyclotrons and synchrotrons used in proton therapy centers have an energy range between 70 - 250 MeV. They differ in size, where the average diameter of cyclotrons is around 5 m but synchrotrons in proton therapy have an average diameter greater than 10 m.

Proton radiation therapy consists of two main beam delivery systems; passive scattering systems and active beam scanning delivery systems.

3.4.1 Passive Scattering Systems

For passive scattering systems, scattering materials (scatterers) inside the treatment head are used to spread the beam laterally. Small fields typically use a single scatterer whereas larger fields place a second scatterer further downstream, which is designed to ensure a uniform, flat lateral dose profile. To produce a uniform dose distribution with depth, i.e. the SOBP, the beam energy is modulated. The two main range modulation techniques for passive scattering systems are the ridge filter and the range modulation wheel. The ridge filter consists of a plate with steps of different thicknesses. Each thickness determines the range of the peak whereas the width of the step determines the weight of the peak. All pristine peaks are delivered simultaneously. The range modulation wheel has steps of varying thicknesses where each step corresponds to a pristine peak in the SOBP. The wheel spins and delivers the pristine peaks sequentially but repeatedly in every cycle of the wheel. As for the ridge filter, the thickness and the width determine the range and the weight of the peak, respectively. Finally, the beam is further shaped laterally and in depth with patient-specific devices; a patient-specific aperture matches the tumor volume and a patient-specific range compensator modulates the distal edge of the beam.

One of the main concerns for passive scattering systems is the production of secondary neutrons in the treatment head. Protons interact with the scattering and range modulation materials, and thus generate neutrons that will cause secondary dose exposure to the patient. Consequently, the risk of second malignancies increases. This is of special concern for children, as children are more sensitive to radiation-induced cancer than adults (ICRP, 1991). Furthermore, smaller patients are typically exposed to a higher neutron contribution from the treatment head. As a consequence, the neutron dose increases with decreasing age of the patient and thus increasing the secondary cancer risk (Kry et al., 2017; Newhauser and Durante, 2011).

3.4.2 Beam Scanning Systems

In beam scanning systems, scanning magnets move the narrow proton beam laterally throughout the tumor volume. The depth of the beam is varied by either changing the energy of the accelerator or at times by using a degrader. Furthermore, mathematical optimization techniques are used to optimize the intensity of the proton beam at each position within the tumor volume. The narrow beam of protons deposited at a given position is called a beamlet or a beam spot. As mentioned above, each beamlet is essentially a Bragg curve longitudinally and a Gaussian transversely where the sigma of the Gaussian determines the spot size of the beam. Beam scanning proton treatment can be performed using a discrete grid system where the beamlets are delivered one by one with beam off-time in between to adjust the magnets (spot scan), or by moving the beam continuously along a predefined trajectory (raster scan). Beam scanning systems can be divided into single field uniform dose (SFUD) delivery in which each beamlet is optimized individually, or multiple field uniform dose (MFUD) delivery, where all beamlets from all fields are optimized simultaneously. MFUD is often called intensity modulated proton therapy (IMPT).

A better dose conformity can be achieved with beam scanning systems in comparison

to passive scattering systems and no patient specific devices are needed. A disadvantage of beam scanning systems may be a higher sensitivity to organ motion during scanning though it depends on the spot size of the beam as well as whether spot scan or raster scan is being used. However, the production of secondary neutrons is significantly reduced compared to passive scattering systems as beam scanning systems generally require negligible amount of range and modulation materials.

3.5 Treatment Planning

The goal of external beam radiation therapy is to achieve a uniform dose distribution inside the the tumor volume while maintaining the lowest possible dose to surrounding healthy tissues (organs at risk, OARs). To ensure the best possible treatment, an individual treatment plan is created for each patient. Imaging information of the patient's anatomy is acquired, mainly by using computed tomography (CT). On each slide of the CT scan, the outlines of the tumor and OARs are delineated, following the guidelines of ICRU (ICRU, 1993a, 1999, 2007). Other medical imaging techniques may be used in parallel with CT, such as magnetic resonance imaging (MRI) and positron emission tomography (PET).

The tumor volume may be defined as the gross tumor volume (GTV), the clinical target volume (CTV), and the planning target volume (PTV). A physician delineates the GTV, which represents the visible, palpable or clinically demonstrable tumor location. The CTV contains the GTV and accounts for suspected microscopic regional spread of the tumor. The CTV is further expanded into PTV with an additional margin, to account for uncertainties arising from e.g. tumor motion and setup errors of positioning the patient in the treatment room.

To achieve the desired dose distribution, a prescription dose is determined for the tumor as well as the fraction dose and total number of treatment fractions. Furthermore, clinical dose constraints may be applied; for the tumor the dose constraints ensure that no overdosing or underdosing occurs within the volume whereas for the OARs upper dose limit are set. The dose constraints can be expressed, for example, in the following way:

- Deliver no less than 98% and no more than 102% of the prescription dose to the tumor volume.
- At most average dose of xx Gy to OAR volume.
- At most yy% of the OAR volume may receive xx Gy.

Dose-volume histograms (DVHs) condense the 3D dose distribution from each voxel of the CT scan within a volume of interest into a graphical 2D format. Two types of DVHs are used in radiotherapy; differential and cumulative DVHs. The differential DVH represents the percentage or absolute volume of interest receiving a dose within a specified dose interval as a function of dose, whereas the cumulative DVH represents the percentage or absolute volume of interest receiving a certain dose or higher as a function of dose. Treatment plans are often evaluated using dosimetric indices estimated

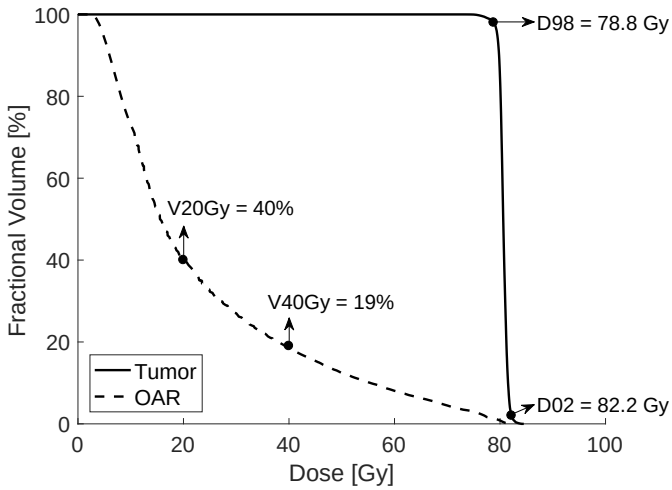

Figure 3.2. Cumulative DVH curve with dose volume indices for a tumor volume (straight) and an OAR (dashed). For the tumor, D02 and D98 are shown, often used to represent the maximum and the minimum tumor dose, respectively. For the OAR, 40% and 19% of the OAR volume receives 20 Gy and 40 Gy or more, respectively.

from a cumulative DVH curve. Figure 3.2 shows an example of a cumulative DVH analysis. The DVH-based indices can be expressed as:

- Mean dose of the tumor or OAR volume.
- Dxx, referring to the maximum dose that covers xx% of the volume.
- VyyGy, referring to the fractional volume of the tumor or OAR receiving yy Gy or more.

Computer simulations are used in radiotherapy to calculate and optimize the delivered dose distribution to a patient. The Monte Carlo (MC) simulation method is considered to be the most accurate method of simulating particle interactions within matter. However, the computation time is long, in order of minutes to hours on standard computers. Therefore, the standard method in the clinic is based on fast analytical dose calculation (ADC) algorithms.

3.5.1 Analytical dose calculations

For photon radiotherapy, analytical dose calculations (ADCs) based on convolution/ superposition techniques are widely used. The calculated dose is considered to give results close to MC simulations while taking much less time. The convolution/superposition algorithms can fundamentally be described as a two-step process (AAPM 85): First, kinetic energy is imparted to charged particles by the interaction of primary photons. This process is expressed by the total energy released per unit mass, or TERMA, and is

dependent upon the primary photon fluence. The charged particles then deposit kinetic energy through ionization and excitation events along a finite track around the photon interaction site. The spatial spread of energy is described by kernels. The dose delivered at any point can be estimated by superimposing the dose contributions from all kernels and weighing in the respective TERMA. For spatially invariant kernels, the dose at any point can be calculated from the convolution of the TERMA with the kernel. The kernels are usually pre-calculated using Monte Carlo simulations.

Analytical dose calculation systems in proton therapy are mostly based on variations of pencil beam algorithms. The dose distribution of a full proton beam may be determined from a convolution of the proton fluence with a pencil beam dose kernel, computed at each depth within the calculation geometry (Schaffner et al., 1999). The kernel represents the dose deposited in water by an infinitesimally narrow proton pencil beam. The dose of the kernel is described by a central axis term, determined from a central axis depth dose profile, and an off axis term, quantifying the diffusion of the protons relative to the beam's central axis. The two terms can either be derived from measurements in water or calculated using Monte Carlo simulations. The density heterogeneities are considered only along the central axis of the pencil beam. Another method is to estimate the dose distribution of a full proton beam by integrating the doses delivered by a set of individual pencil beams (Hong et al., 1996). The dose at the central axis of a single pencil beam is determined from a broad-beam depth dose, either measured in a water phantom or pre-calculated using Monte Carlo simulations, whereas the lateral distribution can be approximated as a Gaussian distribution. For this method, both the central axis and the off axis take density heterogeneities into account.

3.5.2 Monte Carlo simulations

The Monte Carlo (MC) simulation method is the most accurate method of simulating particle interactions within matter. Random number sampling from probability density functions are used to generate tracks of individual particles. The probability density functions represent the interaction probabilities of the particles. Each primary particle may create a cascade of secondary particles which all have to be simulated. The transport process is terminated when all particles are either absorbed or have left the tracking geometry.

For photon transport, a direct simulation of all physical interactions can be applied. However, for charged particles, simulating all interactions may be unrealistic as the number of interaction is very large. A so-called Class II condensed history technique was developed to solve this problem (Berger, 1963). The Class II algorithm groups minor interactions together, i.e. small energy losses and angular deflections of the particles are condensed into a single step. However, "catastrophic" events, in which the loss or deflection is very large, are treated separately. These events might result in the creation of secondary electrons, bremstrahlung photons, or in nuclear interactions.

The central limit theorem states that for a sufficiently large number of histories, N, the result of a quantity of interest, calculated by the Monte Carlo method, follows a Gaussian distribution and consequently has an estimated mean value, $\bar{x}$, and an

uncertainty of the mean that follows

$$\sigma(\bar{x}) \propto \frac{1}{\sqrt{N}} \tag{3.5}$$

Hence, increasing the number of histories will decrease the uncertainty of the simulated quantity of interest.

4 Proton Radiobiology

4.1 DNA damage

Ionizing radiation may cause damage to the deoxyribonucleic acid (DNA) in the cell nucleus by inducing DNA strand breaks. Single-strand breaks (SSBs) are rarely lethal to the cell as they are quickly repaired using the opposite, homologous strand as a template. However, an incorrect repair may result in mutation. By contrast, if the strand breaks are on both strands and in close proximity, it can cause double-strand breaks (DSBs). Consequently, no complementary strand is available as a template for repair. As a result, double-strand breaks may result in cell death, carcinogenesis, and mutation and are considered to be the primary contributor of radiation-induced biological effects (Hall and Giaccia, 2006).

Cells have two main processes to repair DSB: homologous recombination (HR) and non-homologous end joining (NHEJ). In HR, information from the homologous undamaged chromatid/chromosome is used for the repair. The repair process is dependent on the phase of the cell cycle, and occurs primarily in the late S/G2 phase when the undamaged sister chromatid is available as a template. The DSB is repaired without a loss of genetic information. In NHEJ, the structure of the DNA is restored without requiring homologous DNA. Damaged or mismatched DNA ends at the DSB site are removed, and subsequently the DNA strands are ligated together. This process is a much faster repair mechanism compared to HR, however a loss of genetic information at the repair site may occur.

During the repair processes, a number of lesions fail to repair resulting in cell death. For proliferating cells, the term cell death is typically used for the loss of the capacity for sustained proliferation. Mitotic death, in which cells fail to complete mitosis correctly, is the dominant mechanism following irradiation. Another important mechanism is apoptosis, programmed cell death, in which the cell death is highly regulated. In contrast, the term cell survival refers to cells that have retained their reproductive capacity.

Ionizing radiation can cause DNA damage either directly by ionizing the DNA (direct effect), or indirectly by producing free radicals that damage the DNA (indirect effect). A free radical is electrically neutral atom or molecule that contains an unpaired orbital electron in the outer shell, making it highly reactive. Free radicals can diffuse a short distance to reach the DNA. For high LET radiation, i.e. a dense ionizing radiation, direct effects are more pronounced whereas for low LET, i.e. a sparsely ionizing radiation, the DNA damage is mainly caused by indirect effects (Hall and Giaccia, 2006).

4.2 The Linear Quadratic Model

The most common expression to describe the relationship between the absorbed dose and the fraction of surviving cells is the linear-quadratic (LQ) model. The model relates the survival probability of a cell, i.e. the surviving fraction S, to the dose D

$$S = e^{-\alpha D - \beta G D^2} \tag{4.1}$$

Here, α and β characterize the intrinsic sensitivity of a cell or tissue to radiation dose, in units Gy^{-1} and Gy^{-2}, respectively, and are often expressed as the ratio α/β having units Gy. The factor G is the generalized (Lea-Catcheside) dose protraction factor (Sachs et al., 1997) and accounts for dose fractionation/protraction during radiotherapy. It is defined to take values between 0 and 1. For $G = 1$, equation 4.1 describes a dose D delivered in a single dose fraction

$$S = e^{-\alpha D - \beta D^2} \tag{4.2}$$

whereas $G < 1$ is interpreted as a reduction in cell killing due to repair which occurs between dose fractions. For n identical well-separate fractions of dose d, $G = 1/n$ and the survival probability becomes

$$S = \left(e^{-\alpha d - \beta d^2/n}\right) = e^{-D(\alpha + \beta d)} \tag{4.3}$$

where D is the total dose, $D = nd$.

4.3 The α and β Parameters

As mentioned in the previous section, the radiosensitivity of a cell or tissue is frequently defined in terms of the α/β ratio. Early-responding tissues, i.e. organs containing rapidly proliferating cells, tend to have high α/β ratios. These include e.g. skin and bone-marrow. By contrast, late-responding tissues having slowly or nonproliferating cells such as lung, kidney or spinal cord, usually have lower α/β ratios. For photon radiation, the α/β ratio (expressed as $(\alpha/\beta)_x$ ratio) for early-responding tissues is considered to be in the range of 8-15 Gy whereas for late-responding tissues, the $(\alpha/\beta)_x$ ratio is between 1-4 Gy (Joiner and van der Kogel, 2019). As cancer is defined as uncontrolled proliferation of cells, historically the $(\alpha/\beta)_x$ ratio was assumed to be high, or around 10 Gy (Williams et al., 1985). For some tumors, like head and neck, cervix, bladder and liver tumors, this assumption holds. However, estimates of the $(\alpha/\beta)_x$ ratio for breast tumors, rhabdomyosarcoma and liposarcoma indicate lower $(\alpha/\beta)_x$ ratios of around 4 Gy and prostate tumors have showed values of $(\alpha/\beta)_x$ = 1.5 Gy (van Leeuwen et al., 2018).

Figure 4.1 shows the impact of the α/β ratio on cell survival curves calculated using the LQ dose response model (section 4.2). The survival is typically presented on a log scale. For a single fraction, figure 4.1(a), a pronounced curvature is seen for cells having low α/β ratios, often referred to as the shouldered dose response. The

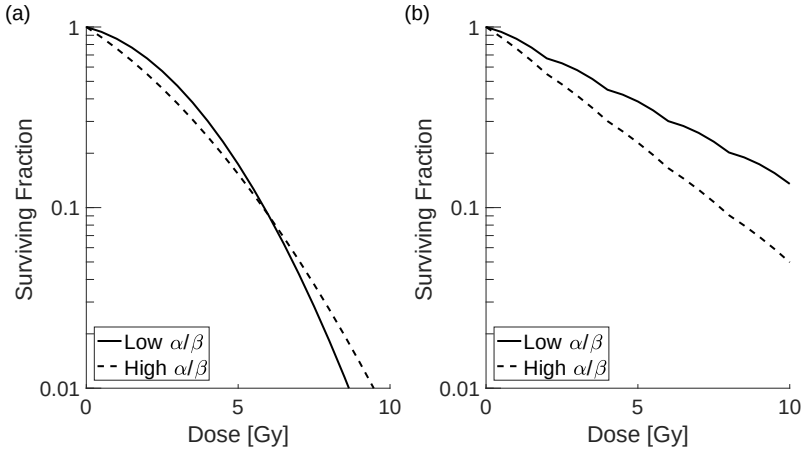

Figure 4.1. Illustration of cell survival curves estimated using the LQ model for cell lines with high and low α/β ratios. (a) Responses for a single unit dose. A shouldered response is seen for cells having low α/β ratios, while cells with high α/β ratios have a nearly constant cell killing rate with dose. (b) Impact of dose fractionation effect, with well separated 2 Gy dose fractions. A significant sparing effect is seen for cells having low α/β ratios.

curvature is determined by the β parameter whereas α represents the initial linear slope. In terms of cell killing, the α and β parameters are often described as measures of the amount of lethal and sub-lethal cell damage, respectively. Furthermore, the survival curves for a single fraction of early and late-responding tissues intersect each other, leading to lower surviving fraction for late-responding tissues at high doses, see figure 4.1(a). Figure 4.1(b) shows the significance dose fractionation in radiation treatment may have on different tissues. By allowing late-responding tissue to recover between fractions of a minimum of 6 h (Fowler, 1989), radiation-induced damage may be fully repaired, thus repeating the shape of the cell survival curve for the following fraction. As a consequence, fractionation tends to spare late-responding tissues relative to tissues having high α/β ratios, such as many tumors.

4.4 The Relative Biological Effectiveness

The relative biological effectiveness (RBE) is defined as the ratio of physical doses required by two radiation modalities to produce the same biological effect or clinical endpoint X. For protons, the RBE is defined as

$$\text{RBE(Endpoint X)} = \frac{D_x(\text{Endpoint X})}{D_p(\text{Endpoint X})} \tag{4.4}$$

where D_x is the dose of a reference radiation (usually ^{60}Co γ rays or MV X-rays) and D_p is the proton dose. Within the LQ framework, see equation (4.2), proton and photon dose are isoeffective if

$$\alpha_x D_x + \beta_x D_x^2 = \alpha_p D_p + \beta_p D_p^2 \tag{4.5}$$

Therefore, the RBE can be defined as

$$\mathrm{RBE}(D_p, \alpha_p, \beta_p, \alpha_x, \beta_x) = \frac{\sqrt{\alpha_x^2 + 4\beta_x D_p(\alpha_p + \beta_p D_p)} - \alpha_x}{2\beta_x D_p} \tag{4.6}$$

Here, α_p and β_p are the radiosensitivity parameters of the LQ model for protons, and α_x and β_x are the LQ parameters for the reference photon radiation. The physical proton dose, D_p, is multiplied with the RBE to obtain a photon equivalent dose having the unit Gy(RBE).

Experimental evidence indicate that RBE depends on physical parameters such as LET, dose, dose rate and fractionation (Paganetti et al., 2002; Paganetti, 2014). Furthermore, RBE may be dependent on biological parameters which include tissue type, intrinsic radiosensitivity, cell cycle phase, proliferation rate, oxygen concentration of the tissue and the relevant biological endpoint (Durante and Loeffler, 2010; Paganetti, 2014; McMahon, 2018).

4.4.1 RBE models

Numerous RBE models have been developed to determine and understand variable proton RBE in tissues. The models are either phenomenological, in which a radiobiological model is fitted to empirical data, or biophysical based on a more mechanistic approach.

Phenomenological Models

The majority of the RBE models are phenomenological, based on the LQ model and use empirical data from *in vitro* proton irradiation of various cell lines in which cell survival is the biological endpoint. The dependence of α_p and β_p on $\mathrm{LET_d}$ and $(\alpha/\beta)_x$ for different models (see equation (4.6)) can be defined as

$$\alpha_p = \alpha_x \left(p_0 + p_1 \frac{\mathrm{LET_d}}{(\alpha/\beta)_x} \right) \tag{4.7}$$

$$\beta_p = \beta_x \left(p_2 + p_3\, h(\mathrm{LET_d}) \right) \tag{4.8}$$

The p_0, p_1, p_2 and p_3 correspond to model-specific fitted parameters whereas the function $h(\mathrm{LET_d})$ varies between models.

Table 4.2 represents the fitted parameters as well as $h(\mathrm{LET}_d)$ for three selected RBE models based on the LQ model and fitted to different experimental datasets of clonogenic cell survival. The selected models are hereafter referred to as the CAR model (Carabe et al., 2012), the McN model (McNamara et al., 2016), and the WED model

Table 4.2. Recommended parameters for selected empirical proton RBE models based on a similar formalism of the LQ model.

Model	$h(\mathrm{LET_d})$	p_0	p_1	p_2	p_3
CAR	$\mathrm{LET_d}/(\alpha/\beta)_x$	0.843	0.413644	1.09	0.01612
McN	$\sqrt{(\alpha/\beta)_x}\,\mathrm{LET_d}$	0.99064	0.35605	1.1012	-0.0039
WED	1	1	0.434	1	0

(Wedenberg et al., 2013). Table 4.3 summarizes the datasets used to fit the models as well as the range of the $(\alpha/\beta)_x$ ratio and the $\mathrm{LET_d}$. The CAR was derived using a single cell line, V-79, whereas the WED and the McN models used multiple cell lines. The fits by CAR and WED are based on a subset of the experimental dataset used by McN.

Biophysical Models

Ideally, mechanistic models would mathematically connect the underlying biological processes, initiated by both physical and chemical interactions of radiation within a cell, to clinical outcomes, such as tumor control or normal tissue complications. However, such modeling is extremely complex and does not currently exist. Therefore, biophysical models, i.e. mechanistic inspired models, have been developed. A common approach is to estimate the RBE for cell survival by linking the radiosensitivity parameters in the LQ model to the induction and biological processing of sublethal damage, predominantly DNA DSB, which are further converted into more lethal forms of damage, such as chromosome aberrations. One example of such model is the Repair-Misrepair-Fixation (RMF) model (Carlson et al., 2008; Frese et al., 2012; Stewart et al., 2015). The model is frequently combined with the Monte Carlo Damage Simulation (MCDS) algorithm which predicts initial DSB induction (Semenenko and Stewart, 2004, 2006; Stewart et al., 2011). In the RMF model, the DSB induction is linked to cell death by mitotic

Table 4.3. Overview of key values of all datasets used to fit selected empirical proton RBE models.

Model	Cell Line	Number of data points	$(\alpha/\beta)_x$ range [Gy]	$\mathrm{LET_d}$ range [keV μm^{-1}]
CAR	V79	44	2.0 – 2.8	1.0 – 20.0
McN	Multiple	285	0.1 – 29.5	0.2 – 20.0
WED	Multiple	19	2.7 – 69.5	7.7 – 30.0

death, apoptosis, or other cell death modes. For a reference radiation with known radiation sensitivity parameters α_x and β_x, the radiosensitivity parameters for protons are defined as (Frese et al., 2012)

$$\alpha_p = \alpha_x \left(\frac{\Sigma}{\Sigma_x}\right)\left[1 + \frac{2}{(\alpha/\beta)_x \Sigma_x}\left(\Sigma\,\bar{z}_{\mathrm{F}} - \Sigma_x\,\bar{z}_{\mathrm{F}x}\right)\right] \tag{4.9}$$

$$\beta_p = \beta_x \left(\frac{\Sigma}{\Sigma_x}\right)^2 \tag{4.10}$$

Here, Σ is the initial number of DSB per Gray per giga base pair, expressed in units $\mathrm{Gy}^{-1}\mathrm{Gbp}^{-1}$. Furthermore, the parameter $\bar{z}_{\mathrm{F}}$ represent the frequency-mean specific energy, expressed in units Gy and can be approximated as

$$\bar{z}_{\mathrm{F}} \approx \frac{\mathrm{LET_d}}{\rho\,\delta^2} \tag{4.11}$$

where ρ is the mass density of a target cell nucleus having a diameter δ.

As for the $\mathrm{LET_d}$ calculations, see section 2.2.4, the α_p and β_p parameters can be computed on a voxel-by-voxel bases. For a discrete set of N overlapping radiation beams, the radiosensitivity parameters in voxel v are defined as

$$\alpha_p(v) = \frac{\sum_{i=1}^{N} \alpha_{p,i}(v) D_i(v)}{\sum_{i=1}^{N} D_i(v)} \tag{4.12}$$

$$\sqrt{\beta_p(v)} = \frac{\sum_{i=1}^{N} \sqrt{\beta_{p,i}(v)} D_i(v)}{\sum_{i=1}^{N} D_i(v)} \tag{4.13}$$

where $\alpha_{p,i}(v)$, $\beta_{p,i}(v)$ and $D_i(v)$ are the α_p, β_p and the dose distribution from beam i in voxel v, respectively.

4.5 Outcome Modeling

The probability of achieving local tumor control, i.e. inactivation of all clonogenic tumor cells, can be described using tumor control probability (TCP) models. Furthermore, normal tissue complication probability (NTCP) models describe the probability of severe complications in the surrounding normal tissue. Both TCP and NTCP approximate a sigmoidal shape when plotted linearly against dose, see figure 4.2. The aim of radiotherapy is to maximize TCP while minimizing NTCP.

4.5.1 Modeling of Tumor Control Probability

Assuming heterogeneous irradiation in a tumor, the overall TCP can be formulated as the product of the probability of killing all clonogenic tumor cells in each voxel of the

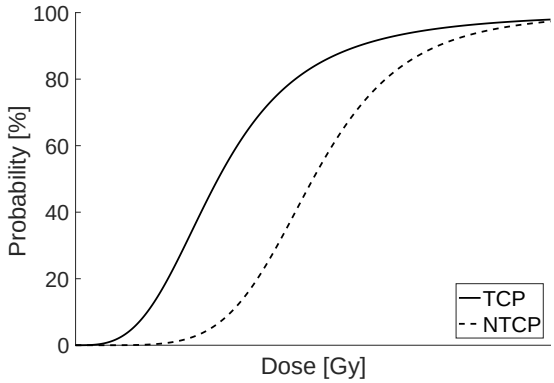

Figure 4.2. Dose-response curve for tumor control probability (TCP) and normal tissue complication probability (NTCP).

tumor (Li et al., 2012)

$$\mathrm{TCP} = \prod_{i=1}^{M} P(D_i)^{v_i} \tag{4.14}$$

Here, M is the total number of voxels, $P(D_i)$ denotes the probability that no clonogenic tumor cells are present in the voxel and v_i is the voxel volume relative to tumor volume, $v_i = V_i/V_{\mathrm{total}}$, irradiated with a dose D_i.

Several formulations of $P(D_i)$ models have been proposed, in which some are phenomenological while others are biophysical. The logistic model (Schultheiss et al., 1983; Goitein and Schultheiss, 1985) is an example of a phenomenological model in which the probability function is predicted using a logistic function

$$P(D_i) = \frac{1}{1 + (\mathrm{TCP}_{50}/D_i)^{4\gamma}} \tag{4.15}$$

Here, TCP_{50} is the tumor dose at which 50% of tumors are controlled and γ is the maximum value of the normalized slope gradient. A more mechanistic approach of estimating $P(D_i)$ is often based on the assumption that the number of surviving clonogenic tumor cells can be defined using Poisson statistics (Munro and Gilbert, 1961). As the probability that no clonogenic tumor cells survive is of interest, the zero-order term of the Poisson distribution is used to define the probability function

$$P(D_i) = e^{-N_0 S} \tag{4.16}$$

where N_0 represents the initial number of clonogenic tumor cells and $N_0 S$ is the average number of surviving clonocenic cells in which S is the surviving fraction after a dose D_i of radiation.

4.5.2 Modeling of Normal Tissue Complication Probability

In general, the dose-response relationship for normal tissue depends on the amount of irradiated normal tissue or organ. Therefore, it is critical to accurately account for the so-called volume effect, that is how the probability of a complication alters with a change in the irradiated volume. The most common phenomenological NTCP model is the Lyman-Kutcher-Burman (LKB) model (Lyman, 1985; Kutcher and Burman, 1989) in which the NTCP depends upon volume as well as dose and is represented by an error function

$$\mathrm{NTCP} = \frac{1}{\sqrt{2\pi}} \int_{-\infty}^{t} e^{-t^2/2} \mathrm{d}t \tag{4.17}$$

$$t = \frac{D_{\mathrm{eff}} - \mathrm{TD}_{50}}{m\,\mathrm{TD}_{50}} \tag{4.18}$$

$$D_{\mathrm{eff}} = \left(\sum_{i}^{M} v_i D_i^{1/n} \right)^n \tag{4.19}$$

where D_{eff} represents the effective volume. Furthermore, TD_{50} is the dose given to the entire organ that results in 50% complication risk, m represents the steepness of the dose–response curve and v_i is the voxel volume relative to tumor volume receiving a dose D_i. Finally, n is a tissue-specific parameter that describes the volume effect. For n close to zero, the volume effect is small which suggests that the NTCP correlates with the mean dose of the organ. However, for n close to unity, the volume effect is large, implying that the NTCP correlates with the maximum dose in the organ.

The effective volume D_{eff} is conceptually identical to the generalized equivalent uniform dose (gEUD) (Niemierko, 1997, 1999), in which the tissue-specific parameter for gEUD is defined as $a = 1/n$. For normal tissues, the gEUD refers to the uniform dose that provides the same biological effect as for a given non-uniform dose distribution.

Another approach to model NTCP classifies the organs as either serial, parallel or a mixture of the two, depending on how the so-called functional subunits (FSUs) of the organs are organized (Withers et al., 1988). The FSUs are structurally well defined tissue compartments, e.g. nephrons of the kidney. Serial organs, such as the spinal cord and the brain stem, have the FSUs structured in a series. The organ may lose its function if one FSU is incapacitated. In contrast, parallel organs, such as the lungs and the kidneys, assume independent FSUs. The organs can function even when a substantial fraction of FSUs has been damaged. Consequently, a volume threshold for the organ may exist. The relative seriality model (Källman et al., 1992) takes the organization of the FSUs into account by including a parameter s which is equal to unity for a fully serial organ or zero for a fully parallel organ. The NTCP is given by

$$\mathrm{NTCP} = \left\{ 1 - \prod_{i=1}^{M} [1 - P(D_i)^s]^{v_i} \right\}^{1/s} \tag{4.20}$$

where v_i is the voxel volume relative to the total organ volume receiving a dose D_i. The probability function, $P(D_i)$, is often based on the Poisson statistical model of cell kill and is defined as

$$P(D_i) = 2^{\exp\{e\gamma(1-D_i/\mathrm{TD}_{50})\}} \tag{4.21}$$

where γ is the maximum value of the normalized slope gradient and TD_{50} is the dose given to the entire organ that results in a 50% complication risk.

5 Specific Aims of this Research

In order to benefit from decades of clinical practice obtained with photon radiation treatments, dose prescriptions in photon therapy are used as the basis for proton therapy. Currently, proton therapy treatment sites are assuming a constant proton relative biological effectiveness (RBE) of 1.1 in both tumor and normal tissues. Therefore, proton therapy patients receive a 10% lower prescribed dose compared to photon therapy. Applying a constant RBE of 1.1 in clinical practice is judged to be reasonable by the ICRU (ICRU, 2007) and the International Atomic Energy Agency (IAEA) (IAEA, 2008). Historically, the RBE of 1.1 was an average value reported for a reference radiation of ^{60}Co at the center of a target volume, for a fraction dose of 2 Gy(RBE), and averaged over various endpoints. However, it has been shown (Paganetti et al., 2002; Paganetti, 2014) that the proton RBE varies as a function of both physical parameters such as dose and linear energy transfer (LET) as well as on biological parameters including tissue type (represented with the $(\alpha/\beta)_x$ ratio), endpoint, cell cycle phase and oxygenation level.

For the energy range used in clinical proton therapy the RBE increases with increasing LET, decreasing dose and with decreasing $(\alpha/\beta)_x$ ratio. A review in 2014 (Paganetti, 2014) analyzed the average RBE values for cell line data from over 70 reports. Using clonogenic cell survival as the endpoint, the average RBE value in the center of a spread-out-Bragg peak (SOBP) for a 2 Gy(RBE) fraction size was reported to be around 1.15. However, due to the LET increase with depth, the average RBE value increased to around 1.35 at the distal edge and to around 1.7 at the fall-off region. Figure 5.1 exemplifies the impact of a variable RBE. Dose distributions for SOBPs were produced using Monte Carlo calculations with the double scattering delivery system at Francis H. Burr Proton Center at the Massachusetts General Hospital. The SOBPs have a range of 15 cm and a modulation width of 5 cm. The figure shows a physical dose distribution with a prescribed dose of (a) 2 Gy and (b) 15 Gy at the center of the SOBP. Furthermore, two biological dose distributions are seen; the physical dose is scaled by a fixed RBE of 1.1 (RBE-fixed) and by a variable RBE (RBE-weighted) based on the McN model with $(\alpha/\beta)_x$ ratios of 2 and 10 Gy. The shaded region resembles a hypothetical location of a tumor within the SOBPs. The figure also demonstrates how the respective dose-averaged LET distribution ($\mathrm{LET_d}$) in the target region increases with depth. Consequently, the average RBE-weighted dose in the target is affected. Furthermore, the position of the distal dose fall-off is shifted in the RBE-weighted dose distribution, which is clearly evident for $(\alpha/\beta)_x$ of 2 Gy and dose per fraction of 2 Gy. It has been shown that this shift in the biological dose distribution can be up to 4 mm compared to the physical dose distribution (Paganetti and Goitein, 2000; Carabe et al., 2012; Paganetti, 2014; Grün et al., 2013).

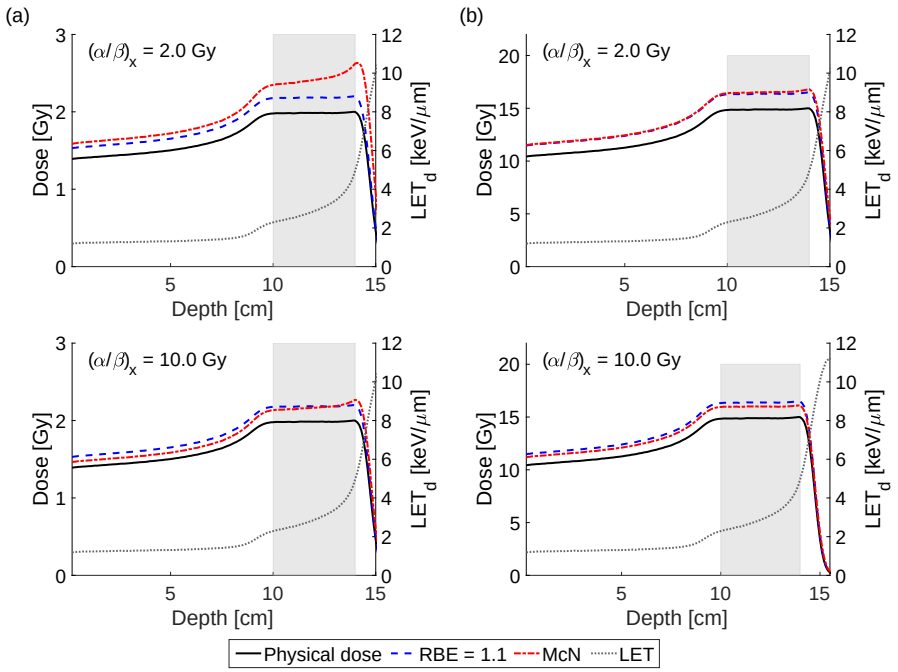

Figure 5.1. Example of depth dose distributions for four simple SOBPs in water. The physical dose is shown by a black solid curve with a prescribed dose of (a) 2 Gy or (b) 15 Gy at the center of the SOBP, the blue dashed curve shows the physical dose scaled by a fixed RBE value of 1.1, while the dashed-dotted curves represents the RBE-weighted dose calculated using different RBE models (RBE-weighted). The respective LET_d curves are shown as a grey dotted curve. The SOBPs have a range of 15 cm. The top figures have $(\alpha/\beta)_x$ = 2 Gy whereas $(\alpha/\beta)_x$ = 10 Gy for the lower figures.

Throughout this work, the primary focus is to evaluate the clinical impact as well as the biological uncertainties on using a variable RBE compared to a constant RBE value of 1.1 in proton therapy. This is accomplished through the analyses of clinical data from ongoing clinical trials and through Monte Carlo simulations. The uncertainty associated with the RBE variation due to the uncertainty in the $(\alpha/\beta)_x$ ratio will be evaluated as well as the choice of the RBE weighted models.

Paper I evaluates the clinical impact of RBE variations in proton therapy for prostate cancer due to the uncertainty in the $(\alpha/\beta)_x$ ratio. Patients receiving either passive scattered proton therapy (PSPT) or intensity modulated proton therapy (IMPT) are compared to patients treated with 7-field intensity modulated photon therapy (IMRT). Two RBE models are used to predict the variable RBE; the phenomenological McN model and the biophysical RMF model. Furthermore, tumor control probabilities (TCP) and normal tissue complication probabilities (NTCP) are assessed. Paper II assesses the biological uncertainties in proton therapy due to the assumptions of using a fixed RBE of 1.1 compared to a variable RBE, particularly for small fields as they are subject

to elevated LET values throughout the field. The McN model is used to evaluate the variable RBE. Furthermore, the clinically used range uncertainty margin of of 3.5% + 1 mm is reduced to illustrate the interplay between range uncertainty margins and a potential RBE effect. Paper III examines the clinical impact of using a variable RBE in proton beam scanning treatment (PBS) for left-sided breast cancer versus the assumption of a fixed RBE of 1.1, particularly in the context of comparisons with photon-based three-dimensional conformal radiotherapy (3DCRT) and volumetric modulated arc therapy (VMAT). Furthermore, a one-to-one plan comparison between PBS and 3DCRT is analyzed. The work is primarily concerned with the risk of normal tissue complications and consequently normal tissue toxicity probabilities for different endpoints are evaluated. The variable RBE is calculated using the McN model. Finally, three different phenomenological RBE models, namely the CAR, McN and WED models, are used to evaluate the variable RBE effect in patients receiving proton therapy for soft tissue sarcoma. The results were presented at the American Association of Physicists in Medicine (AAPM).

6 Methods

6.1 Patient Cohort

All patients selected for this doctoral work underwent radiation therapy at Massachusetts General Hospital. Proton therapy patients were treated at the Francis H. Burr Proton Therapy Center whereas patients receiving photon therapy were treated at the Clark Center for Radiation Oncology. All studies were approved by the institutional review board (IRB) at Massachusetts General Hospital.

6.2 Dose Simulations

Proton dose distributions from analytical dose calculations (ADCs) were collected on a voxel-by-voxel basis from the planning systems XiO (CMS, St Louis, MO) and Astroid (.decimal, Sanford, FL) for passive scattering and beam scanning treatments, respectively. For photon treatments, the ADC dose distributions were collected in the form of dose volume histograms (DHVs) from the treatment planning system RayStation (Raysearch Laboratories, Sweden). All ADC treatment plans were optimized by experienced treatment planners following clinical practice.

Monte Carlo (MC) simulations were performed using the Geant4-based TOPAS toolkit (Perl et al., 2012; Agostinelli et al., 2002). For each patient receiving proton therapy, the beam geometry and treatment plan CT image set were imported into TOPAS using an in-house software (Verburg et al., 2016). The number of primary particles applied resulted in an uncertainty in dose to the target of around 2%. Throughout this work, the physical dose scorer was recalculated on a voxel-by-voxel basis and scored as dose-to-water whereas the proton LET scorer was calculated as dose averaged LET values ($\mathrm{LET_d}$) in each voxel. Furthermore, in paper I, the DNA double strand break (DSB) scorer for the RMF model was calculated voxel-by-voxel, which was estimated from the Monte Carlo Damage Simulation (MCMD) software (Stewart et al., 2011). Subsequently, the radiosensitivity parameters for protons, α_p and β_p, were calculated according to equations (4.9) and (4.10). All simulations were run on a research computer cluster at Partners Healthcare. The proton therapy dose plans were not re-optimized but recalculated when using MC simulations as the aim was to provide insight into potential RBE effects in current clinical practice.

The reference radiation was chosen as γ-rays from ^{60}Co having LET_x equal to 0.2 MeV/mm. For the RMF calculations, the RBE for DSB induction was computed by dividing the number of DSB for the protons by the number of DSB for cells irratiated by ^{60}Co γ-rays in vitro, which resulted in 8.32 DSB Gy^{-1} Gbp^{-1} (Stewart et al., 2015).

Finally, the nucleus of a cell was chosen to have a diameter of 5 μm (Frese et al., 2012).

6.3 RBE Modeling

Further analyses on proton therapy cases were performed using the Computational Environment for Radiation therapy Research (CERR) platform (Deasy et al., 2003) running on the computing environment Matlab (Mathwork Inc.). The physical proton dose distributions were scaled by using either a fixed RBE of 1.1 (RBE-fixed) or a variable RBE (RBE-weighted). The variable RBE values were estimated on a voxel-by-voxel basis using the calculations from the appropriate MC proton scorers. For each RBE estimation, different $(\alpha/\beta)_x$ ratios were carefully chosen. Throughout the work, the McNamara model (McN) was used to evaluate the RBE-weighted dose distributions. In paper I, the RBE-weighted dose distributions were further calculated using the repair-misrepair fixation model (RMF). Additionally, DVH analyses using McN, along with the Carabe model (CAR) and the Wedenberg model (WED) were performed on soft tissue sarcoma, see section 7.2.

6.4 Model Evaluation

In paper I, the logistic model (equation 4.15) was considered to predict the TCPs of prostate tumors following proton and photon treatments. The input parameters were obtained from a study by Cheung *et al* (Cheung et al., 2005). In the same paper, the NTCP for bladder and rectum were estimated using the Lyman–Kutcher–Burman model (equation 4.17) with endpoint of Grade $\geq$2 Radiation Therapy Oncology Group (RTOG) late toxicity for rectum (Michalski et al., 2010) and Grade $\geq$2 Late Effects Normal Tissue Task Force (LENT)/ Subjective, Objective, Management, Analytic (SOMA) 5 year toxicity for bladder (Zhu et al., 2016).

Paper III estimated the NTCP for the heart with two different endpoints for patients receiving either photon or proton radiation treatment for left-sided breast cancer. A linear model proposed by Darby *et al* (Darby et al., 2013) estimated the risk of major coronary events whereas the relative seriality model (equation 4.20) was used to estimate NTCP for the heart with cardiac mortality as the endpoint (Gagliardi et al., 1996). The paper further evaluated the toxicity risk to the LAD using a logistic model proposed by Moigier *et al* (Moignier et al., 2015) to evaluate the increase in risk of coronary stenosis. Finally, the paper estimated the NTCP using the relative seriality model (equation 4.20) having radiation pneumonitis of two different grades as the endpoint (Rancati et al., 2007; Gagliardi et al., 2000).

6.5 Monte Carlo Patient Population

As a patient population might have a distribution of $(\alpha/\beta)_x$ values, random sampling was performed to evaluate the spread in TCP and NTCP due to the $(\alpha/\beta)_x$ uncertainty.

In paper I and III, a Gaussian distribution of $(\alpha/\beta)_x$ ratios was created in which the nominal $(\alpha/\beta)_x$ ratio was set as the mean value and the standard deviation was estimated from the reported 95% confidence intervals. To ensure positive $(\alpha/\beta)_x$ values, each Gaussian distribution was truncated bilaterally at the distance from the mean value to zero. For each patient, thousands of random $(\alpha/\beta)_x$ values were extracted from the truncated Gaussian distribution and with the LET_d and the physical dose distributions obtained from the MC simulations, the corresponding RBE-weighted dose distributions were estimated. The cumulative DVHs for each RBE-weighted dose distribution were stored and consequently the TCP and NTCP values were estimated for each generated DVH.

Furthermore, in paper I, the cumulative DVHs of the photon patients were bootstrapped to compare the proton results to the photon data. The bootstrap method is a re-sampling technique that relies on random sampling with replacement from an existing sample data to create a number of resamples (Efron, 1979). Thousands of bootstrap replicates were generated from the original cumulative DVH data. Subsequently, the TCP and NTCP values were estimated, thus reflecting a range of plausible outcome probabilities.

6.6 Statistical Hypothesis Testing

Statistical analysis of comparisons between proton treatment calculations having a fixed RBE of 1.1 to a variable RBE were performed using the Wilcoxon signed rank test, a nonparametric test for matched or paired samples (paper III). Furthermore, proton treatment comparisons to photon treatments were assessed: for different patient groups the Wilcoxon rank sum test was used, a nonparametric test for independent samples (paper I and paper III), whereas for the same patient group the statistical analysis were performed using the Wilcoxon signed rank test (paper III). The null hypothesis was that the medians of two samples are equal. The statistical significance was defined as rejecting the null hypothesis at the 5% level in paper I whereas in paper III, the statistical significance was defined as rejecting the null hypothesis at the 1% level to account for multiple comparisons.

7 Results

7.1 RMF Model Comparison

The RMF model was implemented into the TOPAS simulation tool. To ensure accurate results for the RMF model, comparisons were made between the TOPAS calculations and results from a previous analysis by Frese *et al* (Frese et al., 2012). SOBPs were simulated according to the double scattering delivery system at Massachusetts General Hospital, having a depth 15 cm and modulation width of 5 cm. Figure 7.1 shows the results for a physical dose of 1 Gy and chordoma tissue type, with $\alpha_x = 0.1$ Gy^{-1} and $\beta_x = 0.05$ Gy^{-2}. The calculated scorers, i.e. α_p, β_p, $\mathrm{LET_d}$ and DBS, were compared to figure 3 in Frese *et al*. Furthermore, table 7.4 demonstrates the average RBE value in

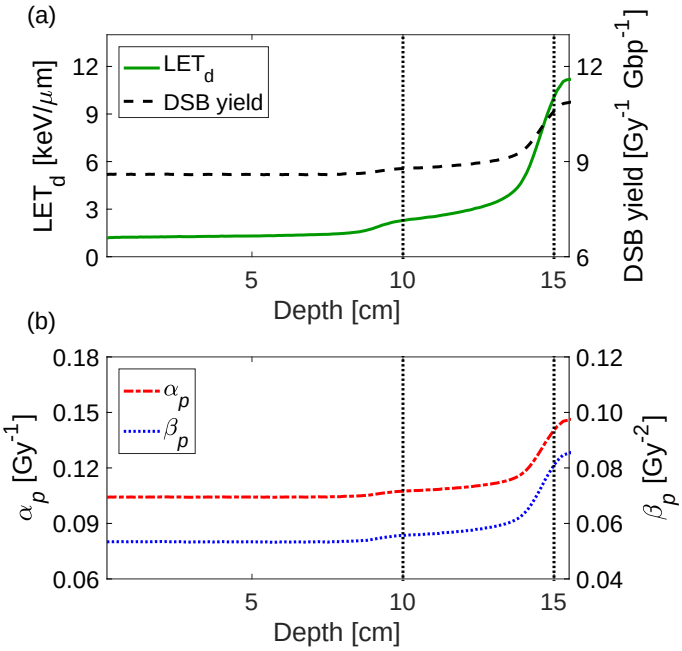

Figure 7.1. The parameters α_p, β_p, LET_d and DBS calculated for the RMF model, to compare with figure 3 in Frese et al, (Frese et al., 2012). Dotted lines show proximal (z = 10 cm) and distal edges (z = 15 cm) of the SOBP.

the SOBPs optimized for a range of physical doses as well as the percentage difference between the calculated values in this work and the reported average RBE values from Frese *et al* (Frese et al., 2012). As can be seen, the difference is <2%. A larger difference was observed for RBE values estimated at proximal and distal edges (results not shown) with the largest difference being 4%. This can be explained as the SOBPs in this work were produced using Monte Carlo calculations with the double scattering delivery system at the Francis H. Burr Proton Center at Massachusetts General Hospital and are therefore somewhat different in shape to the ones produced in Frese's article. The RMF model installed using TOPAS was considered to be accurate based on all parameters estimated.

Table 7.4. The average RBE within an SOBP having modulation width of 5 cm values for a range of tissue radiosensitivities and physical doses. Values calculated for this work to be compared to values from a previous analysis by Frese et al (Frese et al., 2012); the percentage difference is displayed.

	$(\alpha/\beta)_x$ = 2 Gy		$(\alpha/\beta)_x$ = 10 Gy	
Dose [Gy]	This work	Difference - Frese	This work	Difference - Frese
0.1	1.13	0%	1.10	0.9%
1	1.12	0.9%	1.10	0.9%
2	1.11	0.9%	1.10	0.9%
5	1.10	0.9%	1.10	1.9%
10	1.10	1.9%	1.10	1.9%

7.2 Dose and Biological Uncertainties in Sarcoma

Oral presentation at the American Association of Physicists in Medicine (AAPM) in Washington DC - July 2016.

Marteinsdottir M, Schuemann J, Paganetti H.

Purpose

To understand the magnitude and clinical impact of key uncertainties in proton therapy potentially affecting the analysis of clinical trials, namely the assumption of using a constant relative biological effectiveness (RBE) of 1.1 (RBE-fixed) compared to variable RBE (RBE-weighted) for proton therapy and the use of analytical dose calculation (ADC) methods.

Methods

Dose distributions of 10 clinical cases of soft tissue sarcoma (liposarcoma, undifferentiated pleomorphic sarcoma and leiomyosarcoma) were re-calculated on a voxel-by-voxel basis using the Monte Carlo (MC) simulation tool TOPAS (Perl et al., 2012; Agostinelli et al., 2002). In parallel, the dose averaged LET values (LET_d) were estimated in each voxel. Each patient received a beam scanning treatment where the number of fields varied between 1 and 4 fields. The prescription doses were between 30.6 and 50.4 Gy(RBE) for a dose of 1.8 Gy(RBE) per fraction. The range of the target volumes was between 412.3 and 4593.9 cm^3.

Differences between using a constant RBE of 1.1 were compared to three different RBE models; the CAR model (Carabe et al., 2012), the McN model (McNamara et al., 2016), and the WED model (Wedenberg et al., 2013). In addition, the proton RBE-weighted dose distributions were compared to the analytical dose calculations (ADC), collected from the Astroid planning system. Comparisons were performed using dosimetric indices based on dose-volume histogram (DVH) analyses. The $(\alpha/\beta)_x$ ratio for the target (tumor) region was set to 10 Gy as cancer often has high $(\alpha/\beta)_x$ ratio due to its uncontrolled proliferation. However, it has been shown that rhabdomyosarcoma and liposarcoma indicate lower $(\alpha/\beta)_x$ ratios of around 4 Gy (van Leeuwen et al., 2018) and for liposarcoma it has shown to be low as 0.4 Gy (Thames and Suit, 1986). Therefore, the analyses were repeated for low $(\alpha/\beta)_x$ ratios of 4 and 0.4 Gy.

Results

Figure 7.2 shows the cumulative DVHs for the target of one clinical case for an $(\alpha/\beta)_x$ ratio of 10 Gy whereas DVH analysis for all 10 cases and all three $(\alpha/\beta)_x$ ratios can be seen in figure 7.3. All ADC dosimetric indices were up to 4% larger compared to MC calculations with RBE as 1.1, indicating an overestimation in the target dose when calculated with ADC. This has been demonstrated before (Schuemann et al., 2015). Furthermore, the figure displays a clear dependence on the choice of the $(\alpha/\beta)_x$ ratio as well as the variable RBE model. For the McN and WED models with $(\alpha/\beta)_x$ ratios

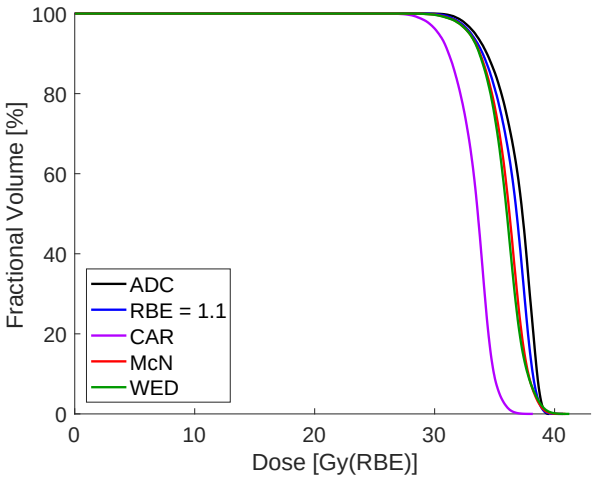

Figure 7.2. Cumulative DVH curve for the tumor of one exemplary clinical case for $(\alpha/\beta)_x$ = 10 Gy.

of 10 Gy, the mean dose, D95, D50 and D02 (dose values covering 95%, 50% and 2% of the target volume, respectively) were up to 4% lower than for MC calculations with a fixed RBE of 1.1. This was not the case for the CAR model where the dosimetric indices were between 7-9% lower than for MC calculations with a fixed RBE. The results suggest that for an $(\alpha/\beta)_x$ ratio of 10 Gy, the calculated RBE within the target may be below 1.1 for all three RBE models. The differences for V90 (the percentage of the target volume covered by 90% of the prescription dose) for $(\alpha/\beta)_x$ ratio of 10 Gy were up to 11% for the McN and WED models, whereas for the CAR model the difference was up to 48%.

Lowering the $(\alpha/\beta)_x$ ratio resulted in an increase in the target dose for all three RBE models. Applying an $(\alpha/\beta)_x$ ratio of 0.4 Gy resulted in a positive difference in all dosimetric indices between a variable RBE and a fixed RBE for all RBE models, demonstrating that the variable RBE-weighted dose distributions are larger than distributions having a fixed RBE of 1.1. The largest difference is seen for the CAR model, where the difference for the mean dose, D95, D50 and D02 was between 18-34% larger than for MC calculations with a fixed RBE of 1.1. This difference was lower for the McN and the WED models, or between 12-20% and 8-19%, respectively.

The different dosimetric results estimated using the CAR model compared to the McN and the WED models may be explained by the fact that the CAR model was fitted to experiments using the V-79 cells having a small range of $(\alpha/\beta)_x$ ratios, or between 2-2.8 Gy (see table 4.3). This might limit the application of the CAR model (Rørvik et al., 2018; Ödén et al., 2017).

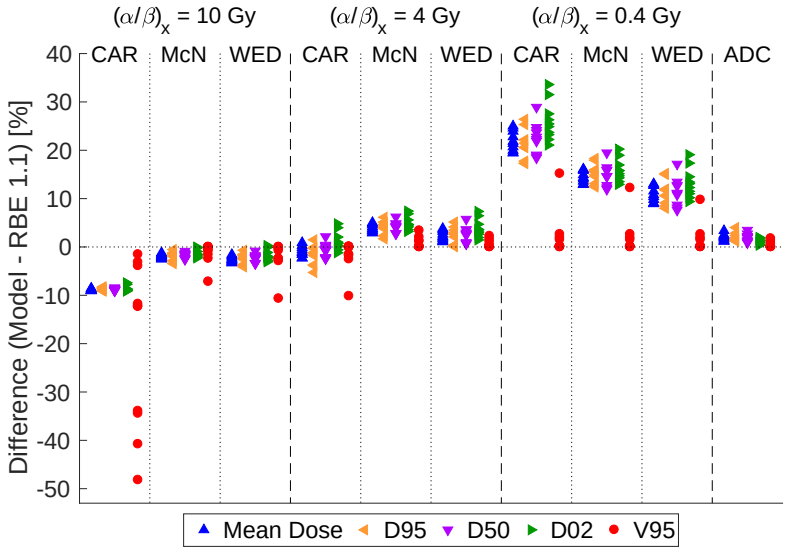

Figure 7.3. Percentage difference subtracting the dosimetric indices calculated by the three variable RBE models and ADC from the constant RBE of 1.1 calculated with MC simulations. Each data point represents results from one patient. DXX is the maximum dose covering the XX% of the target volume; V95 is the percentage of the target volume covered by 95% of the prescribed dose. The results are grouped by different $(\alpha/\beta)_x$ ratios.

Conclusion

Interpretation of clinical trials on sarcoma may depend on the dose calculation method, i.e. on whether ADC or MC simulations are used. In addition, the RBE-weighted dose distribution depends notably on which RBE model is utilized and the choice of $(\alpha/\beta)_x$ ratio. Performing an RBE uncertainty analysis is recommended for trial analysis.

7.3 Paper I - Applying a Variable Relative Biological Effectiveness (RBE) Might Affect the Analysis of Clinical Trials Comparing Photon and Proton Therapy for Prostate Cancer

Marteinsdottir M, Paganetti H.

Phys. Med. Biol. 64 (2019) 115027 (13pp). DOI: 10.1088/1361-6560/ab2144

Summary

Applying external beam radiation therapy (EBRT) of high total dose (>70 Gy) to localized prostate cancer is considered a standard treatment option. For such a high dose treatment, it is important to minimize the dose to the normal tissue, such as the rectum and the bladder, to reduce further complications. The most commonly used EBRT is the photon based intensity modulated radiation therapy (IMRT). Another radiation therapy option is proton beam therapy (PBT) which, due to the physical characteristics of protons, reduces the volume of the normal tissue exposed to radiation. However, it is essential to understand how a variable RBE in proton therapy and its uncertainty due to uncertainties in the $(\alpha/\beta)_x$ ratio impacts comparisons between IMRT and PBT.

In this paper, two PBT techniques, i.e. passive scattered proton therapy (PSPT) and intensity modulated proton therapy (IMPT), and IMRT were considered. Monte Carlo simulations were performed using the Geant4-based TOPAS toolkit (Perl et al., 2012; Agostinelli et al., 2002). Dose was scored as dose-to-water and LET values as dose averaged LET values (LET_d) in each voxel. The variable RBE was calculated according to two RBE models, the phenomenological McNamara model (McNamara et al., 2016) and the biophysical RMF model (Carlson et al., 2008; Frese et al., 2012; Stewart et al., 2015). The results showed that disregarding variable RBE may lead to either underestimation or overestimation of the expected tumor control probability (TCP) and normal tissue complication probabilities (NTCP). This depends on which RBE model is used to estimate the RBE as well as which $(\alpha/\beta)_x$ ratio. It is therefore recommended for future clinical trials to incorporate a larger uncertainty on the sample size calculations for the proton arm.

Main Results

- Using the McN model, the RBE weighted dose distribution was heavily influenced by the $(\alpha/\beta)_x$ ratio. The estimated dosimetric indices calculated for $(\alpha/\beta)_x$ ratio of 1.5 Gy were between 10%–11% larger compared to using a fixed RBE of 1.1. However, this difference decreased to 2%–3% when increasing the $(\alpha/\beta)_x$ to 4.96 Gy. For the RMF model, the results changed very little with the $(\alpha/\beta)_x$ ratio. The

dosimetric indices estimated using the RMF model were 1%–3% lower compared to using a fixed RBE of 1.1, irrelevant of the $(\alpha/\beta)_x$ ratio. This further indicates a lower RBE than 1.1.

- Applying a variable RBE predicted by the McN model revealed an increase in the average TCP value of up to 6% for PBT compared to IMRT, with the largest increase for the $(\alpha/\beta)_x$ ratio of 1.5 Gy. The average TPC value for PBT having an $(\alpha/\beta)_x$ of 4.96 Gy was only around 1% larger than for IMRT. For the RMF model, the average TCP values for PBT were around 2% lower than for IMRT with little variation as a function of $(\alpha/\beta)_x$. Figure 7.4 shows the TCP calculated for the prostate for all treatment modalities.

- The application of the McN model increased the NTCP for both rectum and bladder compared to applying a fixed RBE of 1.1, whereas the NTCP decreased when using the RMF model.

- As a patient population might have a distribution of $(\alpha/\beta)_x$ values, random sampling was performed using the McN model, to evaluate the spread in TCP and NTCP due to the $(\alpha/\beta)_x$ uncertainty. The average TCP values from the random sampling were around 2% larger for PSPT than for IMRT and around 3% larger for IMPT. Evaluation of the spread in NTCP due to the $(\alpha/\beta)_x$ ratio revealed a large relative standard deviation for all modalities, or between 30%–40%. This large variation was primarily due to inter-patient variability.

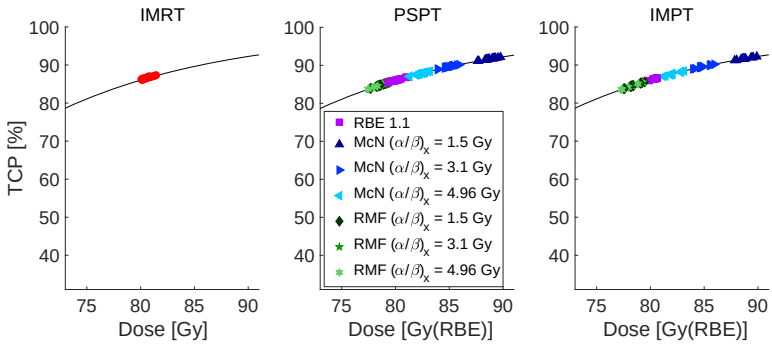

Figure 7.4. TCP calculated for the prostate for all treatment modalities. Each data point corresponds to one patient. The solid line represents the TCP curve for each modality.

7.4 Paper II - Impact of Uncertainties in Range and RBE on Small Field Proton Therapy

Marteinsdottir M, Schuemann J, Paganetti H.

Phys. Med. Biol. 64 (2019) 205005 (9pp). DOI: 10.1088/1361-6560/ab448f

Summary

For proton therapy, the relative biological effectiveness (RBE) of 1.1 is being applied in clinical practice. However, for the energy range used in clinical proton therapy the RBE increases with increasing linear energy transfer (LET), decreasing $(\alpha/\beta)_x$ ratio and with decreasing dose (Paganetti et al., 2002; Paganetti, 2014). Consequently, the RBE increases with depth. Disregarding these RBE variations might lead to underestimation or overestimation of the dose to the target and organs at risk. Furthermore, it is essential to predict the range of proton beams as accurately as possible in treatment planning and delivery. Due to the physical properties of protons, an underestimation of the range may result in parts of the target not receiving any dose. For that reason, an uncertainty margin is applied to ensure target coverage. The uncertainty margin is frequently defined as 3.5% of the prescribed range in water in beam direction +1 mm.

This study investigated how varying the $(\alpha/\beta)_x$ ratio affected the RBE for small fields in proton therapy. As potential RBE effects are typically more pronounced in the distal part of a field, a bigger clinical impact of RBE uncertainties in small fields is expected. The dose distributions and dose averaged LET values (LET_d) were calculated on a voxel-by-voxel basis using the Monte Carlo (MC) toolkit TOPAS (Perl et al., 2012; Agostinelli et al., 2002). The RBE calculations were performed using the McNamara RBE model (McNamara et al., 2016). Additionally, the impact of reducing the clinically used range uncertainty margin as well as changing the dose per fraction were investigated. The results demonstrated that the uncertainty in RBE due to the uncertainty associated with the $(\alpha/\beta)_x$ ratio was larger than the impact of reducing the applied range uncertainty margin. Furthermore, the impact of a variable RBE is more relevant for small doses per fraction of 2 Gy(RBE) than for stereotactic dose levels of 13-16 Gy(RBE) per fraction.

Main Results

- For stereotactic dose levels, increasing $(\alpha/\beta)_x$ ratio decreased the mean value of the RBE in the target (RBE_{mean}). However, reducing only the range margin resulted in a minuscule difference in RBE_{mean}. The largest difference was less than 0.1% and 0.3% for a range reduction to 2.5% + 1 mm and 0% + 1 mm, respectively. Figure 7.5 illustrates the mean value of RBE in the target for stereotactic dose levels, calculated for four different $(\alpha/\beta)_x$ ratios and three

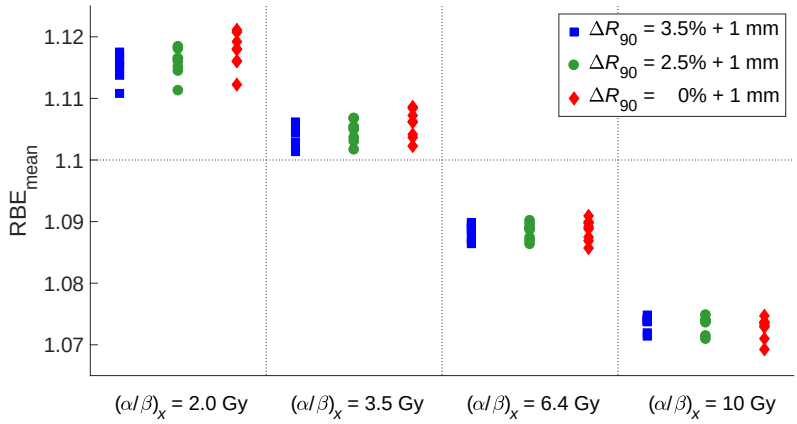

Figure 7.5. The mean value of RBE in the target volume. Results for four different $(\alpha/\beta)_x$ ratios and three different range uncertainty margins for stereotactic dose levels of 13–16 Gy(RBE).

different generic range uncertainty margins.

- Varying the RBE resulted in a small difference in the dosimetric indices compared to a fixed RBE of 1.1 for stereotactic dose levels and clinically used range uncertainty margins of 3.5% + 1 mm. The average value of RBE_{mean} within the target for all patients was 1.12 for an $(\alpha/\beta)_x$ of 2 Gy but 1.07 for an $(\alpha/\beta)_x$ of 10 Gy.

- For scaled doses of 2 Gy(RBE), the RBE_{mean} was larger than 1.1 for all $(\alpha/\beta)_x$ ratios. The reduction in range from 3.5% + 1 mm to 2.5% + 1 mm resulted in a difference in RBE_{mean} of around 1%, independent of the $(\alpha/\beta)_x$ ratio, but up to 3.0% by reducing the range to 0% + 1 mm. Figure 7.6 displays the mean value of RBE in the target for scaled doses of 2 Gy(RBE). The RBE_{mean} is calculated for four different $(\alpha/\beta)_x$ ratios and three different generic range uncertainty margins.

- A difference of up to 19% was seen in the dosimetric indices between a variable RBE having an $(\alpha/\beta)_x$ ratio of 2 Gy and a fixed RBE of 1.1 for scaled doses of 2 Gy(RBE) per fraction and a range uncertainty margin of 3.5% + 1 mm. The average value of RBE_{mean} in the target was 1.27. However, increasing the $(\alpha/\beta)_x$ to 10 Gy resulted in less than a 3% difference in the dosimetric indices and an average value of RBE_{mean} of 1.13.

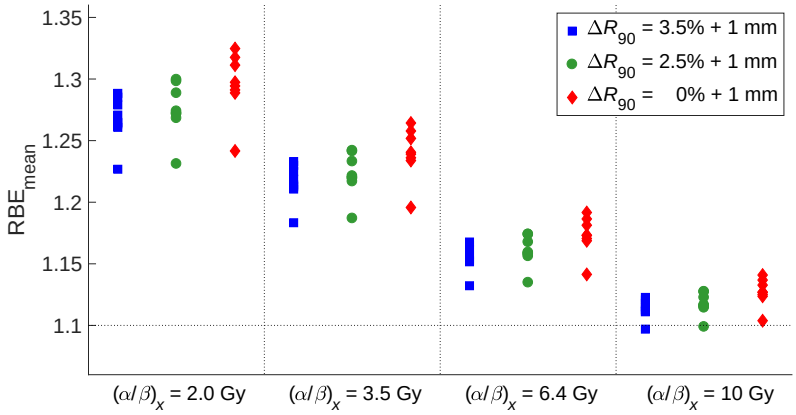

Figure 7.6. The mean value of RBE in the target volume. Results for four different $(\alpha/\beta)_x$ ratios and three different range uncertainty margins for a dose of 2 Gy(RBE).

7.5 Paper III - Impact of Variable RBE for Left-Sided Breast Cancer when Estimating Normal Tissue Complications in the Heart and Lung.

Marteinsdottir M, Wang C, McNamara A, Depauw N, Jungwook S, Paganetti H.

Phys. Med. Biol. 66 (2021) 035023 (15pp). DOI: 10.1088/1361-6560/abd230

Summary

Radiation therapy for left-sided breast cancer implies irradiating organs close to the breast, such as the heart and the left lung, and thus increasing the risk of late toxicity. A common radiation therapy for breast cancer following breast-conserving surgery or mastectomy is the photon based three-dimensional conformal radiotherapy (3DCRT). However, dose hotspots within the target and surrounding organs may be created for large breast sizes. Intensity modulated radiotherapy (IMRT) and volumetric modulated arc therapy (VMAT) allow for an improved radiation conformity and homogeneity, thus reducing hotspots. This, however, results in larger volumes of surrounding organs receiving a low to intermediate dose. An alternative to photon-based radiation therapy for breast cancer is proton beam therapy. Treatment setup often consists of a single field which generates a homogeneous dose distribution to the breast target volume. This configuration unavoidably positions the heart and the lung downstream of the target. As the relative biological effectiveness (RBE) increases with depth, it is therefore important to analyze the impact of a variable RBE compared to a fixed RBE value of 1.1 to the heart and the left lung for a single field proton therapy setup.

Dose distributions and dose averaged LET values (LET_d) for patients treated for left-sided breast cancer in proton beam scanning treatment (PBS) were calculated using the Monte Carlo toolkit TOPAS (Perl et al., 2012; Agostinelli et al., 2002). The McNamara model (McNamara et al., 2016) was used for the evaluation of a variable RBE. The work focused on the risk of normal tissue complications for different endpoints to the entire heart wall, left anterior descending artery (LAD) and left lung. Furthermore, the estimated risk of complications for patients receiving proton therapy were compared to the estimated risk of normal tissue complications for patients treated with 3DCRT and VMAT. Finally, eight 3DCRT patients were re-planned for PBS to allow for a one-to-one comparison. The results, displayed in table 7.5, showed that applying a variable RBE for PBS could have a substantial effect on the dose distributions, especially for the left lung. Consequently, the benefit of PBS estimated with a fixed RBE in relation to the conventional 3DCRT for the left lung decreased when a variable RBE was applied. A clear disadvantage is seen for VMAT over both PBS and 3DCRT in the mean dose to the heart and to the LAD. However, the results may be biased as VMAT treatments are often prescribed when 3DCRT fails due to high heart and lung doses. The one-to-one

Table 7.5. Median (range) of estimated normal tissue complications for appropriate endpoints.

	Protons - PBS		Photons	
Endpoint	RBE 1.1	McN	IMRT	VMAT
	Heart - NTCP [%]			
Major coronary events	1.7*° (1.6-1.7)	1.7° (1.6-1.8)	1.7 (1.7-1.8)	2.1 (2.0-2.2)
Cardiac mortality	0.0* (0.0-0.0)	0.0* (0.0-0.1)	0.0 (0.0-0.0)	0.0 (0.0-0.1)
	OR			
Coronary stenosis	1.1*° (1.0-1.2)	1.1*° (1.0-1.3)	1.2 (1.2-1.6)	1.5 (1.3-2.7)
	Left lung - NTCP [%]			
Pneumonitis, Grade 0-2	12.1*° (3.0-14.1)	26.5 (9.7-28.5)	26.0 (13.6-37.9)	32.6 (16.7-40.9)
Pneumonitis, Grade 2	1.1*° (0.3-1.3)	2.7 (0.8-3.1)	2.4 (1.0-4.1)	4.2 (1.9-5.9)

*Statistically significant difference between 3DCRT against PBS for 1% level.
°Statistically significant difference between VMAT against PBS for 1% level.
Abbreviations: PBS = proton beam scanning. RBE = relative biological effectiveness. RBE 1.1 = fixed RBE of 1.1. McN = McNamara RBE model. 3DCRT = three-dimensional conformal radiotherapy. VMAT = volumetric modulated arc therapy. NTCP = normal tissue complication probability. OR = odds ratio.

plan comparison on eight patients between PBS and 3DCRT showed similar results.

Main Results

- Areas with high LET_d values (>12 keV/μm), located mostly in the heart and the left lung, were accompanied with low dose values (<2.5 Gy(RBE)). Yet, applying a variable RBE increased all dosimetric indices compared to the fixed RBE for each organ.
- The normal tissue toxicity probability increased for all organs when applying a variable RBE compared to a fixed RBE of 1.1
- Applying a variable RBE resulted in a small increase of 2.4% in the risk of major coronary complications to the heart for PBS compared to a fixed RBE of 1.1, whereas the normal tissue toxicity for the LAD increased by 5.6%. Furthermore, applying a variable RBE increased the estimated normal tissue toxicity for the left lung by a factor > 2.1.

- The mean dose to the heart for PBS having a fixed RBE was significantly lower compared to the photon modalities. However, applying a variable RBE increased the mean dose, resulting in no statistically significant difference when comparing to 3DCRT.
- The risk of major coronary complications was significantly lower for PBS having a fixed RBE compared to 3DCRT. However, no statistically significant difference was observed when applying a variable RBE.
- The mean dose to the LAD for PBS was significantly lower when compared to both 3DCRT and VMAT, irrespective of using a fixed or a variable RBE.
- The normal tissue toxicity for the LAD was significantly lower for PBS compared to the photon modalities for both a fixed or a variable RBE.
- The mean dose to the left lung was significantly lower for PBS with a fixed RBE of 1.1 in relation to both 3DCRT and VMAT. However, applying a variable RBE increased the mean dose for PBS by 2.5 Gy(RBE), thereby eliminating the statistical difference in the mean dose between the proton and photon modalities.
- The estimated normal tissue toxicity to the left lung for PBS with a fixed RBE was significantly lower in relation to both 3DCRT and VMAT. However, no statistically significant difference to 3DCRT and VMAT was seen when applying a variable RBE.
- For the heart and the left lung, the dosimetric analysis and the estimated NTCP results of the re-planned PBS patients were similar to the clinically treated PBS patients. However, a small difference was seen in the dose distribution to the LAD, where the re-planned PBS patients received a slightly higher dose compared to the clinically treated PBS patients. This difference can be explained by a small change in clinical practice between the recently re-planned patients and the retrospective clinically treated PBS patients.

8 Concluding Remarks

Despite the vast amount of scientific literature on variable RBE for the energy range used in clinical proton therapy, a constant RBE of 1.1 is currently being applied in clinical practice. The main objectives of this work were to increase the understanding and assess the clinical impact of RBE variations in proton therapy, compared to using a constant RBE value of 1.1. Dosimetric indices based on DVH analysis were performed, along with TCP and NTCP modeling for various treatment sites. Different RBE models were investigated for various $(\alpha/\beta)_x$ ratios. Furthermore, the effect on RBE in target volumes while reducing the range uncertainties was assessed.

A limitation to this work is the reliance on empirical RBE models, such as the McN model, using clonogenic cell survival *in vitro* as an endpoint as this may not reflect true RBE values *in vivo*. That being said, the RBE for clonogenic cell survival *in vitro* can serve as an estimate of trends to guide treatment planning decisions. However, further verification of the RBE models should be made and compared with clinical data. Another limitation is integrating photon TCP and NTCP models to proton therapy. Interpreting absolute values of the outcome models should be done with caution as the values of the input parameters for the outcome models are fitted using data from photon therapy and without considering variations in model parameters based on variations in the $(\alpha/\beta)_x$ ratio. Furthermore, the dose distribution for organs at risk while using protons is considerably different from those using photons. To this day, outcome data from patients treated with proton radiation therapy are relatively low resulting in an inadequate statistical data for most endpoints. However, more proton therapy outcome data will be available in the future as the number of proton radiotherapy centers is increasing.

This work demonstrated that variations in proton RBE are caused mainly by the uncertainty associated with the $(\alpha/\beta)_x$ ratios when calculated using the phenomenological RBE models, such as the McN model. This was, however, not the case for the RMF model, which is a biophysical model and based on a more mechanical approach.The RBE weighted dose distributions estimated using the RMF model did not vary much with the $(\alpha/\beta)_x$ ratio. Furthermore, the results indicated lower RBE values than 1.1. The discrepancy in the results between the two models can be explained by their approaches in estimating the RBE values. The McN model is fitted to empirical data of clonogenic cell survival whereas the RMF model parameters are based on a more limited set of experimental data as it connects DSBs and chromosomal damage to RBE variations. Finally, reducing the range uncertainty margin did not affect the mean RBE in the target significantly. The uncertainty in RBE due to the uncertainty associated with the $(\alpha/\beta)_x$ ratio seems larger than the impact of the applied range uncertainty margin on RBE.

In conclusion, disregarding variations in the RBE might impact comparisons of

proton and photon therapy treatments, and consequently should be considered when performing outcome analysis for proton therapy.

9 Summary of Papers

Paper I

Applying a variable relative biological effectiveness (RBE) might affect the analysis of clinical trials comparing photon and proton therapy for prostate cancer.

Marteinsdottir M, Paganetti H.

Phys. Med. Biol. 64 (2019) 115027 (13pp)

Applying a variable relative biological effectiveness (RBE) might affect the analysis of clinical trials comparing photon and proton therapy for prostate cancer

Maria Marteinsdottir[1,2], Harald Paganetti[1,3*]

[1]Department of Radiation Oncology, Massachusetts General Hospital, Boston, MA 02114, USA
[2]Department of Physics, University of Iceland, 101 Reykjavik, Iceland
[3]Harvard Medical School, Boston, MA 02114, USA
* hpaganetti@mgh.harvard.edu

Abstract

The purpose of this study was the evaluation of the impact of a variable relative biological effectiveness (RBE) compared to a constant RBE value of 1.1 in proton therapy prostate trials due to uncertainties in α/β ratio.

Twenty patients receiving passive scattered proton therapy (PSPT) and fifteen patients receiving intensity modulated proton therapy (IMPT) were compared to twenty patients treated with 7-field intensity modulated photon therapy (IMRT). For proton beam therapy (PBT), the RBE was estimated using two different RBE models. Tumor control probabilities (TCP) and normal tissue complication probabilities (NTCP) were assessed.

For one of the RBE models, dosimetric indices assuming a low α/β were ~10-11% larger compared to using a fixed RBE. A different model resulted in 1-3% lower values independent of α/β. Comparing PBT with IMRT revealed a negligible difference in TCP for a fixed RBE. Applying a variable RBE revealed an increase in TCP by 6% for PBT compared to IMRT for one model but a decrease of 2% for the other. Variable RBE values in PSPT resulted in an increase in NTCP for rectum from 7% to 11% for a fixed RBE with one model but a decrease to 6% for another. For IMPT, NTCP increased from 5% to 9% for a fixed RBE for one model but decreased to 3% using the other. The NTCP for bladder increased for PSPT for both models, from 11% to 19% and 14%, respectively. For IMPT, the NTCP increased from 12% to 17% using one model but decreased to 11% with the other.

In radiation therapy for prostate cancer, disregarding variable RBE may lead to either underestimation or overestimation of the expected TCP and NTCP, depending on the RBE model and α/β. This should be considered when estimating uncertainties when comparing PBT and IMRT outcomes in clinical trials.

1 Introduction

Application of radiation therapy (RT) to localized prostate cancer has long been regarded as a standard treatment option. A high total dose of >70 Gy for external beam radiation therapy (EBRT) is considered necessary to control the tumor growth (Hanks et al. 2002; Peeters et al. 2006; Pollack et al. 2000), however increasing the dose might increase normal tissue complications. It has been argued that reducing the volume of rectum receiving low doses (<50 Gy) may lead to decrease in severe problems with bowel urgency and bowel frequency (Hoppe et al. 2015). Advanced EBRT techniques are used to reduce these complications.

The most commonly used is photon based intensity modulated radiation therapy (IMRT). Another application is proton beam therapy (PBT) which, due to the physical characteristics of protons, reduces the volume of the normal tissue exposed to radiation.

As proton therapy is a more expensive technique than IMRT for prostate cancer, it is essential to accurately estimate its overall benefit. Therefore, outcome in quality of life and toxicity are of importance. Several clinical trials have estimated outcome data of IMRT and proton therapy, Table 1 shows a summary of late gastrointestinal (GI) and genitourinary (GU) toxicity results for Grade 2 or larger.

Direct comparison of toxicity data from different studies is often difficult. The clinical trials need to have the same endpoints and grading system and treatments must be based on the same technical standards. Furthermore, follow up time needs to be considered when estimating outcome. Nihei et al. (Nihei et al. 2011) showed that the late toxicity of Grade 2 or later in GI and GU doubled when increasing the follow up time from 2 years to 3.6 years. Therefore, it might be of no surprise that Table 1 reveals various results. For IMRT, the toxicity results from Vora et al. (Vora et al. 2007) and De Meerleer et al. (De Meerleer et al. 2007) are similar in GI and GU within about 20% and both reports have similar median dose and use the RTOG grading system. Yet, a study by Eade et al. (Eade et al. 2008) has a much lower toxicity rate of 2.4% and 3.5% for GI and GU, respectively, for similar median dose and same grading system.

When comparing PBT, the toxicity results are also quite different. Slater et al. (Slater et al. 1998) reported a 21% toxicity in rectum and 5% toxicity in bladder whereas Pugh et al. (Pugh et al. 2013) reported a larger toxicity in bladder compared to rectum, 13.4% compared to 9.6%. This difference is perhaps explained with a better treatment optimization as PBT technique might be more up to date for Pugh et al. The criteria for the toxicity results reported by Nihei et al. (Nihei et al. 2011) and Mendenhall et al. (Mendenhall et al. 2012) were defined by NCI-CTC. Nihei et al. had 7.8% toxicity of Grade 2 or larger for GU, in contrast to GU 24% toxicity rate reported by Mendenhall et al.

The comparison between proton based and photon based treatment techniques is also impacted by the relative biological effectiveness (RBE). The clinical practice of using a standard RBE of 1.1 assumes that the physical proton dose is biologically equivalent to a 10% higher photon dose. It has been shown that accounting for a variable RBE is of importance when analyzing proton therapy outcome (Chen et al. 2018) The RBE varies, for instance, as a function of the tissue specific parameter α/β ratio with lower α/β being associated with higher RBE values (Paganetti 2014; Jones 2017). The α/β ratio for prostate cancer is a heavily debated issue. In 1999, Brenner and Hall (Brenner & Hall 1999) derived a low α/β ratio of 1.5 Gy from clinically observed outcome data of 134 and 233 patients after permanent implant brachytherapy and EBRT, respectively. This result was questioned by King and Mayo in 2000 (King & Mayo 2000) due to its low radiosensitivity parameter α and an irrational low number of clonogens. They suggested that by taking heterogeneity partially into account, the α/β ratio would increase to 4.96 Gy. Brenner and Hall replied by including heterogeneity and obtained a new α/β estimation of 2.1 Gy. Other studies have supported low value of α/β ratio of around 1.5 Gy. Fowler et al. in 2001 (Fowler et al. 2001) reviewed seventeen clinical studies from which they estimated an α/β ratio of 1.49 Gy. A retrospective study on nearly 6000 prostate cancer patients by Miralbell et al. (Miralbell et al. 2012) derived an α/β ratio of 1.4 Gy. Additionally, a meta-analysis by Dasu and Toma-Dasu (Dasu & Toma-Dasu 2012) in 2012 on >14000 prostate cancer patients led to α/β ratios between 1.0 and 1.7 Gy. The analysis was corrected for the overall treatment time. These low values were further supported in the CHHiP phase III trial in 2016 (Dearnaley et al. 2016) based on >3000 prostate cancer patients at which an estimate of 1.8 Gy was reported. However, the data analysis did not consider the overall treatment duration. A meta-analysis in 2018 by Vogelius and Bentzen (Vogelius & Bentzen 2018) of >10000 prostate cancer patients reported an α/β ratio of 1.2 Gy and 2.7 Gy without and with the overall treatment time effect, respectively. Furthermore, a study by Wang et al. in 2003 (Wang et al. 2003) analyzed the data from Fowler et al. (2001) and data from a study by Levegrun et al. in 2001 (Levegrün et al. 2001) in which biopsy outcome of >100 prostate cancer patients were used. Wang et al. included tumor cell repopulation and derived an α/β ratio of 3.1 Gy. However, a retrospective analysis on

hypofractionation by Pollack et al. in 2009 of >300 prostate cancer patients (Pollack et al. 2009) concluded that the α/β ratio could possible by 6.5 Gy or even higher.

The question arises how a variable RBE and its uncertainty due to uncertainties in α/β impacts the interpretation of clinical trials comparing PBT and IMRT. For an RBE of 1.1, the TCPs between the two modules should be by definition identical whereas NTCP differences would vary due to interpatient variations. However, to account for uncertainty in TCP and NTCP due to RBE, it is important to explore a range of plausible α/β ratios. The goal of this study is to understand the impact of RBE uncertainty on the evaluation of prostate clinical trials on PBT versus IMRT. This uncertainty arises for example from the uncertainty in α/β ratio, the analytical versus Monte Carlo dose calculations as well as the RBE weighted dose calculation models. TCPs with varying α/β ratios as well as NTCPs for rectum and bladder were calculated for patients receiving passive scattered proton therapy (PSPT) and intensity modulated proton therapy (IMPT), as well as patients treated with intensity modulated photon therapy (IMRT).

Table 1. A summary of late gastrointestinal (GI) and genitourinary (GU) toxicity results for Grade 2 or larger.

	Treatment	Dose [Gy](photons) [Gy(RBE)](protons)	Number of patients	Follow up in years	Grading System	≥ 2 GI [%]	≥ 2 GU [%]
Vora et al. 2007 (Vora et al. 2007)	IMRT	70.2 – 77.4	145	4	RTOG	23	23
Eade et al. 2008 (Eade et al. 2008)	IMRT	74 – 78	216	3.75	Modified RTOG	2.4	3.5
De Meerleer et al. 2007 (De Meerleer et al. 2007)	IMRT	74 – 76	133	3	Modified RTOG	17	19
Zelefsky et al. 2008 (Zelefsky et al. 2008)	IMRT	81	741	10	NCI-CTC	5	20
Hoppe et al. 2013 (Hoppe et al. 2013)	IMRT	75.5 – 79.4	204	2	EPIC	11†	11‡
Hoppe et al. 2013 (Hoppe et al. 2013)	PBS	76 – 83	1243	2	EPIC	7†	10‡
Nihei et al. 2011 (Nihei et al. 2011)	PBS	74	124	3.6	NCI-CTC	4.1	7.8
Slater et al. 1998 (Slater et al. 1998)	PBS	75 – 76	643	3	RTOG	21	5.4
Mendenhall et al. 2012 (Mendenhall et al. 2012)	PBS	78	211	2	NCI-CTC	5	24
Pugh et al. 2013 (Pugh et al. 2013)	PBS	76	291	2	Modified RTOG	9.6	13.4

Abbreviations: IMRT = Intensity Modulated Radiation Therapy. PBT = proton beam therapy. RTOG = Radiation Therapy Oncology Group. NCI-CTC = National Cancer Institute Common Toxicity Criteria. EPIC = Expanded Prostate Cancer Index Composite.
Gy(RBE) = Gy × 1.1
† Overall bowel problems
‡ Overall urinary problems

2 Methods

2.1 Patient cohort and dose calculations

20 patients receiving passive scattered proton therapy (PSPT) and 15 patients receiving intensity modulated proton therapy (IMPT) were selected. All patients were treated to 79.2 Gy(RBE) to the prostate in 44 fractions (with the exception of 4 IMPT patients receiving 70 Gy in 28 fractions that were normalized for this study to match the fractionation scheme; clinical constrains for bladder and rectum were not exceeded after the conversion). The dose distributions from analytical dose calculations (ADCs) were collected from the planning systems XiO and Astroid (in-house) for PSPT and IMPT patients, respectively. To account for proton range uncertainty, a generic range uncertainty margins of 3.5% of the prescribed range in water in beam direction + 1 mm were applied for PSPT. For IMPT, different volume of interest was created by expanding the PTV distally to each beam by 2.5% of the water equivalent target depth. In addition, 20 patients treated with 7-field intensity modulated photon therapy (IMRT) were considered, receiving a total dose of 79.2 Gy in 44 fractions. The IMRT plans were calculated using the RayStation planning system.

2.2 Modeling of the relative biological effectiveness

The Monte Carlo (MC) simulation tool TOPAS (Perl et al. 2012; Agostinelli et al. 2002) was used to evaluate different variable RBE models. Two scorers were calculated voxel-by-voxel; the proton linear energy transfer distribution (LET_d) and the DNA double strand break (DSB) which is estimated from the Monte Carlo Damage Simulation (MCMD) software (Stewart et al. 2011). The dose distribution was scaled by using either a fixed RBE of 1.1 or a variable RBE according to the McNamara model (McN) (McNamara et al. 2016) and the Repair-Misrepair Fixation model (RMF) (Carlson et al. 2008; Frese et al. 2012; Stewart et al. 2016). The McN model is a phenomenological RBE proton model and is based on the linear-quadratic model. It used empirical data of clonogenic cell survival from a collection of over 70 experimental reports on proton RBE (Paganetti 2014) to establish its non-linear regression fit. The model is a function of the physical dose, the tissue specific parameters α_x and β_x for X-ray (referred to as α and β from here) and LET_d. The RMF model is based on a more mechanical approach. It predicts DSB induced by radiation within the cell and subsequently links α and β to DSB induction. Therefore, the model is dependent on the α and β parameters, the particle type and energy as well as the physical dose.

As mentioned in the Introduction, multiple α/β ratios for prostate carcinoma have been reported in the literature. However, as it is essential to obtain separate α and β values for the RMF model calculations, the following references reporting these values were selected for further analysis on the prostate; 1.5, 3.1 and 4.96 Gy having α of 0.036, 0.15 and 0.346 Gy^{-1}, respectively (Brenner & Hall 1999), (Wang et al. 2003) (King & Mayo 2000). These α/β ratios were chosen as references to evaluate the impact α/β ratios have on TCP for PBT. For the rectum, an α/β ratio of 3 Gy for late rectal toxicity was selected (Marzi et al. 2009; Pedersen et al. 2018). Higher values have been reported. Deore et al. (Deore et al. 1993) estimated an α/β ratio of 3.87 Gy for late rectal toxicity, whereas for late intestinal morbidity the ratio was calculated by Dische et al. to be 4.3 Gy (Dische et al. 1999). Furthermore, Brenner (Brenner 2004) reported an α/β ratio of 5.4 Gy for late rectal toxicity. However, the choice of a low α/β ratio of 3 Gy was considered to be conservative. The α/β ratio for bladder has been reported to be between 3.4 and 4.5 Gy for symptomatic bladder contracture and volume loss (Perez et al. 1997; Perez 1997). Marks et al. (Marks et al. 1995) suggested an α/β ratio of 6 Gy. As for the rectum, a conservative value was considered and therefore an α/β ratio of 4 Gy was selected as suggested by others (Pedersen et al. 2018; Koukourakis et al. 2007).

2.3 DVH analysis

The dosimetric indices based on dose-volume histogram (DVH) analyses were estimated for each treatment. The dose that covers xx% of the volume of interest, referred as Dxx, was used for the prostate calculations. Three indices were calculated; D98 which represents the minimum target dose, D50 representing the median dose and D02 as the maximum dose. For normal tissue calculations, rectum and bladder were used for further evaluations. For each organ, VxxGy, which refers to the fractional volume of the normal tissue receiving xx Gy (photons) or Gy(RBE) (protons), was calculated.

2.4 TCP calculations

A logistic model was considered to predict the TCP of the prostate tumor (Goitein & Schultheiss 1985; Schultheiss et al. 1983) where the sigmoidal shape of the dose-response curve is phenomenologically described by a logistic function. The TCP is calculated for tumor irradiated with dose D as

$$TCP = \frac{1}{1 + \left(\frac{TCP_{50}}{D}\right)^{4\gamma_{50}}}$$

where TCP_{50} is the tumor dose at which 50% of tumors are controlled and γ_{50} is the slope of the dose response curve. The input parameters TCP_{50} and γ_{50} were obtained from a study by Cheung et al. (Cheung et al. 2005) of 387 intermediate-risk prostate cancer patients treated with external beam radiotherapy where the biochemical failure definition was a PSA rise of >2 ng/mL above the current PSA nadir (CN + 2). These parameters were fitted to photon treatments. The considered α/β ratio used for the fit was not specified.

2.5 NTCP calculations

The Lyman–Kutcher–Burman NTCP model was used for bladder and rectum. The parameters applied for rectum were n = 0.09, m = 0.13, TD50 = 76.9 Gy for the endpoint of Grade ≥2 RTOG late toxicity (Michalski et al. 2010) whereas for bladder the parameters were n = 0.09, m = 0.17, TD50 = 78.68 Gy with Grade ≥2 LENT/SOMA 5 year toxicity as the endpoint (Zhu et al. 2016).

$$NTCP = \frac{1}{\sqrt{2\pi}}\int_{-\infty}^{t} e^{\frac{x^2}{2}}\,dx$$

$$t = \frac{D_{eff} - TD_{50}}{mTD_{50}}$$

$$D_{eff} = \left(\sum_i v_i D_i^{1/n}\right)^n$$

The parameter TD50 is the dose of 50% response probability. As for TCP, the parameters for both organs were fitted for photon treatment without reporting the α/β ratio.

2.6 Random α/β values and bootstrap

To evaluate how variable α/β ratios considered for RBE calculations will impact the TCP and NTCP results, α/β ratios were randomly selected from a Gaussian distribution. Each proton modality had 4000 different α/β ratios selected, divided equally between the patients. Furthermore, the corresponding RBE weighted dose distribution was calculated as well as the associated TCP and NTCP.

For TCP calculations, the mean value and the standard deviation was chosen to be 3.25 Gy and 0.6 Gy, respectively. A distribution was created which had α/β values between 1.5 Gy and 5 Gy. These parameters were chosen to include the range of α/β values evaluated in this study. To calculate the NTCP, the mean value for bladder was set as 4 Gy and the standard deviation as 0.2 Gy. This created a distribution within the 95% confidence interval published by Perez et al. (Perez 1997; Perez et al. 1997). The same standard deviation was chosen for rectum, having a mean value of 3 Gy. To more accurately compare the proton results to the photon data, the DVHs of the 20 IMRT patients were bootstrapped, to reach the same number of distributions.

2.7 Statistics

All proton calculations were compared to photon IMRT and statistical analysis performed using the Wilcoxon rank sum test using MATLAB version 2016b (Mathwork Inc).

3 Results

3.1 Planned dose comparison for PBT – ADC and MC

Figure 1 compares dose-volume histograms (DVHs) for the two proton modalities calculated using ADC and MC, both algorithms calculated having fixed RBE of 1.1. The results are presented for prostate (PTV7920), rectum and bladder. Considering the prostate results: applying MC calculation results in approximately 1-2% lower dose compared to ADC, hence indicating an underdosage of the target when using ADC in the clinic. This has been demonstrated before (Schuemann et al. 2015). The difference between the two calculation algorithms in mean dose, D98 and D50 is statistically significant ($p < 0.05$). For rectum and bladder, it is evident that clinical constrains are not exceeded, with the exception of one PSPT patient having minor deviation of V75Gy < 20% instead of 15% for bladder. The dosimetric indices mean dose, V30Gy, V50Gy, V70Gy and V75Gy for both organs are not statistically significantly different between the two calculation algorithms. As the purpose of this paper is to investigate the uncertainty in RBE when analyzing clinical trials comparing protons and photons, further analysis will be done using MC for protons normalized to the prescribed target dose. Normalized MC doses were derived by scaling the MC dose distribution so that the D95 index estimated by the MC dose calculation method matches the D95 index predicted by the ADC.

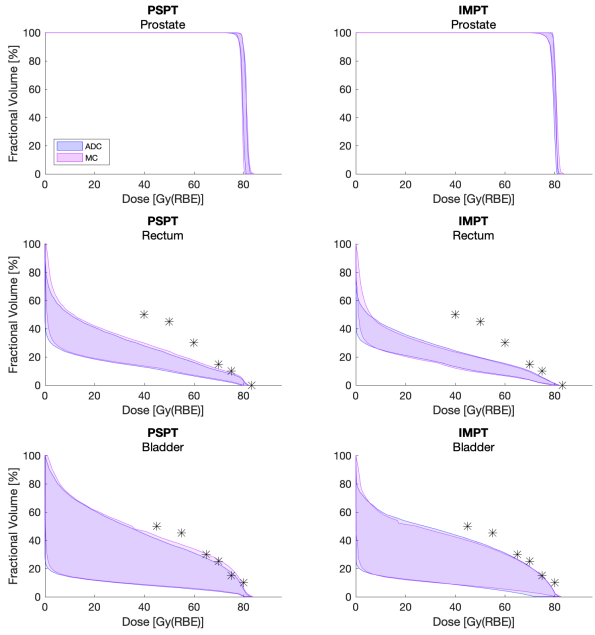

Figure 1. Dose-volume histograms for prostate (PTV7920), rectum and bladder for ADC and MC, having fixed RBE of 1.1. The stars represents clinical dose constraints for each organ.

3.2 RBE-weighted dose comparisons – Prostate

Figure 2 compares the dose-volume histograms (DVHs) for the prostate (PTV7920) from the three different treatment modalities, i.e. PSPT, IMPT and IMRT. The proton data assume a fixed RBE of 1.1 as well as variable RBE calculated with two different variable RBE models, i.e. McN and RMF. For the McN model, a large variation can be seen with α/β ratio, whereas the α/β ratio had negligible effect on the target dose distribution for the RMF model (<0.3%). The figure also displays the LETVH for the proton therapies, their mean and maximum values. The elevated LET values for IMPT compared to PSPT result in a slightly larger target dose when using the McN model.

The target dose coverages, as shown in Figure 2, are further analyzed in Table 2. The difference between dosimetric indices of PBT based on a fixed RBE of 1.1 and IMRT is less than 0.7%, as expected due to the dose normalization, see subsection 3.1. Applying a variable RBE predicted by the McN model results in statistically significant difference in all dosimetric indices between PBT and IMRT, irrespective of α/β ratio. Lowering α/β using the McN model results in an increase in the target dose. For instance, for α/β of 1.5 Gy the RBE weighted mean dose is 10.2% larger for both PSPT and IMPT than for IMRT. However, for α/β of 4.96 Gy the mean dose is 2.1% and 1.9% larger for PSPT and IMPT, respectively, compared to IMRT.

Considering the RMF model, all dosimetric indices calculated for PBT are in fact lower compared to IMRT. The RBE weighted mean dose for PSPT is between 2.4% to 2.7% lower than of IMRT, with the 0.3% variation due to different α/β ratios. The difference is somewhat larger between IMPT and IMRT where the RBE weighted mean dose of IMPT is between 2.7% and 3.0% lower.

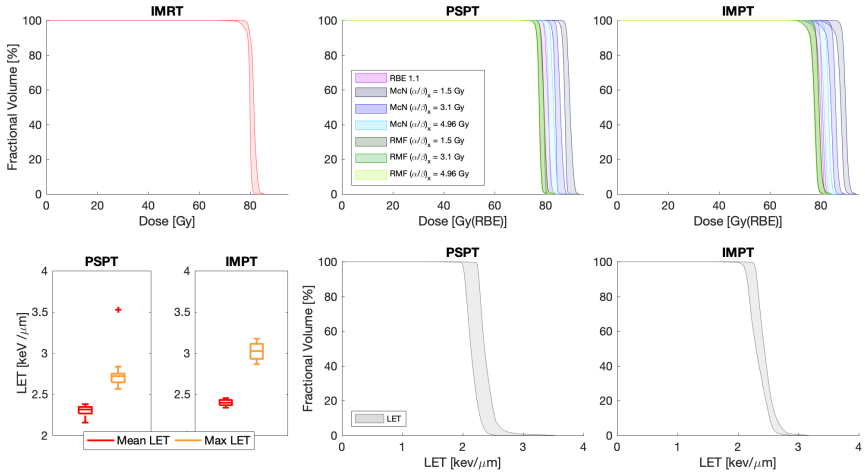

Figure 2. Dose-volume histogram (DVH) for the prostate (PTV7920) for all modalities. Furthermore, LET-volume histogram (LETVH) and boxplot of LET for the proton modalities. The shaded areas in the DVHs and LETVHs indicate the interpatient range for each calculation algorithm. Each box from top to bottom represents the maximum, first quartile, median, third quartile and minimum of the distribution over all patients. The outlier represents data point that fell more than 1.5 times the interquartile range away from the top and bottom of the box.

Table 2. Average and standard deviation of dosimetric indices for prostate. In brackets are p-values from rank test, testing modalities PSPT/IMPT against modality IMRT.

	IMRT	PSPT						
			α/β = 1.5 Gy		α/β = 3.1 Gy		α/β = 4.96 Gy	
Index		RBE 1.1	McN	RMF	McN	RMF	McN	RMF
D_{mean}	80.6 ± 0.4	80.1 ± 0.5	88.8 ± 0.5	78.6 ± 0.5	85.0 ± 0.5	78.5 ± 0.5	82.3 ± 0.5	78.4 ± 0.5
		[< 0.05]	[< 0.05]	[< 0.05]	[< 0.05]	[< 0.05]	[< 0.05]	[< 0.05]
D98	78.3 ± 0.7	78.3 ± 0.5	86.9 ± 0.6	76.7 ± 0.5	83.2 ± 0.6	76.6 ± 0.5	80.5 ± 0.5	76.5 ± 0.5
		[0.60]	[< 0.05]	[< 0.05]	[< 0.05]	[< 0.05]	[< 0.05]	[< 0.05]
D50	79.2 ± 0.4	78.8 ± 0.4	87.4 ± 0.5	77.2 ± 0.4	83.6 ± 0.5	77.1 ± 0.4	81.0 ± 0.5	77.0 ± 0.4
		[< 0.05]	[< 0.05]	[< 0.05]	[< 0.05]	[< 0.05]	[< 0.05]	[< 0.05]
D02	80.6 ± 0.5	80.2 ± 0.5	88.8 ± 0.5	78.6 ± 0.5	85.0 ± 0.5	78.5 ± 0.5	82.3 ± 0.5	78.4 ± 0.5
		[< 0.05]	[< 0.05]	[< 0.05]	[< 0.05]	[< 0.05]	[< 0.05]	[< 0.05]
		IMPT						
			α/β = 1.5 Gy		α/β = 3.1 Gy		α/β = 4.96 Gy	
		RBE 1.1	McN	RMF	McN	RMF	McN	RMF
D_{mean}		80.4 ± 0.2	88.8 ± 0.6	78.4 ± 0.6	84.9 ± 0.6	78.3 ± 0.6	82.1 ± 0.6	78.2 ± 0.6
		[0.60]	[< 0.05]	[< 0.05]	[< 0.05]	[< 0.05]	[< 0.05]	[< 0.05]
D98		78.0 ± 0.9	86.1 ± 1.4	75.9 ± 1.2	82.3 ± 1.4	75.7 ± 1.2	79.6 ± 1.3	75.6 ± 1.2
		[0.16]	[< 0.05]	[< 0.05]	[< 0.05]	[< 0.05]	[< 0.05]	[< 0.05]
D50		78.6 ± 0.6	86.8 ± 1.0	76.6 ± 0.9	83.0 ± 1.0	76.4 ± 0.9	80.3 ± 0.9	76.3 ± 0.9
		[< 0.05]	[< 0.05]	[< 0.05]	[< 0.05]	[< 0.05]	[< 0.05]	[< 0.05]
D02		80.5 ± 0.2	88.8 ± 0.5	78.5 ± 0.5	85.0 ± 0.5	78.3 ± 0.5	82.2 ± 0.5	78.2 ± 0.5
		[0.80]	[< 0.05]	[< 0.05]	[< 0.05]	[< 0.05]	[< 0.05]	[< 0.05]

Proton dosimetric indices are given in Gy(RBE) whereas photon indices are in Gy.
Statistically significant difference for 5% level is marked as <0.05

3.3 RBE-weighted dose comparisons - Normal Tissue

The prostate results for the RMF model in previous subsection show a negligible dependence on the α/β ratio. Therefore, no further analysis using variations in α/β ratios was performed. As mentioned in subsection 2.2, α/β ratios of 3.0 and 4.0 Gy were selected for rectum and bladder, respectively. The DVHs for rectum and bladder are illustrated in Figure 3. For IMRT, all patient cases remain within the clinical constrains. That is also the case for PBT with a fixed RBE of 1.1, as mentioned in section 3.1. However, when applying the McN model, the figure demonstrates that clinical constrains are exceeded in the high dose region for both rectum and bladder, indicating an underestimation in delivered biological dose. The figure also shows that larger fraction of the organs will receive low dose of < 20 Gy for IMRT compared to PBT, however smaller fractions will receive high dose.

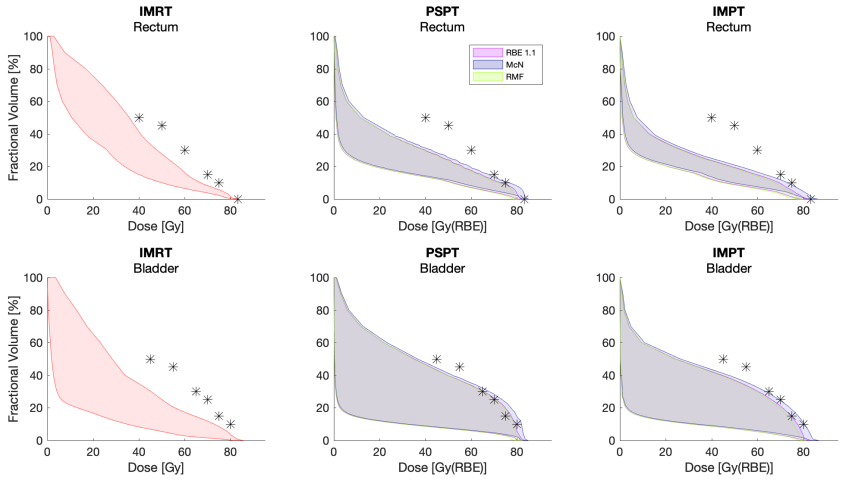

Figure 3 Dose-volume histogram (DVH) for two rectum and bladder. The shaded areas indicate the interpatient range for each calculation algorithm. For variable RBE calculations, the α/β ratio is 3.0 and 4.0 Gy for rectum and bladder, respectively. The stars represents clinical dose constraints for each organ.

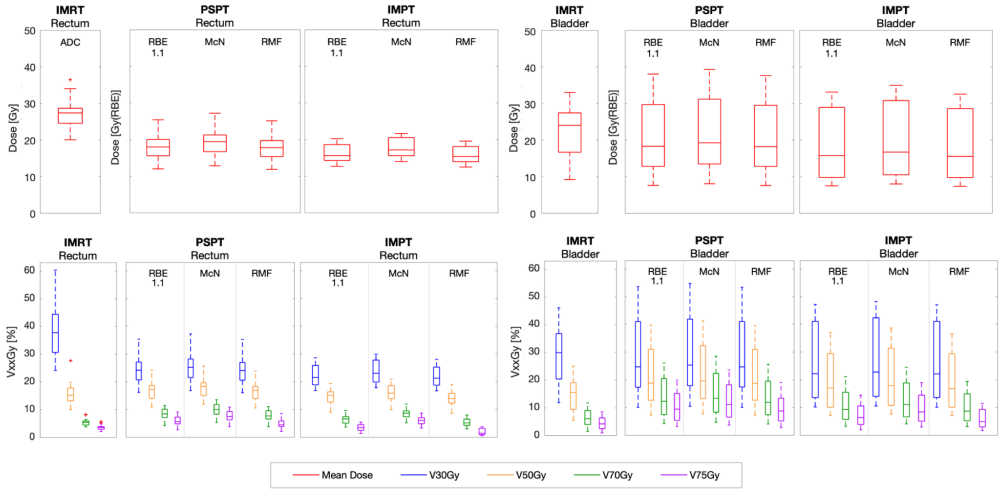

Figure 4. Box plot of dosimetric indices for rectum and bladder, for all modalities. The α/β ratio is 3.0 and 4.0 Gy for rectum and bladder, respectively. VxxGy refers to the fractional volume of the structure receiving xx Gy(RBE). Each box from top to bottom represents the maximum, first quartile, median, third quartile and minimum of the distribution over all patients. The outliers represent data points that fall more than 1.5 times the interquartile range away from the top and bottom of the box.

Table 3. Average and standard deviation of dosimetric indices for rectum and bladder. The α/β ratio is 3.0 and 4.0 Gy for rectum and bladder, respectively. In brackets are p-values from rank test, testing modalities PSPT/IMPT against modality IMRT.

		IMRT	PSPT			IMPT		
Organ	Index		RBE 1.1	McN	RMF	RBE 1.1	McN	RMF
Rectum	D_{mean}	27.0 ± 4.2	18.0 ± 3.6 [< 0.05]	19.3 ± 3.8 [< 0.05]	17.8 ± 3.6 [< 0.05]	16.3 ± 2.5 [< 0.05]	17.8 ± 2.8 [< 0.05]	15.9 ± 2.4 [< 0.05]
	V30Gy	38.3 ± 10.0	24.6 ± 5.3 [< 0.05]	25.6 ± 5.5 [< 0.05]	24.5 ± 5.3 [< 0.05]	22.2 ± 4.0 [< 0.05]	23.6 ± 4.2 [< 0.05]	21.9 ± 3.9 [< 0.05]
	V40Gy	24.2 ± 6.3	20.5 ± 4.5 [0.05]	21.6 ± 4.7 [0.19]	20.3 ± 4.4 [< 0.05]	18.2 ± 3.5 [< 0.05]	19.6 ± 3.7 [< 0.05]	17.8 ± 3.5 [< 0.05]
	V50Gy	15.7 ± 4.0	16.6 ± 3.7 [0.28]	17.7 ± 3.8 [0.07]	16.3 ± 3.6 [0.42]	14.6 ± 2.9 [0.58]	16.0 ± 3.2 [0.70]	14.1 ± 2.8 [0.22]
	V60Gy	9.8 ± 2.3	12.6 ± 2.8 [< 0.05]	13.8 ± 3.0 [< 0.05]	12.2 ± 2.7 [< 0.05]	10.8 ± 2.3 [0.13]	12.4 ± 2.5 [< 0.05]	10.1 ± 2.3 [0.56]
	V70Gy	5.6 ± 1.3	8.4 ± 2.1 [< 0.05]	9.8 ± 2.3 [< 0.05]	7.8 ± 2.0 [< 0.05]	6.4 ± 1.8 [0.18]	8.4 ± 1.9 [< 0.05]	5.3 ± 1.7 [0.70]
	V75Gy	3.5 ± 1.0	5.8 ± 1.7 [< 0.05]	7.6 ± 2.0 [< 0.05]	4.8 ± 1.7 [< 0.05]	3.4 ± 1.3 [0.96]	6.0 ± 1.6 [< 0.05]	1.9 ± 1.2 [< 0.05]
Bladder	D_{mean}	22.3 ± 6.8	20.8 ± 9.6 [0.54]	21.8 ± 9.9 [0.71]	20.6 ± 9.5 [0.51]	18.6 ± 9.3 [0.29]	19.8 ± 9.8 [0.49]	18.4 ± 9.2 [0.25]
	V30Gy	28.8 ± 10.3	28.2 ± 13.6 [0.76]	29.0 ± 13.8 [0.93]	28.2 ± 13.5 [0.76]	26.0 ± 13.4 [0.56]	26.8 ± 13.8 [0.56]	26.0 ± 13.4 [0.54]
	V40Gy	20.7 ± 7.6	24.7 ± 12.0 [0.47]	25.5 ± 12.3 [0.38]	24.7 ± 12.0 [0.47]	22.8 ± 11.9 [0.80]	23.7 ± 12.3 [0.70]	22.7 ± 11.8 [0.80]
	V50Gy	14.5 ± 5.7	21.3 ± 10.5 [< 0.05]	22.1 ± 10.9 [< 0.05]	21.2 ± 10.4 [0.05]	19.4 ± 10.2 [0.20]	20.5 ± 10.8 [0.13]	19.3 ± 10.1 [0.22]
	V60Gy	9.8 ± 4.3	17.7 ± 9.0 [< 0.05]	18.6 ± 9.3 [< 0.05]	17.5 ± 8.8 [< 0.05]	15.6 ± 8.2 [< 0.05]	17.0 ± 9.0 [< 0.05]	15.3 ± 8.1 [< 0.05]
	V70Gy	6.3 ± 3.0	13.3 ± 6.9 [< 0.05]	14.5 ± 7.5 [< 0.05]	12.9 ± 6.7 [< 0.05]	10.7 ± 5.7 [< 0.05]	12.7 ± 6.7 [< 0.05]	10.0 ± 5.4 [0.05]
	V75Gy	4.4 ± 2.2	10.0 ± 5.3 [< 0.05]	11.8 ± 6.2 [< 0.05]	9.2 ± 4.9 [< 0.05]	7.2 ± 3.9 [< 0.05]	9.8 ± 5.3 [< 0.05]	5.9 ± 3.4 [0.24]

VxxGy refers to the fractional volume of the structure receiving xx Gy (photons) or Gy(RBE) (protons). Dose is given in Gy (photons) or Gy(RBE) (protons).
Statistically significant difference for 5% level is marked as <0.05

Figure 4 displays DVH-based analysis for rectum and bladder with Table 3 further reflecting on the results. Larger inter-patient variation is evident for bladder than for rectum. The mean dose of the rectum for IMRT is statistically significantly different compared to PBT, irrelevant of whether the PBT modalities have fixed or variable RBE. Furthermore, statistically significant smaller part of the fractional volume of the rectum is receiving 30 Gy for PBT compared to IMRT. However, IMRT outperforms PSPT in the higher dose region, where statistically significant larger part of the volume is receiving 70 Gy. This has been demonstrated before (Underwood et al. 2016). Additionally, there is no statistically significant difference in the mean dose of the bladder between PBT and IMRT, nor for fractional volume of the bladder receiving dose lower than 30 Gy. This is independent on using either fixed or variable RBE. However, a statistically significant larger volume of the bladder is receiving 70 Gy for PBT for both fixed and variable RBE compared to IMRT, with the exception of IMPT calculated using the RMF model ($p = 0.051$).

The results reveal that application of a variable RBE has a smaller impact on the dosimetric indices of PBT for both rectum and bladder than the potential inter-patient variability.

3.4 Tumor control probability - TCP

Figure 5 and Table 4 represents the TCP values calculated for PBT and IMRT. As expected due to the normalized prescription dose, for a fixed RBE value of 1.1, the average TCP values are within 0.3%. When applying the McN model, all differences in TCP between PBT and IMRT are statistically significant with the exception of PSPT having α/β ratio of 4.96 Gy. Furthermore, all three α/β ratios result in larger TCP

values calculated using the McN model compared to IMRT. The largest difference in TCP is seen for the lowest α/β ratio of 1.5 Gy; the TCP values are up to 6.0% for PSPT and IMPT compared to IMRT. Application of the RMF model reveal lower TCP values for both proton modalities and all α/β ratios compared to IMRT. Furthermore, the differences between average TCP values are statistically significant. The difference in the average TCP value between PBT and IMRT using the RMF model is between 2.0-2.2% and 2.2-2.4% for PSPT and IMPT, respectively. These results are in line with the target coverage calculations in section 3.2.

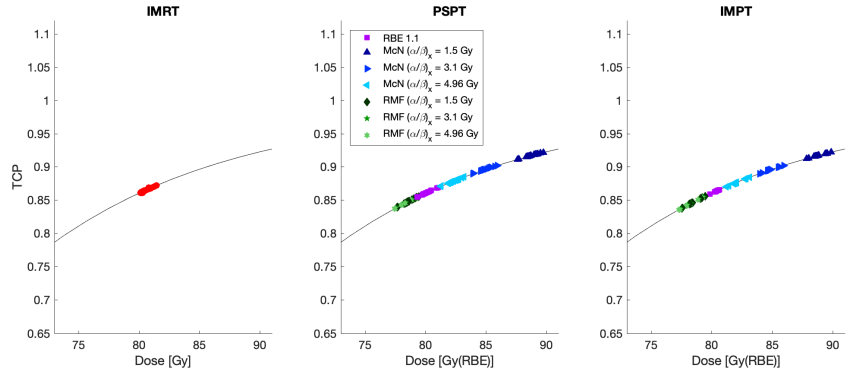

Figure 5. TCP calculated for the prostate (PTV7920) for all treatment modalities. Each data point corresponds to one patient. The solid line represents the TCP curve for each modality.

Table 4. Average and standard deviation of TCP values for prostate. In brackets are p-values from rank test, testing modalities PSPT/IMPT against modality IMRT.

IMRT	PSPT						
		α/β = 1.5 Gy		α/β = 3.1 Gy		α/β = 4.96 Gy	
	RBE 1.1	McN	RMF	McN	RMF	McN	RMF
0.865 ± 0.003	0.862 ± 0.004	0.917 ± 0.003	0.848 ± 0.004	0.896 ± 0.003	0.847 ± 0.004	0.878 ± 0.004	0.846 ± 0.004
	[< 0.05]	[< 0.05]	[< 0.05]	[< 0.05]	[< 0.05]	[< 0.05]	[< 0.05]
	IMPT						
		α/β = 1.5 Gy		α/β = 3.1 Gy		α/β = 4.96 Gy	
	RBE 1.1	McN	RMF	McN	RMF	McN	RMF
	0.864 ± 0.002	0.917 ± 0.003	0.846 ± 0.005	0.896 ± 0.003	0.845 ± 0.005	0.877 ± 0.004	0.844 ± 0.005
	[0.63]	[< 0.05]	[< 0.05]	[< 0.05]	[< 0.05]	[< 0.05]	[< 0.05]

Statistically significant difference for 5% level is marked as <0.05

Figure 6 shows the TCP results of PBT from the random sampling of α/β ratios as well as the TCP of IMRT calculated from bootstrapped DVHs. As seen in previous sections, the impact α/β ratio has on the RMF model is minimal, therefore this evaluation was only performed for the McN model. For all three results, a Gaussian distribution was fitted and the average TCP value and corresponding standard deviation was calculated. Figure 6 exemplifies the impact variable α/β ratios have on TCP for the McN model. As expected, the spread in TCP is larger for PBT than for IMRT due to the variation in α/β ratios. The TCP values for PSPB and IMPT are statistically significant different from IMRT ($p < 0.05$). The wider distribution for PBT caused by the dependency of the RBE on α/β could impact the analysis of clinical trials as the uncertainty is larger and consequently a larger sample size might be required for trial enrollment.

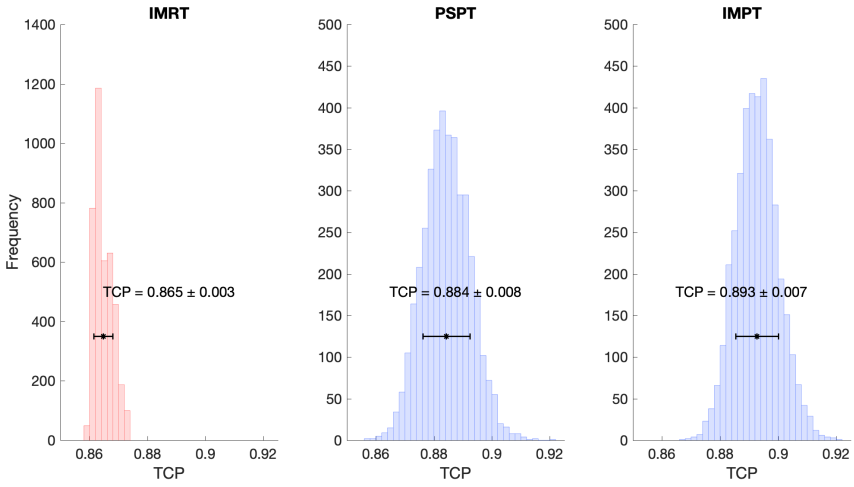

Figure 6. TCP histogram result where random α/β ratios were selected from a Gaussian distributed α/β ratios. For PBT, the results are shown for the McN model.

3.5 Normal tissue complication probability - NTCP

Figure 7 shows the NTCP results for rectum and bladder. The NTCP inter-patient variability is illustrated in Table 5. For rectum, the average NTCP value is statistically significantly larger for PSPT calculated having fixed RBE of 1.1 with relation to IMRT. This is not the case for IMPT where the average NTCP estimated assuming an RBE of 1.1 is close to the average NTCP estimated for IMRT. A change in the IMPT protocol took place during this work, resulting in 5 IMPT patients using injected synthetic hydrogel spacers. Consequently, the dose to the rectum becomes lower (Underwood et al. 2017). Disregarding these 5 patients revealed an average NTCP value for IMPT of 0.051 ± 0.011 when using a constant RBE of 1.1. This alone cannot explain the dissimilarity between the two proton modalities in the NTCP. The NTCP values for rectum are lower for IMPT compared to PSPT, irrespective of using hydrogel spacers. The average NTCP values for both proton modalities increase substantially when applying the McN model causing significantly larger NTCP values compared to IMRT. Applying the RMF model results in NTCP values that are comparable for all three modalities.

For bladder, all average values of NTCP for PBT are larger compared to IMRT. This is irrespective of whether fixed or variable RBE was used and irrespective of the RBE model. Statistically significant difference with relation to IMRT is seen for both proton modalities when applying the McN model, as well as for PSPT using a fixed RBE of 1.1.

Table 5. Average and standard deviation of NTCP values for rectum and bladder. In brackets are p-values from rank test, testing modalities PSPT/IMPT against modality IMRT.

	IMRT	PSPT			IMPT		
Organ		RBE 1.1	McN	RMF	RBE 1.1	McN	RMF
Rectum	0.046 ± 0.013	0.071 ± 0.022 [< 0.05]	0.111 ± 0.030 [< 0.05]	0.056 ± 0.018 [0.06]	0.045 ± 0.014 [0.93]	0.088 ± 0.024 [< 0.05]	0.032 ± 0.011 [< 0.05]
Bladder	0.092 ± 0.035	0.150 ± 0.053 [< 0.05]	0.183 ± 0.065 [< 0.05]	0.135 ± 0.050 [< 0.05]	0.122 ± 0.049 [0.09]	0.169 ± 0.065 [< 0.05]	0.105 ± 0.044 [0.41]

Statistically significant difference for 5% level is marked as <0.05

As for the TCP calculations, randomly selected α/β values were used for the PBT results whereas IMRT was bootstrapped to reach data points of 4000. Also, only the McN model was used for this calculation as the RMF results vary little with the α/β ratio. A Gaussian distribution was fitted to the results and the average NTCP values for rectum and bladder and corresponding standard deviation was evaluated. For both rectum and bladder, the average NTCP values are larger for PBT compared to IMRT, the difference is statistically significant ($p < 0.05$).

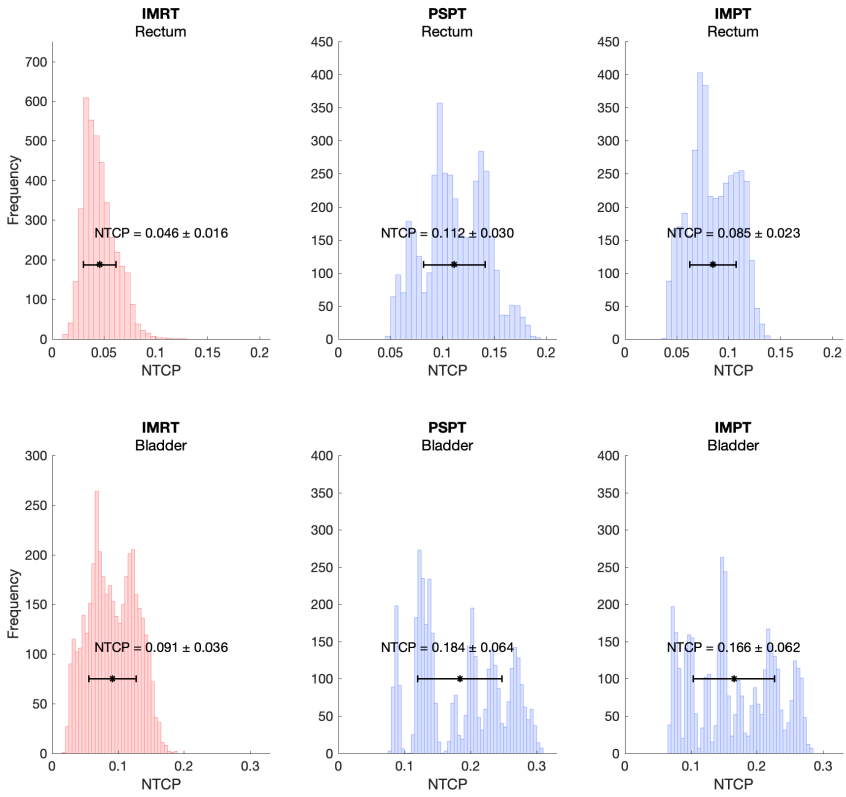

Figure 7. NTCP histogram result for rectum and bladder where random α/β ratios were selected from a Gaussian distributed α/β ratios. For PBT, the results are shown for the McN model.

4 Discussion

This study explored the clinical impact of RBE uncertainty on the dosimetric and outcome evaluation of prostate cancer treatments done with photon or proton therapy. Two PBT techniques, i.e. passive scattered proton therapy (PSPT) and intensity modulated proton therapy (IMPT) and intensity modulated photon therapy (IMRT) were considered. The latter is the predominant radiation treatment for prostate cancer.

The RBE weighted dose distribution was heavily influenced by the α/β ratio if RBE calculations were done by the McN model. The impact of variable RBE values estimated using empirical models based on the linear-quadratic equation has been demonstrated before (Carabe et al. 2013; Pedersen et al. 2018;

Ödén et al. 2017). Carabe et al. analyzed variations in RBE based on LET, α/β ratios and dose per fraction for prostate, brain and liver. The study revealed that RBE increases with increasing LET but decreases with increasing α/β or dose. Pedersen et al. reported that low α/β ratios for the prostate lead to higher biological dose in the target compared to a fixed RBE of 1.1. Furthermore, their study also revealed that the RBE increased with decreasing dose. Ödén et al. predicted up to 15% increase in biological dose to the prostate when applying a variable RBE. These results are in agreement with our study where the dosimetric indices estimated using the McN model and α/β ratio of 1.5 Gy were between 10-11% larger compared to using a fixed RBE of 1.1. This difference decreased to 2-3% when increasing the α/β to 4.96 Gy. The results changed very little with the α/β ratio when applying the RMF model. The dosimetric indices estimated using the RMF model were 1-3% lower compared to using a fixed RBE of 1.1, indicating a lower RBE than 1.1. This is in agreement with Frese et al (Frese et al. 2012) where a small dependence on the α/β ratio was observed as well as RBE < 1.1 when using the RMF model in the energy range of clinical proton beams.

Applying a variable RBE predicted by the McN model revealed an increase in the average TCP value up to 6% for PBT compared to IMRT with the largest increase for α/β ratio of 1.5 Gy. The average TPC value for PBT having an α/β of 4.96 Gy was only ~1% larger than for IMRT. For the RMF model, the average TCP values for PBT were ~2% lower than for IMRT with little variation as a function of α/β.

The application of the McN model increased the NTCP for both rectum and bladder compared to applying a fixed RBE of 1.1, whereas the NTCP decreased when using the RMF model. For the rectum, the average NTCP was larger for IMPT than for IMRT when applying the McN model but lower when the RMF model was used. For the bladder, average values of NTCP for PBT were larger compared to IMRT, for both fixed or variable RBE.

As a patient population might have a distribution of α/β values, random sampling was performed to evaluate the spread in TCP due to the α/β uncertainty. In this case, applying the McN model, the average TCP values from the random sampling were 2% larger for PSPT than for IMRT and 3% larger for IMPT. The relative standard deviation was 0.8% and 0.9% for PSPT and IMPT, respectively. The relative standard deviation was significantly smaller for IMRT as the spread is only due to inter-patient variation, or around 0.3%. The choice of the mean value of 3.25 Gy and standard deviation of 0.6 Gy for the α/β distribution was to incorporate the range of α/β values evaluated in this study. However, as many publications are inclined towards low α/β ratio of 1.5 Gy, the difference in the average TCP values between PBT and IMRT might be even larger. Evaluation on the spread in NTCP due to the α/β ratio revealed a large relative standard deviation for all modalities, or between 30-40%. This large variation was primarily due to inter-patient variability.

The discrepancy in the results between the McN model and the RMF model can be explained by their approaches in predicting variable RBE values. The McN model reflects the experimental relationship between RBE and α/β as the model is fitted to empirical data of clonogenic cell survival. However, the RMF model is based on a more mechanistic approach and connects misrepair or fixation of DSBs and chromosomal damage to RBE variations. The RMF model parameters are based on a more limited set of experimental data compared to the McN model.

This study did not attempt to pinpoint the absolute values of TCP nor NTCP. The uncertainty associated with the TCP and NTCP models has not been addressed. For example, the value of the input parameters for both models were fitted using data from photon therapy and without considering variations in model parameters based on variations in α/β. Different α/β would most likely result in different input parameters for the TCP and NTCP models (Paganetti 2017; Chen et al. 2018).

5 Conclusion

Variations in proton RBE values are caused by variations in α/β. This may impact observed TCP and NTCP values and thus the comparison between photon and proton treatments. The impact seems significant if one

assumes low α/β ratios for tumors or organs at risk as shown here on the example of prostate treatments. Even though uncertainties in α/β and in model predictions on RBE are substantial, this effect should be considered when analyzing clinical trials and deducing statistical significance of trial outcomes. It is therefore recommended for future clinical trials to incorporate a larger uncertainty on the sample size calculations for the proton arm.

Acknowledgement

This work was supported by NIH NCI U19 CA-21239. We would gratefully like to thank Dr. Jan Schuemann, Dr. Maryam Moteabbed and Dr. Jungwook Shin for their valuable support with patient calculations. We would like to thank the Enterprise Research Infrastructure and Services (ERIS) group at Partners Healthcare.

References

Agostinelli, S. et al., 2002. GEANT4: A Simulation toolkit. *Nucl. Instrum. Methods Phys. Res., A*, 506(CERN-IT-2002-003. SLAC-PUB-9350. 3), pp.250–303. 86 p.

Brenner, D.J., 2004. Fractionation and late rectal toxicity. *Radiation Oncology Biology*, 60(4), pp.1013–1015.

Brenner, D.J. & Hall, E.J., 1999. Fractionation and protraction for radiotherapy of prostate carcinoma. *Radiation Oncology Biology*, 43(5), pp.1095–1101.

Carabe, A. et al., 2013. Clinical consequences of relative biological effectiveness variations in proton radiotherapy of the prostate, brain and liver. *Physics in Medicine and Biology*, 58(7), pp.2103–2117.

Carlson, D.J. et al., 2008. Combined use of Monte Carlo DNA damage simulations and deterministic repair models to examine putative mechanisms of cell killing. *Radiation Research*, 169, pp.447–459.

Chen, Y. et al., 2018. Impact of potentially variable RBE in liver proton therapy. *Physics in Medicine and Biology*, 63(19), p.195001.

Cheung, R. et al., 2005. Dose–response characteristics of low- and intermediate-risk prostate cancer treated with external beam radiotherapy. *International Journal of Radiation Oncology*Biology*Physics*, 61(4), pp.993–1002.

Dasu, A. & Toma-Dasu, I., 2012. Prostate alpha/beta revisited – an analysis of clinical results from 14 168 patients. *Acta Oncologica*, 51(8), pp.963–974.

De Meerleer, G.O. et al., 2007. Intensity-modulated radiation therapy for prostate cancer: Late morbidity and results on biochemical control. *Radiotherapy and Oncology*, 82(2), pp.160–166.

Dearnaley, D. et al., 2016. Conventional versus hypofractionated high-dose intensity-modulated radiotherapy for prostate cancer: 5-year outcomes of the randomised, non-inferiority, phase 3 CHHiP trial. *The Lancet. Oncology*, 17(8), pp.1047–1060.

Deore, S.M. et al., 1993. Alpha/beta value and importance of dose per fraction for the late rectal and recto-sigmoid complications. *Strahlentherapie und Onkologie : Organ der Deutschen Rontgengesellschaft ... [et al]*, 169(9), pp.521–526.

Dische, S. et al., 1999. Carcinoma of the cervix and the use of hyperbaric oxygen with radiotherapy: a report of a randomised controlled trial. *Radiotherapy and Oncology*, 53(2), pp.93–98.

Eade, T.N. et al., 2008. A comparison of acute and chronic toxicity for men with low-risk prostate cancer treated with intensity-modulated radiation therapy or 125I permanent implant. *International journal of radiation oncology, biology, physics*, 71(2), pp.338–345.

Fowler, J., Chappell, R. & Ritter, M., 2001. Is alpha/beta for prostate tumors really low? *Radiation Oncology Biology*, 50(4), pp.1021–1031.

Frese, M.C. et al., 2012. A mechanism-based approach to predict the relative biological effectiveness of protons and carbon ions in radiation therapy. *Radiation Oncology Biology*, 83(1), pp.442–450.

Goitein, M. & Schultheiss, T., 1985. Strategies for treating possible tumor extension: some theoretical considerations. *Radiation Oncology Biology*, 11(8), pp.1519–1528.

Hanks, G.E. et al., 2002. Dose response in prostate cancer with 8-12 years' follow-up. *Radiation Oncology Biology*, 54(2), pp.427–435.

Hoppe, B.S. et al., 2013. Comparative effectiveness study of patient-reported outcomes after proton therapy or intensity-modulated radiotherapy for prostate cancer. *Cancer*, 120(7), pp.1076–1082.

Hoppe, B.S., Bryant, C. & Sandler, H.M., 2015. Radiation for prostate cancer: Intensity modulated radiation therapy versus proton beam. *Journal of Urology*, 193(4), pp.1089–1091.

Jones, B., 2017. Clinical radiobiology of proton therapy: modeling of RBE. *Acta oncologica (Stockholm, Sweden)*, 56(11), pp.1374–1378.

King, C.R. & Mayo, C.S., 2000. Is the prostate alpha/beta ratio of 1.5 from Brenner & Hall a modeling artifact? *International journal of radiation oncology, biology, physics*, 47(2), pp.536–537.

Koukourakis, M.I. et al., 2007. Biological dose volume histograms during conformal hypofractionated accelerated radiotherapy for prostate cancer. *Medical Physics*, 34(1), pp.76–80.

Levegrün, S. et al., 2001. Fitting tumor control probability models to biopsy outcome after three-dimensional conformal radiation therapy of prostate cancer: pitfalls in deducing radiobiologic parameters for tumors from clinical data. *Radiation Oncology Biology*, 51(4), pp.1064–1080.

Marks, L.B. et al., 1995. The response of the urinary bladder, urethra, and ureter to radiation and chemotherapy. *Radiation Oncology Biology*, 31(5), pp.1257–1280.

Marzi, S. et al., 2009. Modeling of alpha/beta for late rectal toxicity from a randomized phase II study: conventional versus hypofractionated scheme for localized prostate cancer. *Journal of experimental & clinical cancer research : CR*, 28(1), p.117.

McNamara, A.L., Schuemann, J. & Paganetti, H., 2016. A phenomenological relative biological effectiveness (RBE) model for proton therapy based on all published in vitro cell survival data. *Physics in Medicine and Biology*, pp.8399–8416.

Mendenhall, N.P. et al., 2012. Early Outcomes from Three Prospective Trials of Image-guided Proton Therapy for Prostate Cancer. *Radiation Oncology Biology*, 82(1), pp.213–221.

Michalski, J.M. et al., 2010. Radiation Dose–Volume Effects in Radiation-Induced Rectal Injury. *Radiation Oncology Biology*, 76(3), pp.S123–S129.

Miralbell, R. et al., 2012. Dose-fractionation sensitivity of prostate cancer deduced from radiotherapy outcomes of 5,969 patients in seven international institutional datasets: alpha/beta = 1.4 (0.9-2.2) Gy. *Radiation Oncology Biology*, 82(1), pp.e17–e24.

Nihei, K. et al., 2011. Multi-Institutional Phase II Study of Proton Beam Therapy for Organ-Confined Prostate Cancer Focusing on the Incidence of Late Rectal Toxicities. *Radiation Oncology Biology*, 81(2), pp.390–396.

Ödén, J., Eriksson, K. & Toma-Dasu, I., 2017. Inclusion of a variable RBE into proton and photon plan comparison for various fractionation schedules in prostate radiation therapy. *Medical Physics*, 44(3), pp.810–822.

Paganetti, H., 2017. Relating the proton relative biological effectiveness to tumor control and normal tissue complication probabilities assuming interpatient variability in α/β. *Acta oncologica (Stockholm, Sweden)*, 56(11), pp.1379–1386.

Paganetti, H., 2014. Relative biological effectiveness (RBE) values for proton beam therapy. Variations as a function of biological endpoint, dose, and linear energy transfer. *Physics in Medicine and Biology*, 59(22), pp.R419–R472.

Pedersen, J. et al., 2018. Biological dose and complication probabilities for the rectum and bladder based on linear energy transfer distributions in spot scanning proton therapy of prostate cancer. *Acta Oncologica*, 0(0), pp.1413–1419.

Peeters, S.T.H. et al., 2006. Dose-response in radiotherapy for localized prostate cancer: results of the Dutch multicenter randomized phase III trial comparing 68 Gy of radiotherapy with 78 Gy. *Journal of clinical oncology : official journal of the American Society of Clinical Oncology*, 24(13), pp.1990–1996.

Perez, C.A., 1997. *Uterine cervix. In: Perez CA, Brady LW. editors. Principles and Practice of Radiation Oncology, Ed. 3*, Philadelpia, New York: Lippincott-Raven Publishers.

Perez, C.A., Brady, L.W. & Roti, J., 1997. *Overview. In: Perez CA, Brady LW. editors. Principles and Practice of Radiation Oncology, Ed. 3*, Philadelpia, New York: Lippincott-Raven Publishers.

Perl, J. et al., 2012. TOPAS: An innovative proton Monte Carlo platform for research and clinical applications. *Medical Physics*, 39(11), pp.6818–20.

Pollack, A. et al., 2009. Hypofractionation for prostate cancer: Interim results of a randomized trial. *Radiation Oncology Biology*, 75(3), pp.S81–S82.

Pollack, A. et al., 2000. Preliminary results of a randomized radiotherapy dose-escalation study comparing 70 Gy with 78 Gy for prostate cancer. *Journal of clinical oncology : official journal of the American Society of Clinical Oncology*, 18(23), pp.3904–3911.

Pugh, T.J. et al., 2013. Quality of life and toxicity from passively scattered and spot-scanning proton beam therapy for localized prostate cancer. *Radiation Oncology Biology*, 87(5), pp.946–953.

Schuemann, J. et al., 2015. Assessing the Clinical Impact of Approximations in Analytical Dose Calculations for Proton Therapy. *Radiation Oncology Biology*, 92(5), pp.1157–1164.

Schultheiss, T., Orton, C.G. & Peck, R.A., 1983. Models in radiotherapy:Volume effects. *Medical Physics*, 10(4), pp.1–6.

Slater, J.D. et al., 1998. Conformal proton therapy for prostate carcinoma. *International journal of radiation oncology, biology, physics*, 42(2), pp.299–304.

Stewart, R.D. et al., 2011. Effects of Radiation Quality and Oxygen on Clustered DNA Lesions and Cell Death. *Radiation Research*, 176(5), pp.587–602.

Stewart, R.D. et al., 2016. Rapid MCNP simulation of DNA double strand break (DSB) relative biological effectiveness (RBE) for photons, neutrons, and light ions. *Physics in Medicine and Biology*, pp.8249–8274.

Underwood, T. et al., 2016. Can We Advance Proton Therapy for Prostate? Considering Alternative Beam Angles and Relative Biological Effectiveness Variations When Comparing Against Intensity Modulated Radiation Therapy. *International journal of radiation oncology, biology, physics*, 95(1), pp.454–464.

Underwood, T.S.A. et al., 2017. Hydrogel rectum-prostate spacers mitigate the uncertainties in proton relative biological effectiveness associated with anterior-oblique beams. *Acta oncologica (Stockholm, Sweden)*, 56(4), pp.575–581.

Vogelius, I.R. & Bentzen, S.M., 2018. Dose Response and Fractionation Sensitivity of Prostate Cancer After External Beam Radiation Therapy: A Meta-analysis of Randomized Trials. *International journal of radiation oncology, biology, physics*, 100(4), pp.858–865.

Vora, S.A. et al., 2007. Analysis of biochemical control and prognostic factors in patients treated with either low-dose three-dimensional conformal radiation therapy or high-dose intensity-modulated radiotherapy for localized prostate cancer. *International journal of radiation oncology, biology, physics*, 68(4), pp.1053–1058.

Wang, J.Z., Guerrero, M. & Li, X.A., 2003. How low is the alpha/beta ratio for prostate cancer? *Radiation Oncology Biology*, 55(1), pp.194–203.

Zelefsky, M.J. et al., 2008. Incidence of late rectal and urinary toxicities after three-dimensional conformal radiotherapy and intensity-modulated radiotherapy for localized prostate cancer. *International journal of radiation oncology, biology, physics*, 70(4), pp.1124–1129.

Zhu, J. et al., 2016. The benefit of using bladder sub-volume equivalent uniform dose constraints in prostate intensity-modulated radiotherapy planning. *OncoTargets and therapy*, 9, pp.7537–7544.

Paper II

Impact of uncertainties in range and RBE on small field proton therapy.

Marteinsdottir M, Schuemann J, Paganetti H.

Phys. Med. Biol. 64 (2019) 205005 (9pp)

Impact of uncertainties in range and RBE on small field proton therapy

Maria Marteinsdottir[1,2], Jan Schuemann[1,3], Harald Paganetti[1,3]

[1]Department of Radiation Oncology, Massachusetts General Hospital, Boston, MA 02114, USA
[2]Faculty of Physical Sciences, University of Iceland, Dunhaga 5, IS-107 Reykjavik, Iceland
[3]Harvard Medical School, Boston, MA 02114, USA
* hpaganetti@mgh.harvard.edu

Abstract

To evaluate the clinical impact of biological uncertainties in small field proton therapy due to the assumption of using a constant relative biological effectiveness (RBE) value of 1.1 (RBE-fixed) compared to a variable RBE (RBE-weighted). In this context the impact of the applied range margin was investigated.

Eight patients with arteriovenous malformation (AVM) treated with proton radiosurgery were selected due to the small target volume. Dose distributions were compared for RBE-weighted and RBE-fixed. The impact of RBE was assessed using Monte Carlo (MC) dose calculations for stereotactic doses and doses of 2 Gy(RBE). Four different α/β ratios were investigated. Additionally, dose distributions were recalculated with reduced range margins.

Applying variable RBE values for stereotactic doses resulted in an increase in the mean dose of 1.6% for a low α/β of 2 Gy, but a decrease of 2.6% for an α/β of 10 Gy. However, the mean dose increased to 17.1% and 2.1% for doses of 2 Gy(RBE) and α/β of 2 Gy and 10 Gy, respectively. Reducing range margins from 3.5% + 1 mm to 2.5% + 1 mm resulted in negligible difference in the mean RBE within the target, or 0.1% for stereotactic doses and 0.3% for doses of 2 Gy(RBE). Larger differences were seen for a range reduction to 0% + 1 mm, i.e. 1.1% and 3.0% for stereotactic doses and doses of 2 Gy(RBE), respectively.

Because potential RBE effects are typically more pronounced in the distal part of a field, a bigger clinical impact of RBE uncertainties in small fields is expected. Our study shows that this could be significant for tissues with low α/β and a small dose per fraction. The uncertainty in RBE due to the uncertainty associated with the α/β ratio seems larger than the impact of the applied range uncertainty margin on RBE.

1. Introduction

For proton therapy, the relative biological effectiveness (RBE) is defined as the ratio of the reference photon dose to the proton dose to cause the same level of effect. Currently, a constant RBE of 1.1 is being applied in clinical practice as protons are more biologically effective than photons. Therefore, patients undergoing proton radiotherapy receive 10% lower prescription dose compared to photon radiotherapy. It has, however, been shown (Paganetti et al. 2002; Paganetti 2014) that the RBE depends on different factors, such as the linear energy transfer (LET), dose per fraction and tissue type typically described by the α_x/β_x ratio, a parameter representing tissue radiation sensitivity in the linear-quadratic (LQ) model (McMahon 2018). For the energy range used in clinical proton therapy the RBE increases with increasing LET, decreasing α/β and with decreasing dose. The clinically used generic RBE value of 1.1 disregards these variations. Paganetti (Paganetti 2014) reported average proton RBE values for cell line data from over 70 reports using clonogenic cell survival as endpoint. The average RBE for cell survival in the center of an average Spread Out Bragg Peak (SOBP) for a proton dose of 2 Gy is ~1.15. The RBE increases to ~1.35 at the distal edge and finally the fall-off region shows RBE of ~1.7. These values might however not be representative for in vivo endpoints. Due to the RBE increase at the distal end of proton fields, the biological dose distribution

can be shifted by up to ~4 mm compared to the physical dose distribution (Paganetti 2014; Paganetti & Goitein 2000; Carabe et al. 2012; Grün et al. 2013). Furthermore, the impact of applying variable RBE on clinical cases has previously been studied extensively albeit not with a focus on small fields (Underwood et al. 2016; McNamara et al. 2016; Carabe et al. 2013; Wedenberg & Toma-Dasu 2014; Ödén et al. 2017; Pedersen et al. 2018).

Figure 1 exemplifies the impact of a variable RBE. Dose distributions for different SOBPs were produced using Monte Carlo calculations with the double scattering delivery system at the Francis H. Burr Proton Center at the Massachusetts General Hospital. The four SOBPs have the same range of 15 cm but the top figures have a modulation width of only 1.5 cm, hence representing a small field SOBP, whereas the lower figures have a modulation width of 5 cm. The distributions either show a physical dose with a prescribed dose of 2 Gy at the center of the SOBP, Figure 1(a), or a prescribed dose of 15 Gy, Figure 1(b). Furthermore, a physical dose scaled by a fixed RBE of 1.1 (RBE-fixed) or by a variable RBE based on a model by McNamara et al. (described in section 2.2) with an α_x/β_x value of 3.5 Gy (RBE-weighted) is shown. The figure also demonstrates the respective dose-averaged LET distribution (LET_d) for each modulation width. The shaded regions resemble two hypothetical locations of a tumor within the SOBPs and the corresponding ranges of LET_d. The LET_d in the target region increases with depth and with decreasing modulation width. Consequently, the average RBE-weighted dose in the target estimated using the McNamara model for prescribed dose of 2 Gy is affected by both depth and the width of the SOBP (Figure 1(a)). The average RBE in the shaded region for a small modulation width of 1.5 cm and dose of 2 Gy is 1.22 and 1.17 for a modulation width of 5 cm. In addition, the position of the distal dose fall-off is shifted in the RBE-weighted dose distribution. Larger average RBE values are observed for smaller target volumes as the center of a small target volume is located closer to the distal edge. In contrast, the LET_d has negligible effect on the RBE-weighted dose for a prescribed dose of 15 Gy (Figure 1(b)). The average RBE value in the shaded region for dose of 15 Gy is 1.1 for both the small and large modulation width, respectively. Furthermore, no shift in the distal dose fall-off is evident. The figure further demonstrates that the difference in the LET_d at the distal edge between the small and large modulation width is insignificant, irrelevant of the delivered dose.

It is essential to predict the range of proton beams as accurately as possible in treatment planning and delivery. Due to the physical properties of protons, an underestimation of the range may result in parts of the target not receiving any dose. By means of cautious approach, a generic range uncertainty margin is applied to ensure target coverage, consequently leading to additional irradiation of normal tissue distal to the target volume. The uncertainty margin is frequently defined as 3.5% of the prescribed range in water in beam direction + 1 mm. This margin was introduced by Goitein (Goitein 1985) where the 3.5% factor was ascribed to the CT imaging and its conversion to Hounsfield Units (HU) and water-equivalent densities in tissue. The additional 1 mm reflects the estimated range uncertainty due to setup uncertainty. In a paper by Paganetti (Paganetti 2012) the uncertainties in proton range were estimated to be 2.7% + 1.2 mm for mostly homogeneous patient geometries but 4.6% + 1.2 mm for highly heterogeneous patient geometries. Subsequently, Schuemann et al. (Schuemann et al. 2014) showed that range uncertainty margins have a large variation and can be up to 2.8% + 1.2 mm for liver and prostate treatments, 3.1% + 1.2 mm for whole brain treatments and 6.3% + 1.2 mm for breast, lung and head and neck treatments. A reduction of range uncertainties can be achieved by applying Monte Carlo based dose engines currently not yet implemented in all commercial planning systems. By using Monte Carlo (MC) simulations instead of analytical dose calculation (ADC) the range uncertainty can potentially be reduced to 2.4% + 1.2 mm for all patient geometries.

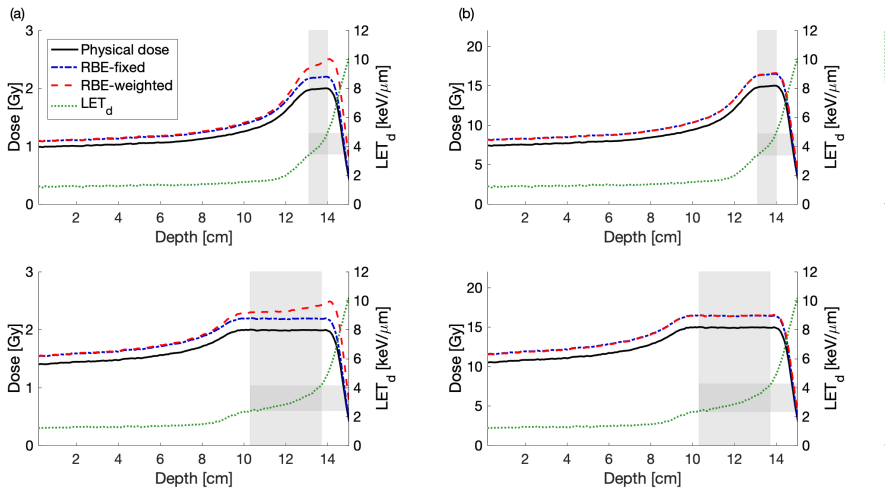

Figure 1. Example of depth dose distributions for four simple SOBPs in water. The physical dose is shown by a black solid curve with a prescribed dose of (a) 2 Gy or (b) 15 Gy at the center of the SOBP, the blue dashed-dotted curve shows the physical dose scaled by a fixed RBE value of 1.1 (RBE-fixed), while the red dashed curve represents the RBE-weighted dose calculated using the McNamara model (RBE-weighted). The SOBPs have a range of 15 cm. The top figures have a modulation width of 1.5 cm whereas the modulation width is 5 cm for the lower figures. The respective LET_d curves are shown as green dotted curve. The shaded regions resemble two hypothetical locations of a tumor within the SOBP and the corresponding ranges of LET_d.

The increasing RBE with depth as well as the range uncertainties do both impact dose to healthy tissue downstream of the target. The purpose of this study is twofold. Firstly, to assess and improve our understanding of the magnitude and clinical impact of the assumption of using a constant RBE of 1.1 compared to variable RBE particularly for small fields subject to elevated LET values throughout the field. Secondly, to assess the effect on RBE in target volumes if range uncertainties were to be reduced.

2. Methods

2.1. Patient cohort and treatment planning

Eight clinical cases with arteriovenous malformations (AVM) treated at the Francis H. Burr Proton Therapy Center at the Massachusetts General Hospital (MGH) were investigated. These cases were selected due to their small target sizes as the analysis is not specific to this disease. The treatments were single-fraction proton beam stereotactic radiosurgery (PSRS) based on a double scattering technique. The prescription doses varied between 13.0 and 16.0 Gy(RBE). To ensure the prescription dose despite scattering effects at apertures correction factors were applied as has been discussed in previous papers (Daartz et al. 2009; Geng et al. 2017). Table 1 summarizes the ranges of parameters of the patient cohort.

Table 1. Summary of patient cohort.

Prescription doses [Gy(RBE)]	Prescribed ranges [mm]	Field diameters [mm]	Target volumes [cc]	Number of beams
13-16	54-122	13.1-20.1	0.191-3.273	4-6

2.2. Dose and RBE simulations

Monte Carlo simulations were performed using the Geant4-based TOPAS toolkit (Perl et al. 2012) which has been thoroughly validated for proton therapy (Testa et al. 2013). The TOPAS version 3.0.p1 was used which is based on Geant4 version 10.02.p01 (Agostinelli et al. 2002). For each patient, the beam geometry and treatment plan CT image set were imported into TOPAS using an in-house software (Verburg et al. 2016). Dose was scored as dose-to-water and LET values as dose averaged LET values (LET_d) per unit density in each voxel (Grassberger et al. 2011).

The variable RBE was calculated according to an empirical RBE model (McNamara et al. 2016). The model is a phenomenological model, based on the LQ model and uses a dataset of over 70 experimental reports on proton RBE (Paganetti 2014) for its non-linear regression fit on 287 experimental data points. It includes a large number of different cell lines reporting α_x/β_x ratios between 0.1 and 29.5 Gy as well as LET_d values below 20 keV/μm. It estimates the RBE as a function of dose, α_x/β_x ratio for X-ray (referred to α/β from here on) for the reference radiation (^{60}Co) and on LET_d and is valid within the parameter space of the underlying experimental data.

2.3. Data Analysis

The impact of various parameters was assessed as follows:

- The α/β ratio: Comparisons were performed between MC calculated dose distributions applying a constant RBE value of 1.1 (RBE-fixed) and a variable RBE (RBE-weighted). To evaluate the impact of α/β on the RBE-weighted dose distributions for AVMs, three different α/β values were chosen. A study by Kocher et al. (Kocher et al. 2004) estimates the α/β ratios for AVMs to be 3.5 Gy in general and 4.6-6.4 Gy for AVMs smaller than 3 cm. However, a study by Karlsson et al (Karlsson et al. 2006) states that AVMs are of the same radiobiological type as its surrounding tissue, i.e. late-responding with a low α/β value. Therefore, α/β ratios of 2, 3.5 and 6.4 Gy were considered in our study. Additionally, as the study is intended not solely for AVMs but for small target volumes in general, an α/β of 10 Gy was chosen to represent generic tumors.
- Range uncertainty: To assess the impact of reducing range uncertainties and thereby shifting the target towards higher LET (RBE) regions, the generic range uncertainty margin (ΔR_∞) of 3.5% + 1 mm was reduced to 2.5% + 1 mm, representing estimated margin requirements when using MC for treatment planning. The range was further reduced to 0% + 1 mm to examine an extreme scenario.
- Prescription dose: As the RBE in general increases with decreasing dose, the prescribed dose was scaled down to 2 Gy(RBE) to study the expected effect of RBE for a standard, not stereotactic, prescription dose in a fractionated treatment.

Comparisons were performed using dosimetric indices based on dose-volume histogram (DVH) analyses. The DVH-based indices analyzed were:

- Mean target dose: The dose averaged over all voxels in the target volume.
- D98: The maximum dose that covers 98% of the target volume (indicating the minimum dose).
- D50: The median target dose.
- D02: The maximum dose that covers 2% of the target volume (indicating the maximum dose).
- V95: The percentage of the target volume covered by 95% of the prescription dose.

In addition, the mean value of the RBE in the target was calculated for each patient for the four different α/β ratios and the three different range uncertainty margins.

3. Results

3.1. Stereotactic dose levels

3.1.1. Impact of variable RBE

Figure 2 presents the DVH analysis results for stereotactic dose levels of 13-16 Gy(RBE). The results are calculated using the clinical range uncertainty margin of 3.5% + 1 mm. Each data point corresponds to the relative difference between MC-calculations assuming a fixed RBE of 1.1 and a variable RBE for one patient. The results are grouped by different α/β ratios. There is a clear dependence on the α/β ratio and the results suggest that for tissues having α/β ratios larger than ~6 Gy, the RBE may be below 1.1. Thus, the target dose would be overestimated when assuming a fixed RBE of 1.1. This discrepancy might become clinically relevant when applying proton stereotactic radiosurgery for brain metastasis delivered with high dose per fraction, as the α/β ratio is considered to be around 10 Gy. It should be noted that these values suffer from a considerable uncertainty because the validity of the LQ model for high doses is questionable (Santacroce et al. 2013; Brown et al. 2014). Consequently, the RBE effect using the constant RBE of 1.1 might be overestimated.

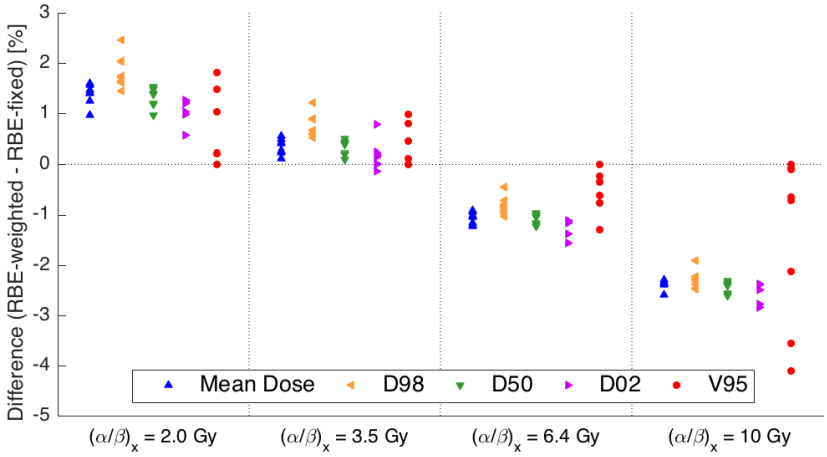

Figure 2. Percentage difference subtracting the dosimetric indices calculated by the variable RBE (RBE-weighted) MC-calculations from the calculations with a constant RBE of 1.1 (RBE-fixed) for stereotactic dose level of 13 - 16 Gy(RBE). DXX is the maximum dose covering the XX% of the target volume; V95 is the percentage of the target volume covered by 95% of the prescribed dose. Results are grouped for four different α/β ratios. The applied range uncertainty margin is 3.5% + 1 mm.

3.1.2. Impact of reducing range uncertainties

Figure 3 exemplifies the dose and LET_d distributions for one patient having the brainstem close to the target. The distributions are shown for the three considered range uncertainty margins. In this example, the treatment plan prescribed four different beam directions. The results are presented for a fixed RBE of 1.1 and a prescribed dose of 16 Gy(RBE). The dose distribution for a generic range margin uncertainty of 3.5% + 1 mm is demonstrated in Figure 3(a), whereas (b) and (c) represent the dose distributions for range margins of 2.5% + 1 mm and 0% + 1 mm, respectively. As can be seen, decreasing the range margin from 3.5% + 1 mm to 2.5% + 1 mm results in around 1.0 mm range reduction in each beam direction as indicated

by a region of reduced dose located outside the target. Furthermore, a small increase in the target dose is evident (Figure 3(e)), reflecting an artifact due to a lack of field flatness and SOBP's non-uniformity often present for small fields. Generating highly uniform (flat) SOBPs for small fields is challenging for proton therapy delivery systems (Testa et al. 2013).

The DVH results for the target (blue) and the brainstem (red) for all range margins are demonstrated in Figure 3(f). For the target, a decrease in the D98 index for range reduction to 0% + 1 mm is evident, thus illustrating more clearly the non-flat SOBP effect. Furthermore, the increase in D02 is demonstrated. Figure 3(g) shows the cumulative LET_d -volume distribution for the target for all range margins. Decreasing the range margin results in an increase in the LET_d as the LET_d affects mainly the distal edge of the dose distribution (see Figure 1) which is being moved towards the target volume for reduced range margins.

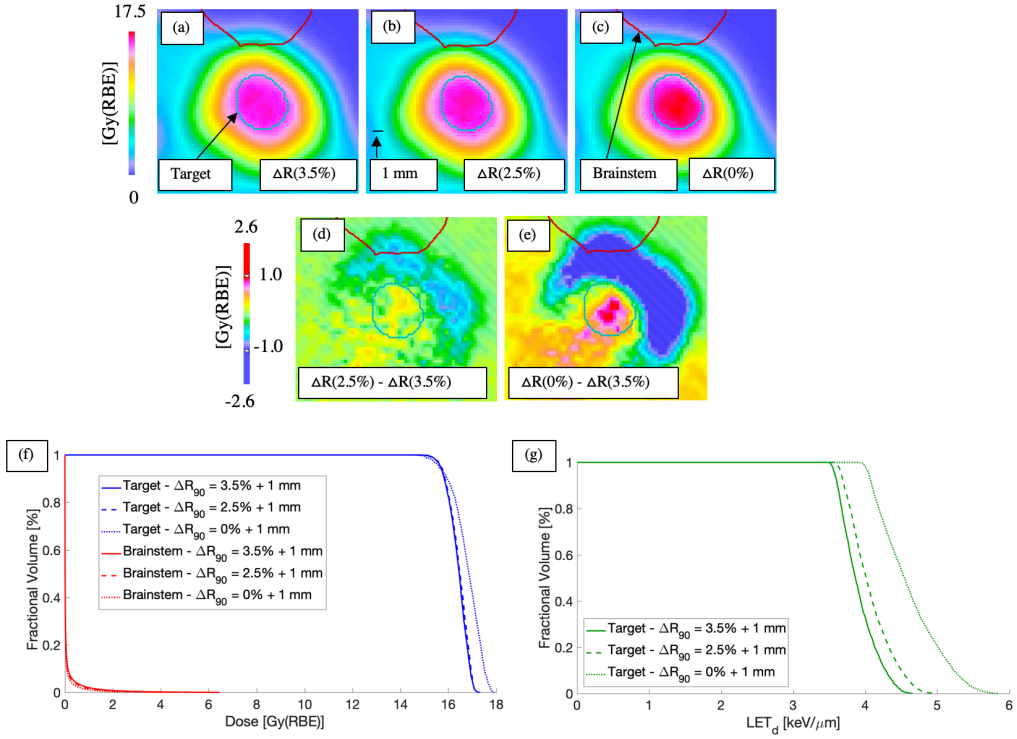

Figure 3. Example of dose distribution for constant RBE value of 1.1 for three different range uncertainty margins ΔR_{∞}. The plan has four different beam directions. (a) $\Delta R_{90} = 3.5\% + 1$ mm, (b) $\Delta R_{90} = 2.5\% + 1$ mm (a scale bar representing 1 mm is displayed), (c) $\Delta R_{90} = 0\% + 1$ mm. (d) The difference between ΔR_{90} of 3.5% and 2.5%. (e) The difference between ΔR_{90} of 3.5% and 0%. (f) The dose-volume histograms for the target and the brainstem. The target and the brainstem are shown in blue and red, respectively. (g) The LET_d -volume histogram for the target.

3.1.3. Impact of variable RBE if range uncertainties are reduced

Figure 4 illustrates the mean value of RBE in the target (RBE_{mean}) for the four different α/β ratios and the three different generic range uncertainty margins. The RBE decreases with increasing α/β ratio. The figure

also demonstrates that for each α/β ratio, reducing only the range margin results in a minuscule difference in the mean value of the RBE. The largest difference is less than 0.1% and 0.3% for a range reduction to 2.5% + 1 mm and 0% + 1 mm, respectively. The results demonstrate that the increase in LET_d within the target does not affect RBE much as the dose per fraction is large.

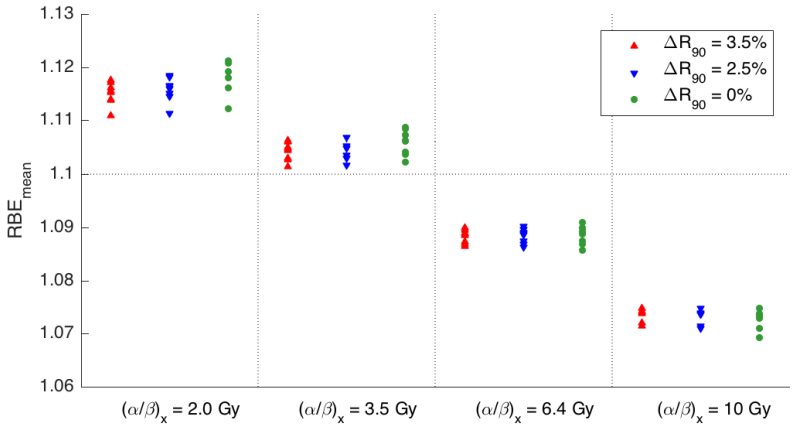

Figure 4. The mean value of RBE in the target volume. Results for four different α/β ratios and three different range uncertainty margins ΔR_{90} for stereotactic dose levels of 13-16 Gy(RBE).

Figure 5 demonstrates the relative differences in the dosimetric indices between MC-calculations based on range uncertainty margins of 3.5% + 1 mm and reduced range uncertainty margins of 2.5% + 1 mm and 0% + 1 mm. Each data point corresponds to one patient. The calculations were performed for an RBE of 1.1 and for a variable RBE with four different α/β ratios. The reduction of the range uncertainty margins from 3.5% + 1 mm to 2.5% + 1 mm resulted in a small difference in all dosimetric indices, illustrated on the left-hand side in Figure 5. This was independent of using either a fixed RBE of 1.1 or a variable RBE with different α/β ratios. The difference is nearly always positive. The maximum increase in mean dose and D50, representing the median dose, was 1.1% when calculated using a range margin of 2.5% + 1 mm compared to using a margin of 3.5% + 1 mm. The D02 index, representing the maximum dose, either increased or decreased, the change was mainly due to inter-patient variation. The D98 index, representing the minimum target dose, decreased only by up to 1% when reducing the range, due to SOBP's non-uniformity for small fields. Thus, the difference between all indices due to a range reduction to 2.5% + 1 mm is within clinical uncertainty.

Reducing the margin to the extreme case of 0% + 1 mm revealed larger differences between the indices (right-hand side on Figure 5). The maximum dose within the target, represented by D02, increased by up to 6% when decreasing the range margin whereas the minimum dose, represented by D98, decreased by up to 4%. The relative difference in all dosimetric indices was similar for both applying a fixed RBE and a variable RBE. The mean dose and the median dose, represented by D50, increased for all patients by up to 4%.

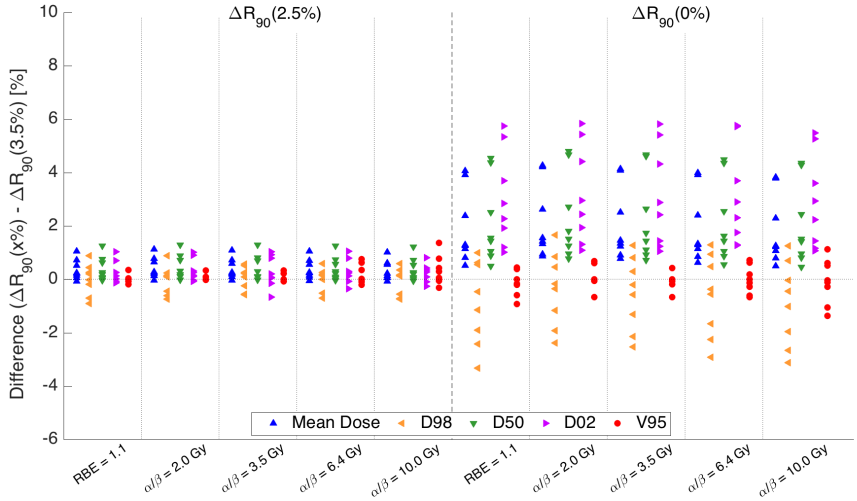

Figure 5. Percentage difference subtracting the dosimetric indices having range uncertainty margins Δ R_{90} of 3.5% + 1 mm from 2.5% + 1 mm and 0% + 1 mm for stereotactic dose levels of 13 – 16 Gy(RBE). Results are calculated for either a fixed RBE of 1.1 or a variable RBE, having four different α/β ratios. DXX is the maximum dose covering the XX% of the target volume; V95 is the percentage of the target volume covered by 95% of the prescribed dose.

3.2. Scaled dose of 2 Gy

3.2.1. Impact of variable RBE

The relative differences in the dosimetric indices for a 2 Gy(RBE) fraction are presented in Figure 6 for range uncertainty margins of 3.5% + 1 mm. The differences are nearly all positive, demonstrating that variable RBE-weighted dose distributions are larger than predicted by a fixed RBE of 1.1. For an α/β ratio of 2 Gy, the dosimetric indices calculated using a variable RBE are up to 19% larger than for a fixed RBE. This difference is somewhat enhanced due to the small size of the target volume compared to larger volumes. For an α/β of 10 Gy the difference is small, indicating that RBE is close to 1.1 in the target. This is different to stereotactic dose levels presented in section 3.1, where applying a variable RBE resulted in a small difference in the target dose of less than ±3% for all α/β values compared to a fixed RBE of 1.1.

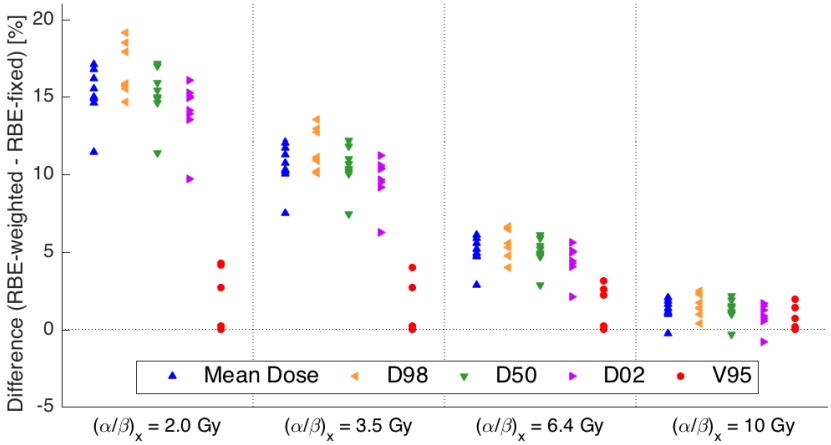

Figure 6. Percentage difference subtracting the dosimetric indices calculated by the variable RBE (RBE-weighted) MC-calculations from the calculations with a constant RBE of 1.1 (RBE-fixed) for dose of 2 Gy(RBE). DXX is the maximum dose covering the XX% of the target volume; V95 is the percentage of the target volume covered by 95% of the prescribed dose. Results are grouped for four different α/β ratios and the range uncertainty margin ΔR_{90} is 3.5% + 1 mm.

3.2.2. Impact of variable RBE if range uncertainties are reduced

The mean value of the RBE in the target, RBE_{mean}, for scaled doses of 2 Gy(RBE) is shown in Figure 7. The RBE is larger than 1.1 for all α/β ratios. The RBE_{mean} for all patients planned for margins of 3.5% + 1 mm and α/β of 10 Gy is close to the clinically used RBE of 1.1. The average value of RBE_{mean} is 1.13 with standard deviation of 0.01. The reduction in range from 3.5% + 1 mm to 2.5% + 1 mm results in a difference in RBE_{mean} of only ~1%, independent of α/β ratio, but up to 3.0% by reducing the range to 0% + 1 mm. This is a larger difference than for stereotactic dose levels where the difference was <0.3%.

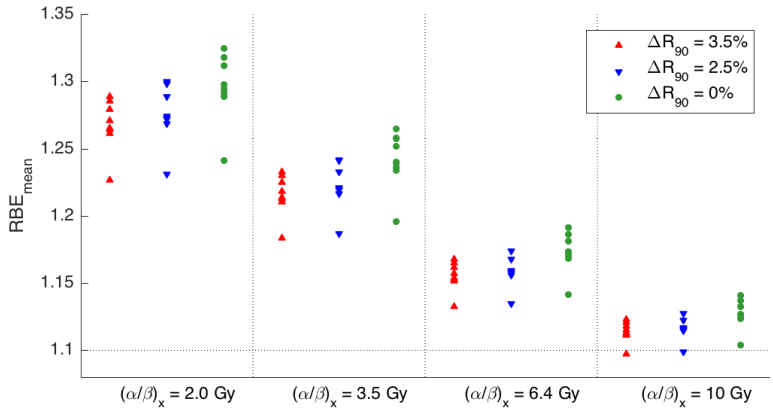

Figure 7. The mean value of RBE in the target volume. Results for four different α/β ratios and three different range uncertainty margins ΔR_{90} for dose of 2 Gy(RBE).

While figure 7 reports the mean RBE, figure 8 compares the differences in dosimetric indices for RBE-weighted doses. The difference in the dosimetric indices between range margins of 3.5% + 1 mm and a reduced margin of 2.5% + 1 mm is small (< 2.4 %). Furthermore, the difference is similar for all α/β ratios. A smaller range uncertainty margin does result in an increase in RBE-weighted dose, clearly demonstrated particularly for the range margin reduction to 0% + 1 mm.

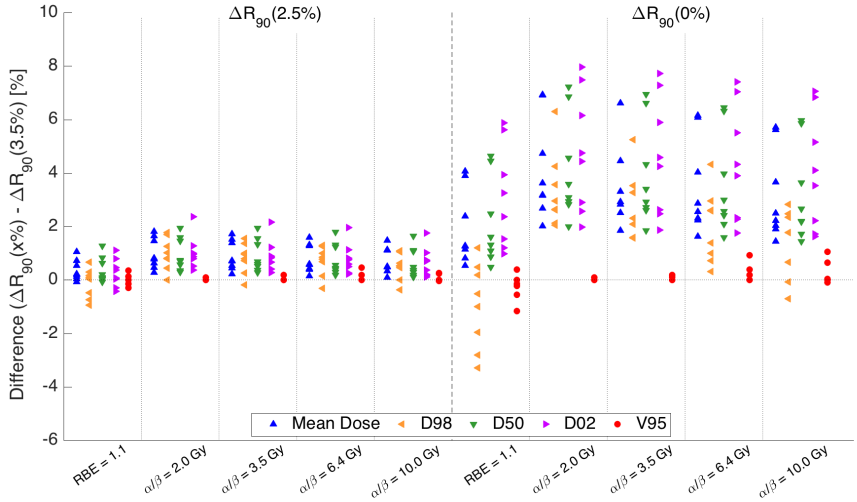

Figure 8. Percentage difference subtracting the dosimetric indices having range uncertainty margins Δ R_{90} of 3.5% + 1 mm from 2.5% + 1 mm and 0% + 1 mm dose of 2 Gy(RBE). Results are calculated for either a fixed RBE of 1.1 or a variable RBE, having four different α/β ratios. DXX is the maximum dose covering the XX% of the target volume; V95 is the percentage of the target volume covered by 95% of the prescribed dose.

4. Discussion

In this study, the impact of varying proton RBE values for small fields was examined as small fields are on average more affected by potential RBE effects. An increase in the average RBE values were observed for smaller target volumes as the center of a small target volume is being shifted towards the distal edge (see Introduction). The use of a variable RBE was investigated and compared to a fixed RBE value of 1.1. Furthermore, to illustrate the interplay between range uncertainty margins and a potential RBE effect, the clinically used range uncertainty margin was reduced.

Varying the RBE resulted in a small difference in the dosimetric indices compared to a fixed RBE of 1.1 for stereotactic dose levels and clinical used range uncertainty margins of 3.5% + 1 mm. For a variable RBE, indices estimated using a low α/β of 2 Gy were up to 3% larger whereas the application of an α/β of 10 Gy resulted in dosimetric indices up to 4% lower than for a fixed RBE. The average value of the mean RBE within the target for all patients was 1.12 for an α/β of 2 Gy but 1.07 for an α/β of 10 Gy. Consequently, ignoring variable RBE may result only in a negligible overestimation in mean target dose for stereotactic dose levels and large α/β values.

Lowering the dose to 2 Gy(RBE) per fraction revealed a large difference in the dosimetric indices between a variable RBE and a fixed RBE for low α/β ratios. For α/β of 2 Gy and range uncertainty margins of 3.5% + 1 mm, the difference was up to 19% with an average value of RBE_{mean} in the target of 1.27.

However, increasing the α/β to 10 Gy resulted in less than 3% difference in the dosimetric indices and an average value of RBE_{mean} of 1.13.

The RBE was calculated using the variable RBE model by McNamara. The model is fitted to empirical data of clonogenic cell survival for α/β ratios between 0.1 and 29.5 Gy and LET_d values below 20 keV/μm and is valid within this parameter space. Comparisons to other models, such as the models by Wedenberg et al. (Wedenberg et al. 2013) and by Carabe et al. (Carabe et al. 2012) have been done before. The most comprehensive comparison was done by Rørvik et al. who compared several published phenomenological models based on the LQ model. The study revealed that the estimated RBE and the RBE-weighted dose varied significantly between different models due to fundamental differences in underlying experimental data, model assumptions and regression techniques. They emphasized the importance of recognizing these fundamental properties in different models when evaluating RBE-weighted dose results. While absolute numbers are model dependent, the relative effects shown in our results will not be affected significantly. In general, all of these models suffer from the underlying data on clonogenic cell survival in vitro and its questionable translation to in vivo endpoints. The resulting uncertainties are likely larger than variations amongst the models.

Reducing the range uncertainty margin from 3.5% + 1 mm to 2.5% + 1 mm exposed a small difference in the mean value of RBE within the target for both stereotactic dose levels and doses of 2 Gy(RBE), or 0.1% and 1%, respectively. Slightly larger differences were observed when reducing the range uncertainty to 0% + 1 mm, where the mean RBE increased by up to 0.3% for stereotactic dose levels and up to 3% for 2 Gy(RBE) per fraction. Note that the maximum RBE-weighted dose at the end of range is located outside the target even for a range margin of 0% + 1 mm (this is clearly illustrated in Figure 1).

This work was based on a double scattering system. Scanned beam delivery would generally result in a more pronounced increase in LET at the distal end for beam scanning due to less scattering in the beam path, hence creating a narrower energy distribution (Paganetti & Schmitz 1996; Paganetti & Goitein 2000; Grassberger & Paganetti 2011; Marteinsdottir & Paganetti 2019). At the same time, the dose fall-off for scanned beam delivery would be sharper thus reducing the distal volume impacted by such an LET increase. While the impact of the delivery system specifications on dose, LET and RBE can be significant in the distal fall-off, the overall trends shown in our work are preserved. A more detailed investigation on how the dose and RBE in the distal fall-off depend on the delivery system is beyond the scope of this work and has been studied previously (Paganetti & Schmitz 1996; Paganetti & Goitein 2000).

This study has limitations. Depending on the double scattering systems and the spot size of the beam scanning systems, the flatness of the SOBP that can be reached may not be as good as for larger fields (see Figure 1). This could have a small impact on the results.

5. Conclusion

In general, it is widely assumed that RBE effects might become more relevant to clinical cases as range reduction methods become more sophisticated. This study focused on small fields where the impact was expected to be larger. It demonstrates that the impact of a variable RBE is relevant for tissues with low α/β ratio only for small doses per fraction, i.e. ~2 Gy. Furthermore, reducing the range margin did not affect the mean RBE in the target significantly. Overall, the uncertainty in RBE due to the uncertainty associated with the α/β ratio was found to be larger than the impact of the applied range uncertainty margin on RBE.

Acknowledgement

This work was supported by NIH NCI U19 CA-21239 (“Improving the Clinical Effectiveness and Understanding of the Biophysical Basis of Proton Therapy”). We would gratefully like to thank Dr. Jungwook Shin for his valuable support. We would like to thank the Enterprise Research Infrastructure and Services (ERIS) group at Partners Healthcare for maintaining the computer cluster.

References

Agostinelli, S. et al., 2002. GEANT4: A Simulation toolkit. *Nucl. Instrum. Methods Phys. Res., A*, 506(CERN-IT-2002-003. SLAC-PUB-9350. 3), pp.250–303. 86 p.

Brown, J.M., Carlson, D.J. & Brenner, D.J., 2014. The Tumor Radiobiology of SRS and SBRT: Are More Than the 5 Rs Involved? *International Journal of Radiation Oncology*Biology*Physics*, 88(2), pp.254–262.

Carabe, A. et al., 2013. Clinical consequences of relative biological effectiveness variations in proton radiotherapy of the prostate, brain and liver. *Physics in Medicine and Biology*, 58(7), pp.2103–2117.

Carabe, A. et al., 2012. Range uncertainty in proton therapy due to variable biological effectiveness. *Physics in Medicine and Biology*, 57(5), pp.1159–1172.

Daartz, J. et al., 2009. Field size dependence of the output factor in passively scattered proton therapy: influence of range, modulation, air gap, and machine settings. *Medical Physics*, 36(7), pp.3205–3210.

Geng, C. et al., 2017. Limitations of analytical dose calculations for small field proton radiosurgery. *Physics in Medicine and Biology*, 62(1), pp.246–257.

Goitein, M., 1985. Calculation of the uncertainty in the dose delivered during radiation therapy. *Medical Physics*, 12(5), pp.608–612.

Grassberger, C. & Paganetti, H., 2011. Elevated LET components in clinical proton beams. *Physics in Medicine and Biology*, 56(20), pp.6677–6691.

Grassberger, C. et al., 2011. Variations in linear energy transfer within clinical proton therapy fields and the potential for biological treatment planning. *International journal of radiation oncology, biology, physics*, 80(5), pp.1559–1566.

Grün, R. et al., 2013. Physical and biological factors determining the effective proton range. *Medical Physics*, 40(11), pp.111716–10.

Karlsson, B. et al., 2006. Calculation of isoeffective doses and the alpha/beta value by comparing results following radiosurgery and radiotherapy for arteriovenous malformations of the brain. *Journal of Neurosurgery*, 105, pp.183–189.

Kocher, M. et al., 2004. Alpha/beta ratio for arteriovenous malformations estimated from obliteration rates after fractionated and single-dose irradiation. *Radiotherapy and Oncology*, 71(1), pp.109–114.

Marteinsdottir, M. & Paganetti, H., 2019. Applying a variable relative biological effectiveness (RBE) might affect the analysis of clinical trials comparing photon and proton therapy for prostate cancer. *Physics in Medicine and Biology*, 64(11), p.115027.

McMahon, S.J., 2018. The linear quadratic model: usage, interpretation and challenges. *Physics in Medicine and Biology*, 64(1), p.01TR01.

McNamara, A.L., Schuemann, J. & Paganetti, H., 2016. A phenomenological relative biological effectiveness (RBE) model for proton therapy based on all published in vitro cell survival data. *Physics in Medicine and Biology*, pp.8399–8416.

Ödén, J., Eriksson, K. & Toma-Dasu, I., 2017. Inclusion of a variable RBE into proton and photon plan comparison for various fractionation schedules in prostate radiation therapy. *Medical Physics*, 44(3), pp.810–822.

Paganetti, H., 2012. Range uncertainties in proton therapy and the role of Monte Carlo simulations. *Physics in Medicine and Biology*, 57(11), pp.R99–R117.

Paganetti, H., 2014. Relative biological effectiveness (RBE) values for proton beam therapy. Variations as a function of biological endpoint, dose, and linear energy transfer. *Physics in Medicine and Biology*, 59(22), pp.R419–R472.

Paganetti, H. & Goitein, M., 2000. Radiobiological significance of beamline dependent proton energy distributions in a spread-out Bragg peak. *Medical Physics*, 27(5), pp.1119–1126.

Paganetti, H. & Schmitz, T., 1996. The influence of the beam modulation technique on dose and RBE in proton radiation therapy. *Physics in Medicine and Biology*, 41(9), pp.1649–1663.

Paganetti, H. et al., 2002. Relative biological effectiveness (RBE) values for proton beam therapy. *International Journal of Radiation Oncology*Biology*Physics*, 53(2), pp.407–421.

Pedersen, J. et al., 2018. Biological dose and complication probabilities for the rectum and bladder based on linear energy transfer distributions in spot scanning proton therapy of prostate cancer. *Acta Oncologica*, 0(0), pp.1413–1419.

Perl, J. et al., 2012. TOPAS: An innovative proton Monte Carlo platform for research and clinical applications. *Medical Physics*, 39(11), pp.6818–20.

Santacroce, A. et al., 2013. Radiobiology of radiosurgery for the central nervous system. *BioMed Research International*, 2013(3-4), pp.362761–9.

Schuemann, J. et al., 2014. Site-specific range uncertainties caused by dose calculation algorithms for proton therapy. *Physics in Medicine and Biology*, 59(15), pp.4007–4031.

Testa, M. et al., 2013. Experimental validation of the TOPAS Monte Carlo system for passive scattering proton therapy. *Medical Physics*, 40(12), pp.121719–16.

Underwood, T. et al., 2016. Can We Advance Proton Therapy for Prostate? Considering Alternative Beam Angles and Relative Biological Effectiveness Variations When Comparing Against Intensity Modulated Radiation Therapy. *International journal of radiation oncology, biology, physics*, 95(1), pp.454–464.

Verburg, J.M. et al., 2016. Automated Monte Carlo Simulation of Proton Therapy Treatment Plans. *Technology in cancer research & treatment*, 15(6), pp.NP35–NP46.

Wedenberg, M. & Toma-Dasu, I., 2014. Disregarding RBE variation in treatment plan comparison may lead to bias in favor of proton plans. *Medical Physics*, 41(9), pp.091706–9.

Wedenberg, M., Lind, B.K. & Hårdemark, B., 2013. A model for the relative biological effectiveness of protons: The tissue specific parameter $\alpha/\beta$of photons is a predictor for the sensitivity to LET changes. *Acta Oncologica*, 52(3), pp.580–588.

Paper III

The impact of variable RBE in proton therapy for left-sided breast cancer when estimating normal tissue complications in the heart and lung.

Marteinsdottir M, Wang C, McNamara A, Depauw N, Jungwook S, Paganetti H.

Phys. Med. Biol. 66 (2021) 035023 (15pp)

The impact of variable RBE in proton therapy for left-sided breast cancer when estimating normal tissue complications in the heart and lung

Maria Marteinsdottir[1,2] (MSc), Chia-Chun Wang[1,3,4] (MD, PhD), Aimee McNamara[1,3] (PhD), Nicolas Depauw[1,3] (PhD), Jungwook Shin[1,3] (PhD), Harald Paganetti[1,3] (PhD)

[1]Department of Radiation Oncology, Massachusetts General Hospital, Boston, MA 02114, USA
[2]Faculty of Physical Sciences, University of Iceland, Dunhaga 5, IS-107 Reykjavik, Iceland
[3]Harvard Medical School, Boston, MA 02114, USA
[4]National Taiwan University Cancer Center, Taipei, Taiwan
* hpaganetti@mgh.harvard.edu

Abstract

The aim of this study was to evaluate the clinical impact of relative biological effectiveness (RBE) variations in proton beam scanning treatment (PBS) for left-sided breast cancer versus the assumption of a fixed RBE of 1.1, particularly in the context of comparisons with photon-based three-dimensional conformal radiotherapy (3DCRT) and volumetric modulated arc therapy (VMAT).

Ten patients receiving radiation treatment to the whole breast/chest wall and regional lymph nodes were selected for each modality. For PBS, the dose distributions were re-calculated with both a fixed RBE and a variable RBE using an empirical RBE model. Dosimetric indices based on dose-volume histogram analysis were calculated for the entire heart wall, left anterior descending artery (LAD) and left lung. Furthermore, normal tissue toxicity probabilities for different endpoints were evaluated.

The results show that applying a variable RBE significantly increases the RBE-weighted dose and consequently the calculated dosimetric indices increases for all organs compared to a fixed RBE. The mean dose to the heart and the maximum dose to the LAD and the left lung are significantly lower for PBS assuming a fixed RBE compared to 3DCRT. However, no statistically significant difference is seen when a variable RBE is applied. For a fixed RBE, lung toxicities are significantly lower compared to 3DCRT but when applying a variable RBE, no statistically significant differences are noted. A disadvantage is seen for VMAT over both PBS and 3DCRT. One-to-one plan comparison on 8 patients between PBS and 3DCRT shows similar results.

We conclude that dosimetric analysis for all organs and toxicity estimation for the left lung might be underestimated when applying a fixed RBE for protons. Potential RBE variations should therefore be considered as uncertainty bands in outcome analysis.

1 Introduction

In the United States, breast cancer is the most common cancer in women (1). It has been shown that the use of adjuvant radiation therapy for breast cancer following both breast-conserving surgery as well as mastectomy reduces recurrence and breast cancer deaths (2-7). However, radiation therapy implies irradiating organs close to the breast, thus increasing the risk of late toxicity. For left-sided breast cancer patients the heart is likely to receive considerable radiation dose. A study by Darby et al. (8) proposed the risk of major coronary events to increase linearly with the mean dose to the heart, with no apparent threshold. Furthermore, Nilsson et al. (9) reported an association between high dose areas in the heart from radiation therapy for breast cancer and coronary artery stenosis, which may contribute to post-treatment cardiac mortality. The highest dose areas are likely to be delivered to the anterior portion of the heart which

includes the left anterior descending coronary artery (LAD). Therefore, it has been suggested that in addition to assessing the dose to the heart it is important to further assess the dose to the LAD when estimating the eligibility of radiation treatment for breast cancer (10). Other important risk factors for breast cancer radiation treatment are lung complications and toxicities in the respiratory system. It has been shown in a study by Kubo et al. (11) that the lung volume within the radiation field is a significant risk factor for radiation pneumonitis and radiation induced bronchiolitis obliterans organizing pneumonia syndrome.

A commonly administered radiation therapy for breast cancer following breast-conserving surgery or mastectomy is three-dimensional conformal radiotherapy (3DCRT). The dose homogeneity for this treatment planning technique is however largely affected by variations in size and shape of the breast. For large breast sizes, hotspots may be created within the target and surrounding organs. Intensity modulated radiotherapy (IMRT) and volumetric modulated arc therapy (VMAT) allow for improved radiation conformity and homogeneity which may reduce hotspots. However, due to the large number of entry points used by these treatment planning techniques, the mean dose to the heart can potentially increase compared to 3DCRT (12-14). Furthermore, larger volumes of surrounding organs receive a low to intermediate dose suggesting an increased risk of secondary malignancies (15-17).

An alternative to photon-based radiation therapy for breast cancer is proton beam therapy. A common treatment setup consists of a single field generating a homogeneous dose distribution to the breast target volume. Organs behind the target volume are spared due to the rapid dose fall-off distal to the target. As protons are more biologically effective than photons, a lower physical dose is needed to cause the same level of biological effect. In clinical practice, the proton dose is scaled by a constant of 1.1, i.e. protons are assumed to be 10% more biologically effective than photons. This is represented by using a fixed relative biological effectiveness (RBE) of 1.1. However, it has been demonstrated *in vitro* that RBE depends on dose, linear energy transfer (LET), tissue type and endpoint (18). The clinical assumption of using a fixed RBE overlooks these variations. In a spread-out Bragg peak (SOBP), the LET and thus RBE values increase with depth and decreasing modulation width. It has been shown that for an α_x/β_x ratio of 3.5 Gy (an α_x/β_x ratio characteristic of late responding normal tissues (19)) and a standard fractionation, the biological dose calculated using a variable RBE estimated with the McNamara RBE model (20) is around 15% larger at the distal edge of SOBP compared to using a fixed RBE of 1.1 but this value depends on the modulation width and the beam characteristics (18,21). The biological dose distribution may also be shifted in relation to the physical dose distribution (22-24).

Comparisons between photon and proton based radiation treatments to left-sided breast cancer have previously been reported (13,25-28). Tommasino et al. (25) demonstrated that with the same level of tumor coverage a significant dose reduction to the heart and left lung is seen for intensity modulated proton therapy (IMPT) compared to IMRT. Ares et al. (13) reported that 3DCRT often compromised target coverage and increased the dose to heart, lung and contralateral breast. Applying IMRT gave better results but at the cost of increasing integral dose. However, IMPT improved the target coverage and reduced the dose to the organs at risk. The risk of cardiac toxicity was estimated in a study by Stick et al. (26). The study revealed that the predicted risk is limited for most patients when using modern photon therapy, yet proton therapy further reduced the risk. However, these studies all assume a fixed proton RBE of 1.1. As the heart and the lung are positioned downstream of the target, the question arises if a variable RBE will affect comparisons between proton and photon treatment options.

The aim of this study was to include estimated RBE variations in proton dose distributions for left-sided breast cancer and to compare to the assumption of using a constant RBE value of 1.1. The work is primarily concerned with the risk of normal tissue complications. Dosimetric analysis along with toxicity estimations for the heart, LAD and left lung were done for patients receiving proton pencil beam scanning (PBS) treatment. Furthermore, the analysis was compared to patients treated with 3DCRT and VMAT.

2 Material and Methods

2.1 Patient Cohort

After approval by our institutional review board (IRB) at Massachusetts General Hospital (protocol number: 2016P001950), 30 patients who received radiation treatment (RT) to the whole breast/chest wall (CW) and regional lymph nodes (i.e. internal mammary lymph nodes (IMN), axillary lymph nodes (AXL) and supraclavicular lymph nodes (SCV)) were selected, 10 patients for each RT modality: PBS, 3DCRT, and VMAT. Additionally, to allow for a one-to-one comparison between modalities, eight of the 3DCRT patients were re-planned for PBS.

Patients treated with PBS received 45.0 GyRBE[1] to the whole breast/chest wall (CW) and regional lymph nodes (AXL, SCV and IMN) with sequential 5.4 GyRBE to only the CW and IMN, a total of 50.4 GyRBE. A total of 28 fractions were administered, with 1.8 GyRBE per fraction. All 10 patients had mastectomies and 9 of the patients received reconstruction using implants before RT. The PBS patients selected had all been treated with a single-field configuration. As the increasing RBE with depth mainly impacts organs at risk downstream of the target, this may maximize the effect in the heart and lung when applying a variable RBE. The PBS treatment plans were optimized by experienced planners using an analytical dose calculation (ADC) algorithm with a fixed RBE of 1.1.

For 3DCRT, 9 patients received 50.4 Gy to the whole breast/CW and regional lymph nodes simultaneously in 28 fractions, whereas 1 patient received 55.8 Gy in 31 fractions due to a treatment break. Three patients had a sequential boost with electrons of 10-14 Gy to the CW. The RT planning technique consisted of one beam to the SCV and 4-6 beams to the CW in which a 3 mm bolus was used for dose build up to 30.6 Gy. All patients had mastectomies, with 6 patients receiving reconstruction using implants. Six of the patients treated with VMAT received 50.4 Gy in 28 fractions to the whole breast/CW and regional lymph nodes whereas three patients received 50.0 Gy in 25 fractions and 1 patient received 58.8 Gy in 25 fractions. The RT planning technique consisted of 4 beams to the treatment area. Seven patients had mastectomies with only two patients not undergoing breast reconstruction prior to treatment.

The RTOG (Radiation Therapy Oncology Group) breast and RadComp (Radiotherapy Comparative Effectiveness) contouring atlases were used for delineation of both target structures and organs at risk (OARs). Target structure included the whole breast/CW, IMN, AXL and SCV. The prosthesis and overlying skin were included in the chest wall target for patients receiving breast reconstruction.

Patients receiving 3DCRT and VMAT were treated using a breath-hold technique. A free-breathing technique was used for patients receiving PBS. This is in accordance to our institutional guidelines. Breath-hold for breast cancer is of limited value in PBS as the proton beam range is not significantly affected by breathing (29,30).

Normal tissue dose constraints follow institutional guidelines which vary between treatment modalities. Constraints to the heart included a maximum mean dose of 1.5 GyRBE for PBS, whereas a maximum mean dose of 2.5 Gy and 5.0 Gy for 3DCRT and VMAT, respectively. For the ipsilateral lung, the constraints included <20% of the lung volume to receive 20 GyRBE for PBS whereas <35% of the lung volume to receive 20 Gy for 3DCRT. For VMAT, the constraints included <65% of the ipsilateral lung volume to receive 5 Gy and <30% to receive 20 Gy. The target coverage was maximized in all cases while meeting normal tissue constraints. Furthermore, all patients were planned by experienced treatment planners following clinical practice (31).

[1] The unit GyRBE is used for RBE-weighted absorbed dose.

2.2 Dose Calculations and Analysis

Dose distributions from analytical dose calculations (ADC) were collected from the treatment planning system RayStation (Raysearch Laboratories, Sweden) for 3DCRT and VMAT and Astroid (.decimal, Sanford, FL) for PBS. The analysis in this work was performed by studying dose plans and did not consider reported clinical outcomes. Dose-volume histogram (DVH) analyses were performed for the heart, LAD, and left lung and following dosimetric indices were calculated:

- Mean dose of the organ volume.
- D02, which is the maximum dose that covers 2% of the volume and represents the maximum organ dose.
- gEUD (generalized equivalent uniform dose), referring to the dose that, if given uniformly to the entire organ, is believed to yield the same complication rate as the true dose distribution.
- VxxGy, referring to the fractional volume of the organ receiving xx Gy (photons) or GyRBE (protons).

The following equation is used to evaluate gEUD:

$$\mathrm{gEUD} = (\sum_{i=1}^{M} v_i \, D_i^a)^{1/a}$$

where M is the total number of DVH dose bins in the anatomic structure of interest, v_i is the fractional organ volume receiving a dose D_i and a is the tissue-specific parameter that describes the volume effect. For normal tissues that are assumed to follow a parallel- organ architecture, a is likely to be close to unity whereas large positive values of a indicate normal tissues following a serial-organ architecture. The tissue-specific parameter a was set to 3 for the heart and the LAD (32). For the left lung, a is set to 1, thus making gEUD equal to the mean dose.

Figure 1 shows examples of typical dose distributions for the three different RT modalities. The patients in the examples all have implants. Furthermore, all received 1.8 Gy per fraction (GyRBE in the case of PBS) for 28 fractions. The 3DCRT patient also received an electron boost of 10 Gy. The maximum dose increase due to electron boosts for all three patients is <0.1 Gy to the heart and LAD and should therefore not interfere with the analysis. This is not the case for the left lung where the dose increase is significant and is therefore considered. The figure also reveals a contralateral breast exposure for VMAT.

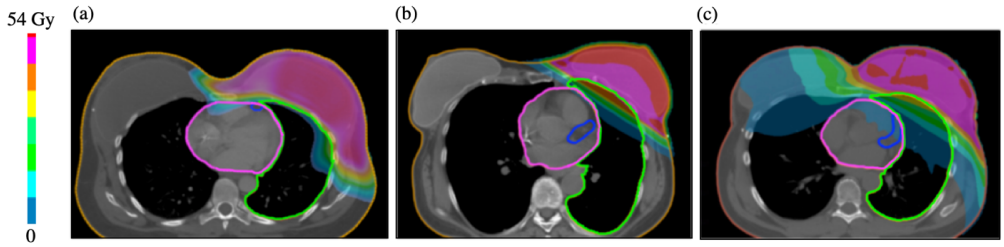

Figure 1. Examples of dose distribution for (a) PBS with RBE = 1.1 (b) 3DCRT (c) VMAT. Skin (orange), heart (pink), LAD (blue) and left lung (green) are contoured.

2.3 Monte Carlo Calculations

For the PBS plans, the dose distributions were recalculated on a voxel-by-voxel basis using the Monte Carlo (MC) toolkit TOPAS (33,34). The number of primary particles applied resulted in an uncertainty in dose to the target of around 2%. Furthermore, the dose-averaged linear energy transfer ($\mathrm{LET_d}$) was calculated

voxel-by-voxel with TOPAS. The McNamara model (20) was used to calculate the relative biological effect (RBE) for clonogenic cell survival for the proton plans. The model is a phenomenological model and is based on the linear-quadratic (LQ) model. It is a function of physical dose, LET_d and the tissue specific parameter α_x/β_x ratio. The α_x/β_x ratio for the heart was chosen to be 3.0 Gy (35). For the LAD, α_x/β_x ratio was estimated to be the same as for the heart whereas for the left lung it was considered to be 4.0 Gy (36). To evaluate the impact on applying a variable RBE, the PBS dose plans were not re-optimized when re-calculated using Monte Carlo (MC) simulations because our aim was to provide insight into potential RBE effects in current clinical practice.

To evaluate the uncertainty associated with each α_x/β_x ratio, a Gaussian distribution of α_x/β_x ratios was created in which the nominal α_x/β_x ratio was set as the mean value and the standard deviation was estimated from the reported 95% confidence intervals. To ensure positive α_x/β_x values, the Gaussian distribution were truncated bilaterally at the distance from the mean value to zero. For each patient, 1000 random α_x/β_x ratios were extracted from the Gaussian distribution, and with the LET_d and the dose distributions obtained from the MC simulations, the corresponding RBE-weighted dose distributions were estimated. The cumulative DVHs for each RBE-weighted dose distribution was stored, resulting in a total of 10000 DVHs for each organ at risk. Finally, the NTCP values were estimated for each generated DVH.

2.4 NTCP

The analysis of the NTCP for the heart was performed with a linear model proposed by Darby et al (8) ($NTCP_{linear}$). The paper estimates that rates of major coronary events increase linearly with the mean dose to the heart by 7.4% per Gy. The proportional increase in rate of major coronary events per Gy of radiation was modeled as

$$\mathrm{NTCP}_{\mathrm{linear}} = B_S(1 + KX)$$

where B_s is the risk of coronary events in the absence of radiation treatment and is considered to be 1.6%, assuming an age of 50 years at time of irradiation and an attained age of 70 years, X is the radiation dose in Gy and K is the increase in the rate of major coronary events per Gy, i.e. 7.4% per Gy. The parameter B_s varies with both the age of irradiation and the attained age, in which 50 and 70 years, respectively, was considered a conservative choice.

The NTCP for the heart was furthermore evaluated using the relative seriality model by Källman et al (37) ($NTCP_{serial}$)

$$\mathrm{NTCP}_{\mathrm{serial}} = \{1 - \prod_{i=1}^{M}[1 - P(D_i)^s]^{v_i}\}^{1/s}$$

Where M is the total number of dose bins and v_i is the fractional volume receiving a dose D_i. The probability function, $P(D_i)$, is based on the Poisson statistical model and is defined as

$$P(D_i) = 2^{\exp[e\gamma\left(1-\frac{D_i}{\mathrm{D50}}\right)]}$$

where γ is the maximum value of the normalized slope gradient, D50 is the dose given to the entire organ that results in 50% complication risk and e is the base of the natural logarithm. The parameters involved in the analysis with cardiac mortality as the endpoint were taken from Gagliardi et al (38) where dose giving 50% of complication probability, D50, is 52.3 Gy, the normalized dose-response gradient γ is 1.28 and the relative sensitivity parameter s is 1.

The normal tissue toxicity to the LAD was estimated using a logistic model by Moignier et al (39). An increase in risk of coronary stenosis is described as

$$\mathrm{OR}_{\mathrm{logistic}} = \mathrm{OR}^{D_{\mathrm{med}}}$$

where OR is the odds ratio and is considered to be 1.049 and D_{med} is the median dose to the LAD.

The relative seriality model was further used to estimate radiation pneumonitis of Grade 0-2 according to modified NCIC-CTC (National Cancer Institute of Canada Common Toxicity Criteria) (40) and Grade 2 (41) where the collection of the clinical data was retrospective. For Grade 0-2 pneumonitis, the parameter D50 is considered to be 16.3 Gy, γ is 1.08 and s is 0.15, whereas for Grade 2 the parameters are 30.1 Gy for D50, 0.966 for γ and 0.012 for *s*.

2.5 Statistics

Statistical analysis on comparisons between PBS calculations having a fixed RBE of 1.1 to a variable RBE were performed using the Wilcoxon signed rank test (section 3.1). Furthermore, PBS comparisons to 3DCRT and VMAT were assessed using the Wilcoxon rank sum test for different patient groups (section 3.2) and the Wilcoxon signed rank test for the same patient group (section 3.3). All tests were performed using MATLAB version 2016b (Mathwork Inc.). We define statistical significance as rejecting the null hypothesis at 1% level to account for multiple comparisons.

3 Results

3.1 Proton Calculations

Figure 2 displays the mean and maximum dose (represented by D02) for the heart, the LAD and the left lung for PBS having a fixed RBE of 1.1 and variable RBE. Furthermore, dosimetric indices of interest, VxxGy, for each organ are shown. Figure 3 displays the mean and maximum dose-averaged linear energy transfer ($\mathrm{LET_d}$) values for the heart, the LAD and the left lung for all patients treated with PBS. Voxels having doses smaller than 1% of the prescription dose are masked off in the $\mathrm{LET_d}$ distributions for the mean and maximum $\mathrm{LET_d}$ calculations, to eliminate hotspots of high $\mathrm{LET_d}$ values located in areas with very low dose values that are clinically in significant. The maximum $\mathrm{LET_d}$ is calculated as the maximum $\mathrm{LET_d}$ received by 0.1% of the volume to further exclude outliers. The figure further exemplifies the dose distribution for PBS having a fixed RBE of 1.1 for one patient and the corresponding $\mathrm{LET_d}$ values. Areas with high $\mathrm{LET_d}$ values (>12 keV/µm), located mostly in the heart and the left lung, are accompanied with low dose values (<2.5 GyRBE). Yet, the application of a variable RBE increases all dosimetric indices compared to the fixed RBE for each organ, as shown in Figure 2. The difference is statistically significant for all estimated indices. Furthermore, the normal tissue toxicity probability increases for all organs when applying a variable RBE, resulting in a statistically significant difference for each organ compared to a fixed RBE. The application of a linear NTCP model to major coronary complications for PBS results in a small increase of ~2.4% when applying a variable RBE compared to fixed RBE of 1.1, whereas the normal tissue toxicity for the LAD increases by ~5.6%. Additionally, applying a variable RBE increases the median value of the estimated NTCP by a factor > 2.1 compared to a fixed RBE for both stages. Estimated risk values can be found in Table 1, Table 2 and Table 3 for the heart, the LAD and the left lung, respectively (statistical analysis are not shown). The increase in the estimated risk values when applying a variable RBE in Table 1 and Table 2 is not evident due to the small number of significant figures.

These results do not consider the uncertainties of the RBE estimation due to the range of α_x/β_x ratios. Figure 4 illustrates the effect of including the uncertainty in the α_x/β_x ratio, where α_x/β_x ratios were randomly selected from a Gaussian distribution. Colorwashed areas in Figure 4 represent this uncertainty in the DVH estimation for one patient. When considering uncertainties in α_x/β_x, the DVH estimation broadens substantially for all organs. Figure 5 shows the spread of estimated NTCP values for all 10

patients, where the NTCP values were calculated 1000 times for each patient resulting in 10000 NTCP estimations. The figure reveals a large spread of NTCP values, where low α_x/β_x ratios increase the risk estimation.

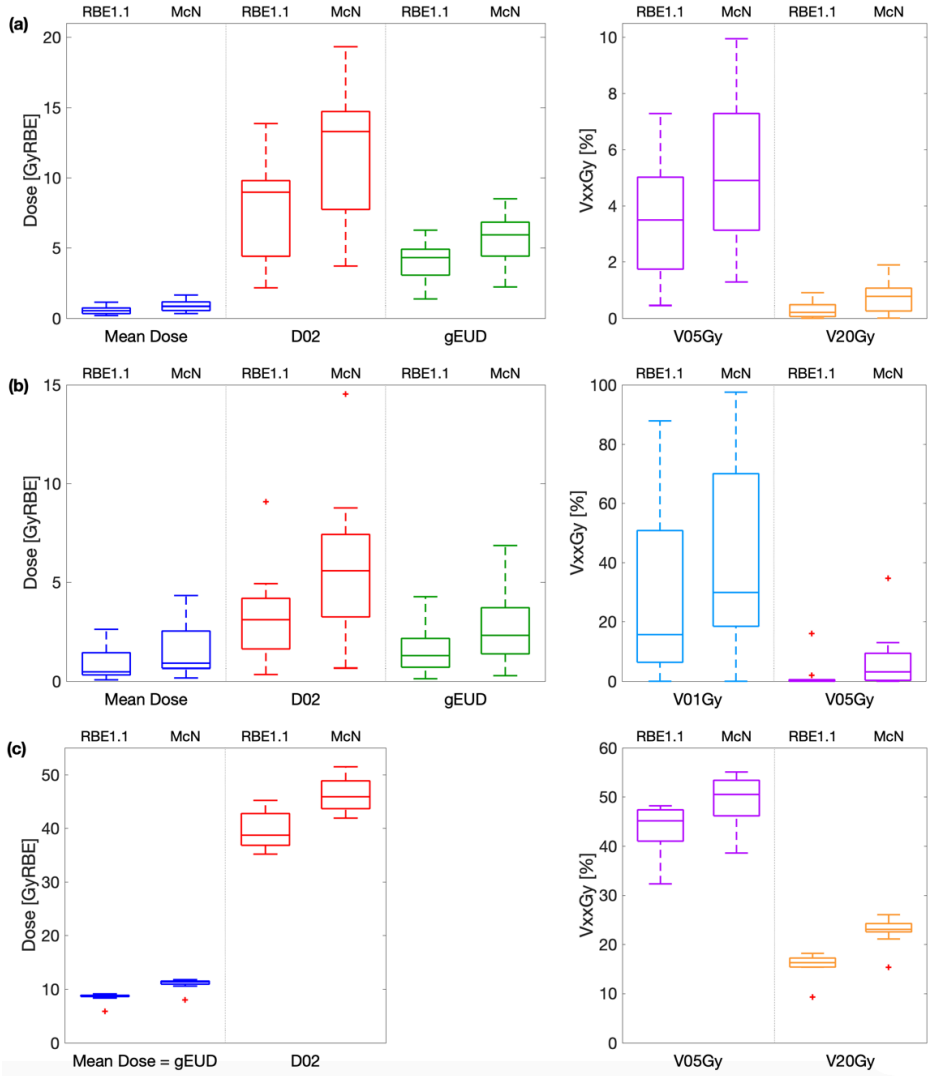

Figure 2. Box plot of dosimetric indices for proton beam scanning; (a) the heart, (b) the LAD, and (c) the left lung. The mean dose, maximum dose (indicated with D02)), gEUD and VxxGy, which refers to the fractional volume of the structure receiving xx GyRBE. Each box from top to bottom represents the maximum, first quartile, median, third quartile and minimum of the distribution over all patients. The outliers, marked with red plus signs, represent data points that fall more than 1.5 times the interquartile range away from the top and bottom of the box. *Abbreviations:* RBE = relative biological effectiveness. RBE1.1 = fixed RBE of 1.1. McN = McNamara RBE model.

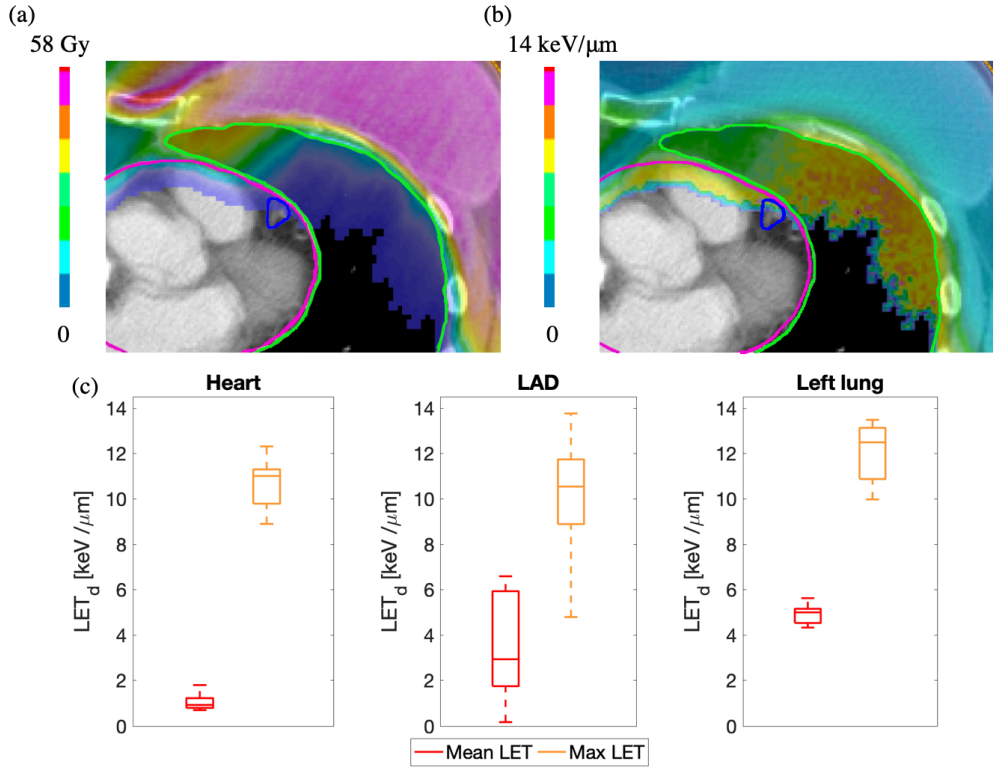

Figure 3. Demonstration of dose distribution for PBS with RBE = 1.1 in (a) and LET_d distribution in (b) for the same plan. Heart (pink), LAD (blue) and left lung (green) are contoured. Voxels having doses smaller than 1% of the prescription dose are masked off for both the dose and the LET_d distribution for better visualization. (c) shows mean LET_d and maximum LET_d values for all patients going through proton beam scanning treatment. Each box from top to bottom represents the maximum, first quartile, median, third quartile and minimum of the distribution over all patients. The outliers, marked with red plus signs, represent data points that fall more than 1.5 times the interquartile range away from the top and bottom of the box.

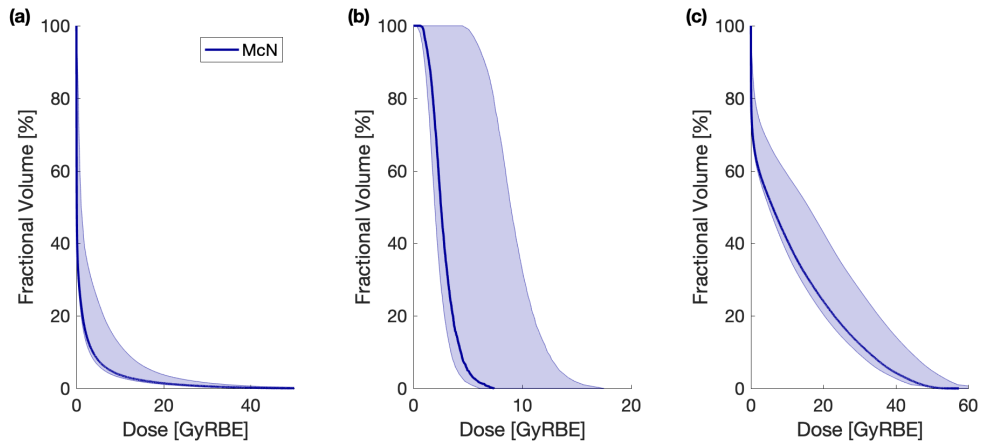

Figure 4. Cumulative dose-volume histograms (DVHs) for one patient calculated using the McN model for proton beam scanning; (a) the heart, (b) the LAD, and (c) the left lung. The solid lines represent α_x/β_x = 3 Gy for the heart and the LAD and α_x/β_x = 4.0 Gy for the left lung. The shaded areas in the DVHs indicate the range of the α_x/β_x ratio, with α_x/β_x extracted randomly from a Gaussian distribution. *Abbreviations:* McN = McNamara RBE model.

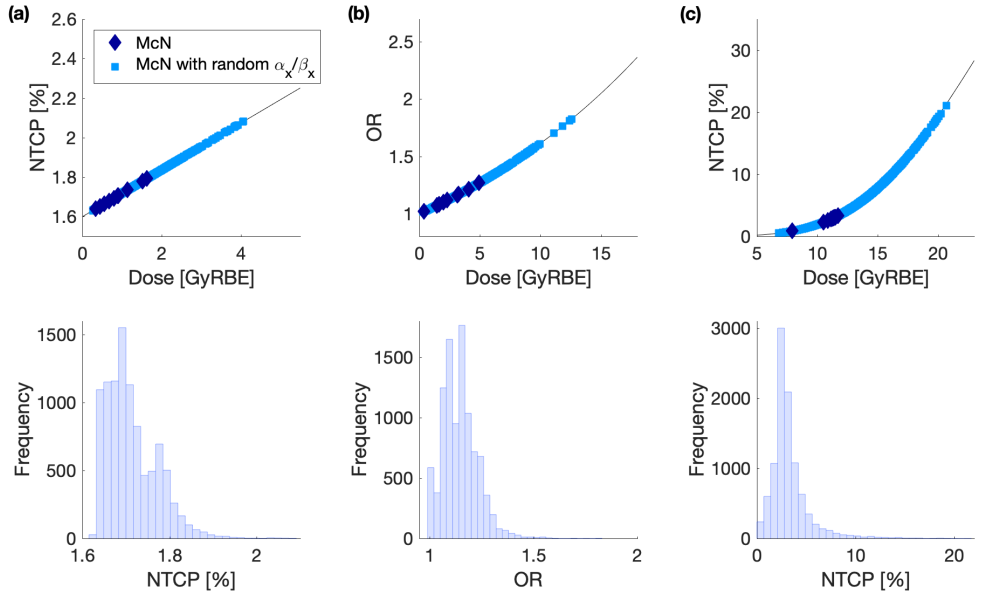

Figure 5. The risk of late toxicities for 10 patients calculated using the McN model for proton beam scanning; (a) the heart - NTCP for the endpoint of major coronary events (b) the LAD - OR for the endpoint of coronary stenosis, and (c) the left lung - NTCP for the endpoint of pneumonitis, Grade 2. Top figures: The dark blue diamonds represent estimated NTCP and OR with α_x/β_x = 3 Gy for the heart and the LAD and α_x/β_x = 4.0 Gy for the left lung. The light blue squared indicate the range of the α_x/β_x ratio, with α_x/β_x extracted randomly from a Gaussian distribution. Lower figures: Histogram results for the randomly extracted α_x/β_x ratios. *Abbreviations:* McN = McNamara RBE model. NTCP = normal tissue complication probability. OR = odds ratio.

3.2 Comparison to Photon Treatments

The dosimetric results from the PBS cohort were further compared to patients treated with 3DCRT and VMAT to assess whether a variable RBE would impact the comparison between these modalities. For the PBS data, the nominal α_x/β_x ratio was applied.

3.2.1 Heart

Table 1 reflects the calculated dosimetric indices within the heart for all modalities. For 3DCRT, all patients are within the clinical constraints of the heart whereas one patient (i.e. 10% of the sample) exceeds the constraints for VMAT, having a mean dose of 5.5 Gy because of difficulties of ensuring dose coverage to the target while simultaneously maintaining the dose constraints to the heart and the left lung. For PBS assuming a fixed RBE of 1.1, all patient cases remain within the clinical constraints, however clinical constraints were exceeded for one patient (10% of the sample) when applying a variable RBE, with mean dose of 1.6 GyRBE.

VMAT is outperformed by both 3DCRT and PBS when comparing the mean dose to the heart. As mentioned in section 2.1, the dose constraints for the mean dose to the heart are significantly higher for VMAT compared to the other modalities (i.e. 5 Gy for VMAT versus 1.5 GyRBE and 2.5 Gy for PBS and 3DCRT, respectively). The mean dose for PBS having a fixed RBE is significantly lower compared to both 3DCRT and VMAT. However, applying a variable RBE increases the mean dose to the heart compared to a fixed RBE, resulting in no statistically significant difference when comparing to 3DCRT. The difference in the maximum dose (D02) between PBS having a fixed RBE and the photon modalities is not statistically significant. However, application of a variable RBE increases the median value of the maximum dose by 4.3 GyRBE leading to a statistically significant higher maximum dose compared to 3DCRT. This is caused by an RBE increase due to the elevated LET values at the end of the proton field located within the heart volume. The median value of the gEUD parameter is significantly lower for IMRT compared to PBS with both a fixed and a variable RBE.

The majority of the heart volume received a low dose of 1 Gy for VMAT for all patients. This is not the case for either 3DCRT or PBS. For 3DCRT, around 35% of the volume of the heart received a dose of 1 Gy, whereas for PBS the volume of the heart covered by a dose of 1 GyRBE is around 7% for a fixed RBE of 1.1, but increases to 10% when applying a variable RBE. For all modalities, the volume of the heart receiving 20 Gy is <1%.

The median value of the linear NTCP model to major coronary complications is lower for PBS with statistical significance in relation to VMAT, irrelevant of using a fixed or a variable RBE. However, the estimated NTCP is significantly lower for PBS (constant RBE) with statistical significance compared to 3DCRT but not statistically significant when a variable RBE is applied. NTCP calculations using the relative seriality model with cardiac mortality as the endpoint revealed negligible probability of complications for all modalities.

Table 1. Heart - Median (range) of dosimetric indices and normal tissue complication probability for the appropriate endpoints.

	Protons - PBS		Photons	
Heart	RBE1.1	McN	3DCRT	VMAT
	Dosimetric Analysis			
Mean dose	0.5*° (0.2-1.1)	0.8° (0.3-1.6)	1.1 (0.7-1.7)	3.9 (3.3-5.5)
D02	9.0 (2.1-13.9)	13.3* (3.7-19.3)	4.2 (3.4-5.5)	9.4 (6.5-19.6)
gEUD	4.3* (1.4-6.3)	5.9* (2.2-8.5)	1.9 (1.5-2.6)	5.3 (3.9-8.7)
V01Gy	7.4*° (4.6-18.3)	9.6*° (7.1-23.7)	34.6 (18.8-65.0)	100.0 (98.7-100.0)
V05Gy	3.5° (0.4-7.3)	4.9*° (1.3-9.9)	0.9 (0.5-2.7)	19.2 (8.8-46.3)
V20Gy	0.2* (0.0-0.9)	0.8* (0.0-1.9)	0.0 (0.0-0.0)	0.3 (0.0-1.9)
V25Gy	0.0* (0.0-0.4)	0.3* (0.0-1.2)	0.0 (0.0-0.0)	0.1 (0.0-1.1)
	NTCP [%]			
Endpoint				
major coronary events	1.7*° (1.6-1.7)	1.7° (1.6-1.8)	1.7 (1.7-1.8)	2.1 (2.0-2.2)
cardiac mortality	0.0* (0.0-0.0)	0.0* (0.0-0.1)	0.0 (0.0-0.0)	0.0 (0.0-0.1)

Mean dose, D02 and gEUD are given in Gy (photons) or GyRBE (protons).
VxxGy refers to the fractional volume of the structure receiving xx Gy (photons) or GyRBE (protons) and is given in [%].
*Statistically significant difference between 3DCRT against PBS for 1% level.
°Statistically significant difference between VMAT against PBS for 1% level.
Abbreviations: 3DCRT = three-dimensional conformal radiotherapy. VMAT = volumetric modulated arc therapy. PBS = proton beam scanning. RBE = relative biological effectiveness. RBE1.1 = fixed RBE of 1.1. McN = McNamara RBE model. NTCP = normal tissue complication probability.

3.2.2 LAD

The dosimetric results and statistical analysis for the LAD are shown in Table 2. The mean dose to the LAD is higher than the mean dose to the heart for all modalities. Furthermore, for PBS the mean dose is significantly lower with statistical significance when compared to the photon modalities, irrelevant of using a fixed or a variable RBE. Furthermore, the gEUD is significantly lower for PBS with a fixed RBE compared to photon modalities. The maximum dose (D02) to the LAD for 3DCRT and VMAT is higher compared to the maximum dose to the heart. This is not the case for PBS where the maximum dose to the LAD is lower than for the heart. Furthermore, the maximum dose is significantly lower for PBS having a fixed RBE of 1.1 in relation to both 3DCRT and VMAT. However, taking a variable RBE into account increases the average maximum dose to the LAD by 2.5 GyRBE, resulting in no statistically significant difference in the maximum dose between PBS and 3DCRT.

Both 3DCRT and PBS outperform VMAT in terms of dose to the LAD. VMAT is significantly larger for all dosimetric indices in relation to PBS. Additionally, 69.7% of the volume of the LAD received a dose of 5 Gy for VMAT compared to 13.6% of the volume for 3DCRT. Comparing to PBS reveals a statistically significant difference as the volume of LAD covered by an RBE-weighted dose of 5 GyRBE is 0.2% and 3.2% for a fixed and variable RBE, respectively.

The application of a normal tissue toxicity model for the LAD (Table 2) reveals a statistically significant reduction in risk for PBS compared to the photon modalities for both a fixed or a variable RBE.

Table 2. LAD - Median (range) of dosimetric indices and odds ratio values for the appropriate endpoint.

	Protons - PBS		Photons	
LAD	RBE1.1	McN	3DCRT	VMAT
	Dosimetric Analysis			
Mean dose	0.5*° (0.1-2.6)	0.9*° (0.2-4.3)	3.3 (2.2-5.5)	6.2 (5.5-12.8)
D02	3.1*° (0.3-9.1)	5.6° (0.7-14.5)	6.9 (5.7-14.5)	12.0 (7.5-31.7)
gEUD	1.3*° (0.1-4.3)	2.3° (0.3-6.9)	3.9 (3.2-7.3)	6.8 (5.6-16.4)
V01Gy	15.6*° (0.0-87.8)	29.9*° (0.0-97.5)	97.4 (72.9-100.0)	100.0 (100.0-100.0)
V05Gy	0.2*° (0.0-16.0)	3.2*° (0.0-34.7)	13.6 (5.1-50.8)	69.7 (60.9-91.9)
	OR			
Endpoint				
coronary stenosis	1.1*° (1.0-1.2)	1.1*° (1.0-1.3)	1.2 (1.2-1.6)	1.5 (1.3-2.7)

Mean dose, D02 and gEUD are given in Gy (photons) or GyRBE (protons).
VxxGy refers to the fractional volume of the structure receiving xx Gy (photons) or GyRBE (protons) and is given in [%].
*Statistically significant difference between 3DCRT against PBS for 1% level.
°Statistically significant difference between VMAT against PBS for 1% level.
Abbreviations: 3DCRT = three-dimensional conformal radiotherapy. VMAT = volumetric modulated arc therapy. PBS = proton beam scanning. RBE = relative biological effectiveness. RBE1.1 = fixed RBE of 1.1. McN = McNamara RBE model. OR = odds ratio.

3.2.3 Left lung

The dosimetric results for the left lung are shown in Table 3. For 3DCRT, all patients remain within the clinical constraints. This is also the case for PBS with a fixed RBE of 1.1 where less than 20% of the lung volume receives 20 GyRBE for all patients. However, the clinical constraints are exceeded for all patients except one (10% of the sample) when applying a variable RBE. For VMAT, two patients (20% of the sample) have a minor excess in the clinical constraints for V05Gy where 66% of the left lung volume received 5 Gy. The mean dose is significantly lower for PBS with a fixed RBE of 1.1 in relation to both 3DCRT and VMAT. However, applying a variable RBE increases the mean dose for PBS by 2.5 GyRBE, hence eliminating the statistical difference in the mean dose between the proton and photon modalities. Similarly, no statistically significant difference is seen in the maximum dose (D02) for PBS after applying a variable RBE compared to both 3DCRT and VMAT.

The volume of the left lung covered by a dose of 5 Gy (GyRBE in the case of PBS) is significantly larger for PBS with a variable RBE compared to 3DCRT but significantly lower in relation to VMAT for both a fixed or a variable RBE. However, a larger volume of the lung received 40 Gy for 3DCRT compared to both PBS and VMAT. The fractional volume, represented by V40Gy, was 12.0% for 3DCRT whereas only 6.1% for VMAT. Furthermore, applying a variable RBE for PBS increases V40Gy from 1.6% for a fixed RBE to 4.4% which is smaller compared to 3DCRT.

Table 3 shows the results of the NTCP calculations for pneumonitis of two different stages. The difference in the estimated NTCP for PBS with a fixed RBE is significantly lower in relation to both 3DCRT and VMAT for both stages but no statistically significant difference to 3DCRT and VMAT can be seen when applying a variable RBE. The calculations were repeated while excluding the three 3DCRT patients receiving electron boost. This resulted in slightly lower NTCP values for both stages without changing the statistical analysis results between 3DCRT and PBS.

Table 3. Left lung - Median (range) of dosimetric indices and normal tissue complication probability values for the appropriate endpoints.

	Protons - PBS		Photons	
Left lung	RBE1.1	McN	3DCRT	VMAT
	Dosimetric Analysis			
Mean dose = gEUD	8.7*° (5.8-9.1)	11.3 (7.9-11.7)	10.9 (8.4-12.8)	12.8 (10.1-14.1)
D02	38.7*° (35.2-45.2)	45.9 (41.9-51.5)	48.6 (43.0-51.1)	46.7 (43.5-51.1)
V05Gy	45.1° (32.3-48.2)	50.5*° (38.6-55.1)	38.7 (28.3-44.8)	61.1 (49.8-66.2)
V20Gy	16.3*° (9.3-18.2)	23.0 (15.3-26.0)	21.7 (16.3-25.8)	22.9 (15.4-26.2)
V40Gy	1.6*° (0.7-4.2)	4.4* (2.7-7.5)	12.0 (6.4-15.9)	6.1 (3.4-8.9)
	NTCP [%]			
Endpoint				
Pneumonitis, Grade 0-2	12.1*° (3.0-14.1)	26.5 (9.7-28.5)	26.0 (13.6-37.9)	32.6 (16.7-40.9)
Pneumonitis, Grade 2	1.1*° (0.3-1.3)	2.7 (0.8-3.1)	2.4 (1.0-4.1)	4.2 (1.9-5.9)

Mean dose, D02 and gEUD are given in Gy (photons) or GyRBE (protons).
VxxGy refers to the fractional volume of the structure receiving xx Gy (photons) or GyRBE (protons) and is given in [%].
*Statistically significant difference between 3DCRT against PBS for 1% level.
°Statistically significant difference between VMAT against PBS for 1% level.
Abbreviations: 3DCRT = three-dimensional conformal radiotherapy. VMAT = volumetric modulated arc therapy. PBS = proton beam scanning. RBE = relative biological effectiveness. RBE1.1 = fixed RBE of 1.1. McN = McNamara RBE model. NTCP = normal tissue complication probability.

3.3 Analysis for the Same Patient Group

The analysis given above presents a fair comparison as patients were analyzed according to the patient specific treatment selection and the treatment actually delivered. Nevertheless, eight of the 3DCRT patients were re-planned for PBS to allow for a one-to-one comparison. For the PBS data, the nominal α_x/β_x ratio was applied.

Figure 6 and Table 4 show the dosimetric results and the estimated toxicity probabilities for the heart, the LAD and the left lung. For the heart and the left lung, the dosimetric analysis and the estimated NTCP results of the re-planned PBS patients were similar to the clinically treated PBS patients. However, a small difference was seen in the dose distribution to the LAD, where the re-planned PBS patients received a slightly higher dose compared to the clinically treated PBS patients. The complication probability for the LAD is therefore no longer statistically significant when applying a variable RBE compared to the 3DCRT. This difference can be explained by a small change in clinical practice between the recently re-planned patients and the retrospective clinically treated PBS patients. The mean dose of the LAD was allowed to be slightly higher than that in current practice, i.e. the expected mean dose to the LAD went from ~1 GyRBE to ~1.5 GyRBE.

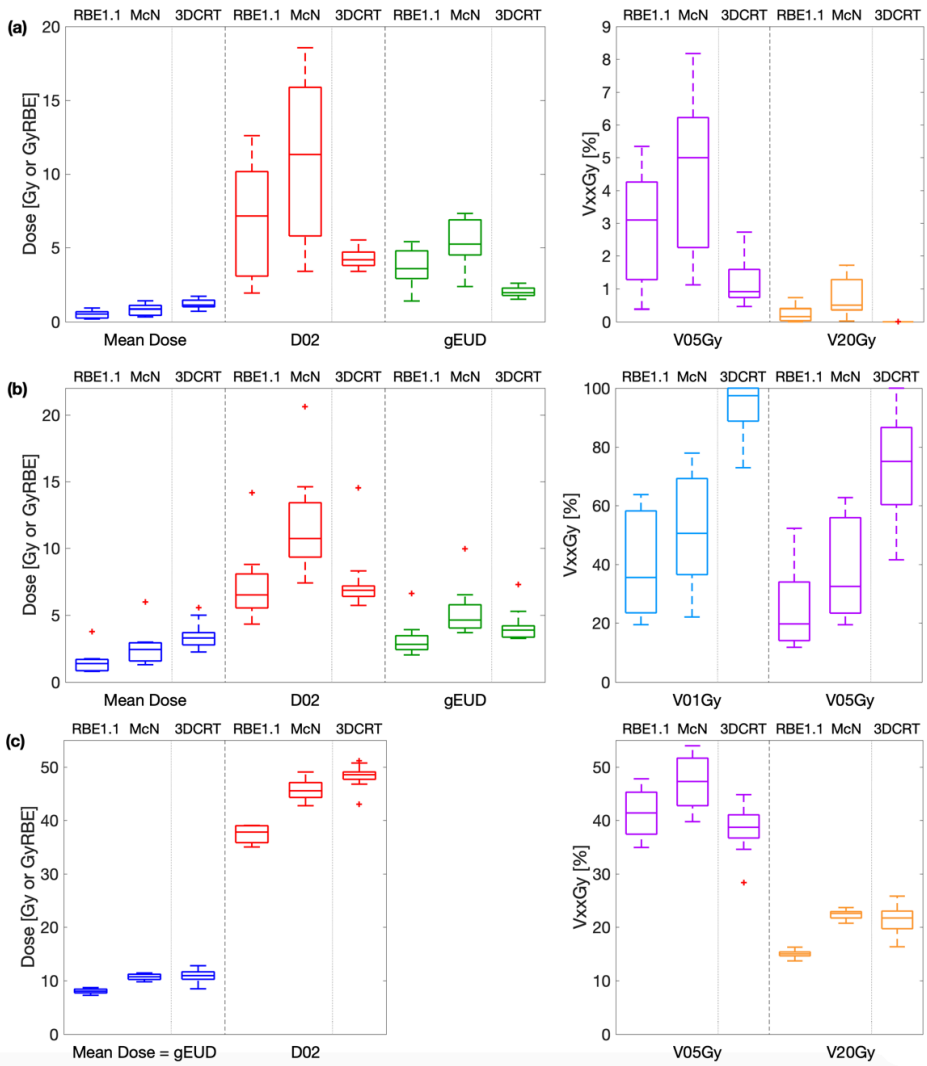

Figure 6. Box plot of dosimetric indices for proton beam scanning; (a) the heart, (b) the LAD, and (c) the left lung. The mean dose, maximum dose (indicated with D02)), gEUD and VxxGy, which refers to the fractional volume of the structure receiving xx Gy (photons) or GyRBE (protons). Each box from top to bottom represents the maximum, first quartile, median, third quartile and minimum of the distribution over all patients. The outliers, marked with red plus signs, represent data points that fall more than 1.5 times the interquartile range away from the top and bottom of the box. *Abbreviations:* RBE = relative biological effectiveness. RBE1.1 = fixed RBE of 1.1. McN = McNamara RBE model. 3DCRT = three-dimensional conformal radiotherapy.

Table 4. Median (range) of estimated toxicity risks for appropriate endpoints.

	Protons - PBS		Photons
Endpoint	RBE1.1	McN	3DCRT
	Heart - NTCP [%]		
major coronary events	1.7* (1.6-1.7)	1.7 (1.6-1.8)	1.7 (1.7-1.8)
cardiac mortality	0.0* (0.0-0.0)	0.0* (0.0-0.0)	0.0 (0.0-0.0)
	LAD - OR		
coronary stenosis	1.1* (1.1-1.4)	1.2 (1.1-1.6)	1.2 (1.2-1.6)
	Left Lung - NTCP [%]		
Pneumonitis, Grade 0-2	9.3* (7.3-11.3)	23.2 (19.5-26.5)	26.0 (13.6-37.9)
Pneumonitis, Grade 2	0.8* (0.6-1.1)	2.2 (1.6-2.8)	2.4 (1.0-4.1)

*Statistically significant difference between 3DCRT against PBS for 1% level.
Abbreviations: 3DCRT = three-dimensional conformal radiotherapy. PBS = proton beam scanning. RBE = relative biological effectiveness. RBE1.1 = fixed RBE of 1.1. McN = McNamara RBE model. NTCP = normal tissue complication probability. OR = odds ratio.

4 Discussion

In this study, the clinical impact of using a variable RBE in proton therapy for left-sided breast cancer was analyzed and compared to using a fixed RBE of 1.1. Dosimetric analysis to organs at risk and NTCP evaluations were performed for 10 patients. Applying a variable RBE significantly increased the RBE-weighted dose and the estimated NTCP for all organs. Incorporating the associated uncertainties of the RBE estimation due to the range of the α_x/β_x ratio revealed a substantial spread in the estimated NTCP values, indicating interpatient variability.

PBS treated patients were compared to 3DCRT and VMAT treatments. Our analysis showed that applying a variable RBE for PBS could have a substantial effect on the dose distributions. However, for the estimated normal tissue toxicity probabilities, the impact due to the variable RBE application was significantly larger for the left lung than for the heart and the LAD with a considerable risk increase of pneumonitis for both stages. Consequently, the benefit of PBS with a fixed RBE in relation to the conventional 3DCRT for the left lung decreased when a variable RBE was applied. s

A clear disadvantage is seen for VMAT over both PBS and 3DCRT in the mean dose to the heart and to the LAD. This can be explained by the higher normal dose tissue constraints to the heart for VMAT, see section 2.1. However, the results may be biased as VMAT treatments are often prescribed when 3DCRT fails due to high heart and lung doses.

Two different toxicity end-points are often considered for the heart; cardiac mortality and major coronary events. It has been reported that for partial irradiation the dosimetric index V25Gy<10% is associated with <1% probability of cardiac mortality (35). This is in line with our results as V25Gy is 0.5% or smaller for all treatment modalities and consequently the estimated NTCP with cardiac mortality as an endpoint is negligible.

Eight 3DCRT patients were re-planned for PBS to allow for a one-to-one comparison. It should be noted that some patients undergoing PBS treatment would not have been considered for 3DCRT treatment due to their complex anatomy, while they might have been selected for VMAT. Therefore, re-planning 3DCRT patients for PBS was considered to reduce biased results against 3DCRT. No significant difference was seen between the re-planned PBS and the clinically treated PBS cases compared to the 3DCRT plans.

A limitation of our study is the reliance of an RBE model for clonogenic cell survival *in vitro*, which may not result in realistic RBE values for the clinical endpoints considered. The RBE for clonogenic cell survival *in vitro* are rough estimates of RBE values related to normal tissue toxicity. For instance, a retrospective analysis of late-phase lung-density changes for breast cancer patients radiated to the chest wall showed that late-phase radiographic changes in the lung might be associated with a proton RBE exceeding 3.0 (42). On the other hand, a recently published study on RBE effects at the end of range in breast cancer patients focusing on rib fractures showed that, at least for this endpoint, RBE from clonogenic cell survival can be a valuable estimate (43). Our study aims at providing guidance for considering potential RBE effects in breast cancer treatment planning. Caution should be taken as RBE values not only depend on endpoint and models but also on α_x/β_x ratios that are associated with uncertainties causing variations in RBE values (21,44,45).

Another potential limitation is the use of outcome models derived from photon data for patients treated with protons. Photon dose distributions are typically more homogeneous to the organs at risk than proton dose distributions, which may limit the applicability of photon therapy derived NTCP models in proton therapy. Though it has been reported that photon based NTCP models for head and neck cancer remained valid for patients treated with proton therapy (46), a recent study concluded that photon based rectal NTCP models either over- or underestimated the clinically observed gastrointestinal morbidity in proton cohorts (47). Integrating photon outcome models to proton therapy and consequently interpret the absolute values of normal tissue toxicity probabilities should therefore be done with caution. As the number of proton radiotherapy centers is increasing worldwide, more proton therapy outcome data will be available in the future. However to date, as normal tissue complications observed in radiation therapy patients are relatively low, there is inadequate statistical data for proton therapy for most endpoints.

A breath-hold technique (BH) was applied for 3DCRT and VMAT whereas for PBS a free-breathing (FB) technique was used. A study by Mast el al. (48) revealed that using BH in left-sided breast cancer 3DCRT treatment lead to a significant dose reduction in the heart and LAD. This is in line with another study by Mast et al. (49) where the dose to the heart, LAD and lung decreased when using deep inspiration breath hold (DIBH) for both IMRT and IMPT. However, a study by Patel et al. (29) reported no significant dosimetric benefits to heart and lung when adding DIBH to PBS treatment. It should be noted that due to range and biological uncertainties associated with protons, it is not known whether observed dose reduction due to BH techniques for proton therapy is clinically relevant.

The PBS patients in this study were treated with a single-field configuration, i.e. high LET values at the distal edge of the SOBP are unavoidably placed in organs at risk positioned downstream of the target volume. Single-field configuration is the treatment of choice at our institution. Applying multiple fields may allow for variable RBE values to influence the treatment planning. Different mathematical approaches have been suggested to incorporate biological uncertainties associated with a variable RBE to IMPT planning, e.g. via robust planning techniques to include the RBE uncertainties (50,51). Others have investigated biological optimization for IMPT by replacing the physical dose with the biological dose (52-54). However, a considerably large uncertainty is associated with the RBE models which may result in clinically unacceptable inaccuracies. Due to uncertainties in RBE values for normal tissue toxicities, purely LET based treatment optimization has been suggested (55-57).

Due to the small number of patients, the statistical tests performed do not include P-values. Therefore, it is not possible to apply multiple correction (e.g. the Bonferroni Correction) to protect for an increased risk of type 1 error (i.e. incorrectly reject the null hypothesis). However, to include correction for multiple comparisons, a 1% significance level instead of the commonly used 5% significance level was considered a reasonable strategy.

The main focus of this study was to evaluate whether expected dosimetric advantages of proton therapy are compromised when incorporating a variable RBE. For this evaluation, the proton PBS results were compared to results from 3DCRT and VMAT photon plans. In addition to RBE for normal tissue toxicities, long-term side effects such as second cancers might have to be considered. It has been shown that VMAT is inferior to PBS and 3DCRT considering the risk of second lung cancers (58).

The purpose of this study was to assess the impact of RBE variations in proton therapy and how it might decrease the dosimetric advantage of PBS compared to photon techniques. Our intention was not to do a treatment planning comparison, which is an independent subject that has been covered by many publications already (13,59-61). All patients considered in this study were planned and treated at the same institution under the same institutional guidelines and planned by experienced planners. However, we cannot rule out that other institutions or planners might have chosen different plan parameters that may have impacted our absolute values.

5 Conclusion

Our study demonstrates how the consideration of RBE might impact comparisons of proton and photon techniques for breast cancer, particularly in terms of normal tissue complications in the heart and lung. PBS offers advantages over 3DCRT and VMAT when analyzing the normal tissue toxicity probability using dosimetric data but the advantages decrease when applying a variable RBE. Even though RBE uncertainties are considerable and treatment plan optimization based on model-based RBE values is currently not feasible, outcome analysis should consider potential RBE effects for protons.

Acknowledgement

This work was supported by NIH NCI U19 CA-21239. We would gratefully like to thank Dr Clemens Grassberger, Dr Jan Schuemann and Dr Andrzej Niemierko for their valuable support. We would like to thank the Enterprise Research Infrastructure and Services (ERIS) group at Partners Healthcare for computer support.

References

1. Torre LA, Bray F, Siegel RL, Ferlay J, Lortet-Tieulent J, Jemal A. Global cancer statistics, 2012. CA Cancer J Clin. 3rd ed. American Cancer Society; 2015 Mar;65(2):87–108.

2. Poortmans PM, Collette S, Kirkove C, Van Limbergen E, Budach V, Struikmans H, et al. Internal Mammary and Medial Supraclavicular Irradiation in Breast Cancer. N Engl J Med. 2015 Jul 23;373(4):317–27.

3. Early Breast Cancer Trialists' Collaborative Group (EBCTCG). Effect of radiotherapy after breast-conserving surgery on 10-year recurrence and 15-year breast cancer death: meta-analysis of individual patient data for 10801 women in 17 randomised trials. The Lancet. Elsevier Ltd; 2011 Nov 12;378(9804):1707–16.

4. Tendulkar RD, Rehman S, Shukla ME, Reddy CA, Moore H, Budd GT, et al. Impact of postmastectomy radiation on locoregional recurrence in breast cancer patients with 1-3 positive lymph nodes treated with modern systemic therapy. Int J Radiat Oncol Biol Phys. 2012 Aug 1;83(5):e577–81.

5. Everett AS, De Los Santos JF, Boggs DH. The Evolving Role of Postmastectomy Radiation Therapy. Surg Clin North Am. 2018 Aug;98(4):801–17.

6. Clarke M, Collins R, Darby S, Davies C, Elphinstone P, Evans V, et al. Effects of radiotherapy and of differences in the extent of surgery for early breast cancer on local recurrence and 15-year survival: an overview of the randomised trials. Lancet. 2005 Dec 17;366(9503):2087–106.

7. Overgaard M, Hansen PS, Overgaard J, Rose C, Andersson M, Bach F, et al. Postoperative radiotherapy in high-risk premenopausal women with breast cancer who receive adjuvant chemotherapy. Danish Breast Cancer Cooperative Group 82b Trial. N Engl J Med. 1997 Oct 2;337(14):949–55.

8. Darby SC, Ewertz M, McGale P, Bennet AM, Blom-Goldman U, Brønnum D, et al. Risk of ischemic heart disease in women after radiotherapy for breast cancer. N Engl J Med. 2013 Mar 14;368(11):987–98.

9. Nilsson G, Holmberg L, Garmo H, Duvernoy O, Sjögren I, Lagerqvist B, et al. Distribution of coronary artery stenosis after radiation for breast cancer. J Clin Oncol. 2012 Feb 1;30(4):380–6.

10. Aznar MC, Korreman S-S, Pedersen AN, Persson GF, Josipovic M, Specht L. Evaluation of dose to cardiac structures during breast irradiation. The British Journal of Radiology. The British Institute of Radiology. 36 Portland Place, London, W1B 1AT; 2011 Aug;84(1004):743–6.

11. Kubo A, Osaki K, Kawanaka T, Furutani S, Ikushima H, Nishitani H. Risk factors for radiation pneumonitis caused by whole breast irradiation following breast-conserving surgery. J Med Invest. The University of Tokushima Faculty of Medicine; 2009 Aug;56(3-4):99–110.

12. Lauche O, Kirova YM, Fenoglietto P, Costa E, Lemanski C, Bourgier C, et al. Helical tomotherapy and volumetric modulated arc therapy: New therapeutic arms in the breast cancer radiotherapy. WJR. 2016;8(8):735–8.

13. Ares C, Khan S, Macartain AM, Heuberger J, Goitein G, Gruber G, et al. Postoperative proton radiotherapy for localized and locoregional breast cancer: potential for clinically relevant improvements? Int J Radiat Oncol Biol Phys. 2010 Mar 1;76(3):685–97.

14. Goddu M, Chaudhari S, Mamalui-Hunter M, Pechenaya OL, Pratt D, Mutic S, et al. Helical Tomotherapy Planning for Left-Sided Breast Cancer Patients with Positive Lymph Nodes: Comparison to Conventional Multiport Breast technique. Radiation Oncology Biology. Elsevier Ltd; 2009 Mar 15;73(4):1243–51.

15. Chung CS, Yock TI, Nelson K, Xu Y, Keating NL, Tarbell NJ. Incidence of second malignancies among patients treated with proton versus photon radiation. Int J Radiat Oncol Biol Phys. 2013 Sep 1;87(1):46–52.

16. Grantzau T, Mellemkjær L, Overgaard J. Second primary cancers after adjuvant radiotherapy in early breast cancer patients: a national population based study under the Danish Breast Cancer Cooperative Group (DBCG). Radiother Oncol. 2013 Jan;106(1):42–9.

17. Grantzau T, Thomsen MS, Væth M, Overgaard J. Risk of second primary lung cancer in women after radiotherapy for breast cancer. Radiother Oncol. 2014 Jun;111(3):366–73.

18. Paganetti H. Relative biological effectiveness (RBE) values for proton beam therapy. Variations as a function of biological endpoint, dose, and linear energy transfer. Phys Med Biol. 2014 Oct 31;59(22):R419–72.

19. Joiner MC, van der Kogel A. Basic Clinical Radiobiology. Boca Raton, FL: CRC Press; 2019.

20. McNamara AL, Schuemann J, Paganetti H. A phenomenological relative biological effectiveness (RBE) model for proton therapy based on all published in vitro cell survival data. Phys Med Biol. IOP Publishing; 2016 Dec 15;60:8399–416.

21. Paganetti H, Goitein M. Radiobiological significance of beamline dependent proton energy distributions in a spread-out Bragg peak. Med Phys. John Wiley & Sons, Ltd; 2000 May 5;27(5):1119–26.

22. Carabe A, Moteabbed M, Depauw N, Schuemann J, Paganetti H. Range uncertainty in proton therapy due to variable biological effectiveness. Phys Med Biol. 2012 Feb 14;57(5):1159–72.

23. Grün R, Friedrich T, Krämer M, Zink K, Durante M, Engenhart-Cabillic R, et al. Physical and biological factors determining the effective proton range. Med Phys. 2013 Nov 30;40(11):111716–10.

24. Tommasino F, Durante M, D'Avino V, Liuzzi R, Conson M, Farace P, et al. Model-based approach for quantitative estimates of skin, heart, and lung toxicity risk for left-side photon and proton irradiation after breast-conserving surgery. Acta Oncol. Taylor & Francis; 2017 May;56(5):730–6.

25. Stick LB, Yu J, Maraldo MV, Aznar MC, Pedersen AN, Bentzen SM, et al. Joint Estimation of Cardiac Toxicity and Recurrence Risks After Comprehensive Nodal Photon Versus Proton Therapy for Breast Cancer. Int J Radiat Oncol Biol Phys. 2017 Mar 15;97(4):754–61.

26. Verma V, Iftekaruddin Z, Badar N, Hartsell W, Han-Chih Chang J, Gondi V, et al. Proton beam radiotherapy as part of comprehensive regional nodal irradiation for locally advanced breast cancer. Radiother Oncol. 2017 May;123(2):294–8.

27. Cuaron JJ, Chon B, Tsai H, Goenka A, DeBlois D, Ho A, et al. Early toxicity in patients treated with postoperative proton therapy for locally advanced breast cancer. Int J Radiat Oncol Biol Phys. 2015 Jun 1;92(2):284–91.

28. Patel SA, Lu H-M, Nyamwanda JA, Jimenez RB, Taghian AG, MacDonald SM, et al. Postmastectomy radiation therapy technique and cardiopulmonary sparing: A dosimetric comparative analysis between photons and protons with free breathing versus deep inspiration breath hold. Pract Radiat Oncol. 2017 Dec;7(6):e377–84.

29. Depauw N, Patel SA, MacDonald SM, Lu H-M. SU-E-T-383: Evaluation of Deep Inspiration Breath-Hold Technique for Post-Mastectomy Proton Pencil Beam Scanning Therapy. Med Phys. 42(6):3421.

30. Depauw N, Batin E, Daartz J, Rosenfeld A, Adams J, Kooy HM, et al. A novel approach to postmastectomy radiation therapy using scanned proton beams. Int J Radiat Oncol Biol Phys. 2015 Feb 1;91(2):427–34.

31. Emami B, Lyman J, Brown A, Cola L, Goitein M, Munzenrider JE, et al. Tolerance of normal tissue to therapeutic irradiation. Radiation Oncology Biology. Elsevier; 1991 May 15;21(1):109–22.

32. Perl J, Shin J, Schuemann J, Faddegon B, Paganetti H. TOPAS: An innovative proton Monte Carlo platform for research and clinical applications. Med Phys. 2012;39(11):6818–20.

33. Agostinelli S, Allison J, Amako K, Apostolakis J, Araújo HM, Arce P, et al. GEANT4: A Simulation toolkit. Nucl Instrum Methods Phys Res, A. 2002 Jul;506(CERN-IT-2002-003. SLAC-PUB-9350. 3):250–303.86p.

34. Gagliardi G, Constine LS, Moiseenko V, Correa C, Pierce LJ, Allen AM, et al. Radiation dose-volume effects in the heart. Int J Radiat Oncol Biol Phys. 2010 Mar 1;76(3 Suppl):S77–85.

35. Bentzen SM, Skoczylas JZ, Bernier J. Quantitative clinical radiobiology of early and late lung reactions. Int J Radiat Biol. 2000 Apr;76(4):453–62.

36. Källman P, Agren A, Brahme A. Tumour and normal tissue responses to fractionated non-uniform dose delivery. Int J Radiat Biol. 1992 Aug;62(2):249–62.

37. Gagliardi G, Lax I, Ottolenghi A, Rutqvist LE. Long-term cardiac mortality after radiotherapy of breast cancer—application of the relative seriality model. The British Journal of Radiology. The British Institute of Radiology; 1996;69(825):839–46.

38. Moignier A, Broggio D, Derreumaux S, Beaudré A, Girinsky T, Paul J-F, et al. Coronary stenosis risk analysis following Hodgkin lymphoma radiotherapy: A study based on patient specific artery segments dose calculation. Radiother Oncol. 2015 Dec;117(3):467–72.

39. Rancati T, Wennberg B, Lind P, Svane G, Gagliardi G. Early clinical and radiological pulmonary complications following breast cancer radiation therapy: NTCP fit with four different models. Radiotherapy and Oncology. 2007 Mar;82(3):308–16.

40. Gagliardi G, Bjöhle J, Lax I, Ottolenghi A, Eriksson F, Liedberg A, et al. Radiation pneumonitis after breast cancer irradiation: analysis of the complication probability using the relative seriality model. Radiation Oncology Biology. 2000 Jan 15;46(2):373–81.

41. Underwood TSA, Grassberger C, Bass R, MacDonald SM, Meyersohn NM, Yeap BY, et al. Asymptomatic Late-phase Radiographic Changes Among Chest-Wall Patients Are Associated With a Proton RBE Exceeding 1.1. Int J Radiat Oncol Biol Phys. 2018 Jul 15;101(4):809–19.

42. Wang C-C, McNamara AL, Shin J, Schuemann J, Grassberger C, Taghian AG, et al. End-of-Range Radiobiological Effect on Rib Fractures in Patients Receiving Proton Therapy for Breast Cancer. Int J Radiat Oncol Biol Phys. 2020 Jul 1;107(3):449–54.

43. Marteinsdottir M, Schuemann J, Paganetti H. Impact of uncertainties in range and RBE on small field proton therapy. Phys Med Biol. 2019 Oct 10;64(20):205005.

44. Marteinsdottir M, Paganetti H. Applying a variable relative biological effectiveness (RBE) might affect the analysis of clinical trials comparing photon and proton therapy for prostate cancer. Phys Med Biol. 2019 Jun 5;64(11):115027.

45. Chen Y, Grassberger C, Li J, Hong TS, Paganetti H. Impact of potentially variable RBE in liver proton therapy. Phys Med Biol. IOP Publishing; 2018 Sep 21;63(19):195001.

46. Blanchard P, Wong AJ, Gunn GB, Garden AS, Mohamed ASR, Rosenthal DI, et al. Toward a model-based patient selection strategy for proton therapy: External validation of photon-derived normal tissue complication probability models in a head and neck proton therapy cohort. Radiother Oncol. 2016 Dec;121(3):381–6.

47. Pedersen J, Flampouri S, Bryant C, Liang X, Mendenhall N, Li Z, et al. Cross-modality applicability of rectal normal tissue complication probability models from photon- to proton-based radiotherapy. Radiother Oncol. 2020 Jan;142:253–60.

48. Mast ME, van Kempen-Harteveld L, Heijenbrok MW, Kalidien Y, Rozema H, Jansen WPA, et al. Left-sided breast cancer radiotherapy with and without breath-hold: does IMRT reduce the cardiac dose even further? Radiother Oncol. 2013 Aug;108(2):248–53.

49. Mast ME, Vredeveld EJ, Credoe HM, van Egmond J, Heijenbrok MW, Hug EB, et al. Whole breast proton irradiation for maximal reduction of heart dose in breast cancer patients. Breast Cancer Res Treat. Springer US; 2014 Nov;148(1):33–9.

50. Ödén J, Eriksson K, Toma-Dasu I. Incorporation of relative biological effectiveness uncertainties into proton plan robustness evaluation. Acta Oncol. Taylor & Francis; 2017 Jun;56(6):769–78.

51. Unkelbach J, Paganetti H. Robust Proton Treatment Planning: Physical and Biological Optimization. Seminars in Radiation Oncology. 2018 Apr;28(2):88–96.

52. Wilkens JJ, Oelfke U. Optimization of radiobiological effects in intensity modulated proton therapy. Med Phys. 2005 Feb;32(2):455–65.

53. Frese MC, Wilkens JJ, Huber PE, Jensen AD, Oelfke U, Taheri-Kadkhoda Z. Application of Constant vs. Variable Relative Biological Effectiveness in Treatment Planning of Intensity-Modulated Proton Therapy. Int J Radiat Oncol Biol Phys. 2011 Jan;79(1):80–8.

54. Guan F, Geng C, Ma D, Bronk L, Kerr M, Li Y, et al. RBE Model-Based Biological Dose Optimization for Proton Radiobiology Studies. Int J Part Ther. The Particle Therapy Co-operative Group; 2018;5(1):160–71.

55. Giantsoudi D, Grassberger C, Craft D, Niemierko A, Trofimov A, Paganetti H. Linear Energy Transfer-Guided Optimization in Intensity Modulated Proton Therapy: Feasibility Study and Clinical Potential. Radiation Oncology Biology. Elsevier Inc; 2013 Sep 1;87(1):216–22.

56. Unkelbach J, Botas P, Giantsoudi D, Gorissen BL, Paganetti H. Reoptimization of Intensity Modulated Proton Therapy Plans Based on Linear Energy Transfer. Int J Radiat Oncol Biol Phys. 2016 Dec 1;96(5):1097–106.

57. Cao W, Khabazian A, Yepes PP, Lim G, Poenisch F, Grosshans DR, et al. Linear energy transfer incorporated intensity modulated proton therapy optimization. Phys Med Biol. 2017 Dec 19;63(1):015013.

58. Paganetti H, Depauw N, Johnson A, Forman RB, Lau J, Jimenez R. The risk for developing a secondary cancer after breast radiation therapy: Comparison of photon and proton techniques. Radiother Oncol. 2020 Aug;149:212–8.

59. Hernandez M, Zhang R, Sanders M, Newhauser W. A treatment planning comparison of volumetric modulated arc therapy and proton therapy for a sample of breast cancer patients treated with post-mastectomy radiotherapy. J Proton Ther. 2015;1(1):119.

60. Jimenez RB, Goma C, Nyamwanda J, Kooy HM, Halabi T, Napolitano BN, et al. Intensity modulated proton therapy for postmastectomy radiation of bilateral implant reconstructed breasts: a treatment planning study. Radiother Oncol. 2013 May;107(2):213–7.

61. Lomax AJ, Cella L, Weber D, Kurtz JM, Miralbell R. Potential role of intensity-modulated photons and protons in the treatment of the breast and regional nodes. Radiation Oncology Biology. 2003 Mar 1;55(3):785–92.

References

Agostinelli, S. et al. (2002). GEANT4: A Simulation toolkit. *Nucl. Instrum. Methods Phys. Res., A*, 506(CERN-IT-2002-003. SLAC-PUB-9350. 3):250–303. 86 p.

Attix, F. H. (1986). *Introduction to Radiological Physics Radiation Dosimetry*. John Wiley & Sons, New York, NY.

Berger, M. J. (1963). Monte Carlo Calculation of the Penetration and Diffusion of Fast Charged Particles. In Alder, B., Frenbach, S., and Rotenberg, M., editors, *Methods in Computational Physics*, pages 135–215. Academic Press, New York, NY.

Carabe, A., Moteabbed, M., Depauw, N., Schuemann, J., and Paganetti, H. (2012). Range uncertainty in proton therapy due to variable biological effectiveness. *Physics in Medicine and Biology*, 57(5):1159–1172.

Carlson, D. J., Stewart, R. D., Semenenko, V. A., and Sandison, G. A. (2008). Combined use of Monte Carlo DNA damage simulations and deterministic repair models to examine putative mechanisms of cell killing. *Radiation Research*, 169:447–459.

Cheung, R., Tucker, S. L., Lee, A. K., de Crevoisier, R., Dong, L., Kamat, A., Pisters, L., and Kuban, D. (2005). Dose–response characteristics of low- and intermediate-risk prostate cancer treated with external beam radiotherapy. *International Journal of Radiation Oncology*Biology*Physics*, 61(4):993–1002.

Darby, S. C., Ewertz, M., McGale, P., Bennet, A. M., Blom-Goldman, U., Brønnum, D., Correa, C., Cutter, D., Gagliardi, G., Gigante, B., Jensen, M.-B., Nisbet, A., Peto, R., Rahimi, K., Taylor, C., and Hall, P. (2013). Risk of ischemic heart disease in women after radiotherapy for breast cancer. *The New England journal of medicine*, 368(11):987–998.

Deasy, J. O., Blanco, A. I., and Clark, V. H. (2003). CERR: a computational environment for radiotherapy research. *Medical physics*, 30(5):979–985.

Durante, M. and Loeffler, J. S. (2010). Charged particles in radiation oncology. *Nature reviews. Clinical oncology*, 7(1):37–43.

Efron, B. (1979). Bootstrap methods: Another look at the jackknife. *The annals fo Statistics*, pages 1–26.

Fowler, J. F. (1989). The linear-quadratic formula and progress in fractionated radiotherapy. *The British Journal of Radiology*, 62(740):679–694.

Frese, M. C., Yu, V. K., Stewart, R. D., and Carlson, D. J. (2012). A mechanism-based approach to predict the relative biological effectiveness of protons and carbon ions in radiation therapy. *Radiation Oncology Biology*, 83(1):442–450.

Gagliardi, G., Bjöhle, J., Lax, I., Ottolenghi, A., Eriksson, F., Liedberg, A., Lind, P., and Rutqvist, L. E. (2000). Radiation pneumonitis after breast cancer irradiation: analysis of the complication probability using the relative seriality model. *Radiation Oncology Biology*, 46(2):373–381.

Gagliardi, G., Lax, I., Ottolenghi, A., and Rutqvist, L. E. (1996). Long-term cardiac mortality after radiotherapy of breast cancer—application of the relative seriality model. *The British Journal of Radiology*, 69(825):839–846.

Goitein, M. and Schultheiss, T. (1985). Strategies for treating possible tumor extension: some theoretical considerations. *Radiation Oncology Biology*, 11(8):1519–1528.

Grassberger, C., Trofimov, A., Lomax, A., and Paganetti, H. (2011). Variations in linear energy transfer within clinical proton therapy fields and the potential for biological treatment planning. *International journal of radiation oncology, biology, physics*, 80(5):1559–1566.

Grün, R., Friedrich, T., Krämer, M., Zink, K., Durante, M., Engenhart-Cabillic, R., and Scholz, M. (2013). Physical and biological factors determining the effective proton range. *Medical Physics*, 40(11):111716–10.

Hall, E. J. and Giaccia, A. J. (2006). *Radiobiology for the Radiologist*. Lippincott Williams & Wilkins, Philadelphia, PA.

Hong, L., Goitein, M., Bucciolini, M., Comiskey, R., Gottschalk, B., Rosenthal, S., Serago, C., and Urie, M. (1996). A pencil beam algorithm for proton dose calculations. *Physics in Medicine and Biology*, 41(8):1305–1330.

IAEA (2008). *Relative Biological Effectiveness in Ion Beam Therapy*. Technical Reports Series. INTERNATIONAL ATOMIC ENERGY AGENCY, Vienna.

ICRP (1991). *Recommendations of the International Commission on Radiological Protection.* ICRP Publication 60. Bergamon Press, Oxford.

ICRU (1993a). *Prescribing, Recording, and Reporting Photon Beam Therapy.* Report 50. International Commission on Radiation Units and Measurements, Bethesda, MD.

ICRU (1993b). *Stopping Powers and Ranges for Protons and Alpha Particles.* Report 49. International Commission on Radiation Units and Measurements, Bethesda, MD.

ICRU (1999). *Prescribing, Recording, and Reporting Photon Beam Therapy.* Report 62. International Commission on Radiation Units and Measurements, Bethesda, MD.

ICRU (2007). *Prescribing, Recording, and Reporting Proton Beam Therapy.* Report 78. International Commission on Radiation Units and Measurements, Bethesda, MD.

ICRU (2011). *Fundamental quantities and units for ionizing radiation.* Report 85a. ICRU, Bethesda, MD.

Janni, J. F. (1982). Proton range energy tables, 1 keV–10 GeV. *Atomic Data and Nuclear Data Tables*, 27:147–529.

Joiner, M. C. and van der Kogel, A. (2019). *Basic Clinical Radiobiology*. CRC Press, Boca Raton, FL.

Källman, P., Agren, A., and Brahme, A. (1992). Tumour and normal tissue responses to fractionated non-uniform dose delivery. *International journal of radiation biology*, 62(2):249–262.

Kry, S. F., Bednarz, B., Howell, R. M., Dauer, L., Followill, D., Klein, E., Paganetti, H., Wang, B., Wuu, C.-S., and George Xu, X. (2017). AAPM TG 158: Measurement and calculation of doses outside the treated volume from external-beam radiation therapy. *Medical Physics*, 44(10):e391–e429.

Kutcher, G. J. and Burman, C. (1989). Calculation of complication probability factors for non-uniform normal tissue irradiation: the effective volume method. *Radiation Oncology Biology*, 16(6):1623–1630.

Li, X. A., Alber, M., Deasy, J. O., Jackson, A., Jee, K. K., Marks, L. B., Martel, M. K.,

Mayo, C., Moiseenko, V., Nahum, A. E., Niemierko, A., Semenenko, V. A., and Yorke, E. D. (2012). The Use and QA of Biologically Related Models for Treatment Planning. Report of AAPM Task Group 166 of the Therapy Physics Committee. *Medical Physics*, 39:1386–1409.

Lyman, J. T. (1985). Complication probability as assessed from dose-volume histograms. *Radiation research. Supplement*, 8:S13–9.

McMahon, S. J. (2018). The linear quadratic model: usage, interpretation and challenges. *Physics in Medicine and Biology*, 64(1):01TR01.

McNamara, A. L., Schuemann, J., and Paganetti, H. (2016). A phenomenological relative biological effectiveness (RBE) model for proton therapy based on all published in vitro cell survival data. *Physics in Medicine and Biology*, 60:8399–8416.

Michalski, J. M., Gay, H., Jackson, A., Tucker, S. L., and Deasy, J. O. (2010). Radiation Dose–Volume Effects in Radiation-Induced Rectal Injury. *Radiation Oncology Biology*, 76(3):S123–S129.

Moignier, A., Broggio, D., Derreumaux, S., Beaudré, A., Girinsky, T., Paul, J.-F., Drubay, D., Lefkopoulos, D., Franck, D., Aubert, B., Deutsch, E., and Bourhis, J. (2015). Coronary stenosis risk analysis following Hodgkin lymphoma radiotherapy: A study based on patient specific artery segments dose calculation. *Radiotherapy and oncology : journal of the European Society for Therapeutic Radiology and Oncology*, 117(3):467–472.

Munro, T. R. and Gilbert, C. W. (1961). The relation between tumour lethal doses and the radiosensitivity of tumour cells. *The British Journal of Radiology*, 34(400):246–251.

Newhauser, W. D. and Durante, M. (2011). Assessing the risk of second malignancies after modern radiotherapy. *Nature Reviews Cancer*, 11(6):438–448.

Newhauser, W. D. and Zhang, R. (2015). The physics of proton therapy. *Physics in Medicine and Biology*, 60(8):R155–209.

Niemierko, A. (1997). Reporting and analyzing dose distributions: A concept of equivalent uniform dose. *Medical Physics*, 24(1):103–110.

Niemierko, A. (1999). A generalized concept of equivalent uniform dose (EUD). *Medical Physics*, 26(1101). Abstract WE-C2-9.

Ödén, J., Eriksson, K., and Toma-Dasu, I. (2017). Inclusion of a variable RBE into proton and photon plan comparison for various fractionation schedules in prostate radiation therapy. *Medical Physics*, 44(3):810–822.

Paganetti, H. (2012). *Proton Therapy Physics*. Series in Medical Physics and Biomedical Engineering. Taylor & Francis Group, Boca Raton.

Paganetti, H. (2014). Relative biological effectiveness (RBE) values for proton beam therapy. Variations as a function of biological endpoint, dose, and linear energy transfer. *Physics in Medicine and Biology*, 59(22):R419–R472.

Paganetti, H. and Goitein, M. (2000). Radiobiological significance of beamline dependent proton energy distributions in a spread-out Bragg peak. *Medical Physics*, 27(5):1119–1126.

Paganetti, H., Niemierko, A., Ancukiewicz, M., Gerweck, L. E., Goitein, M., Loeffler, J. S., and Suit, H. D. (2002). Relative biological effectiveness (RBE) values for proton beam therapy. *International Journal of Radiation Oncology*Biology*Physics*, 53(2):407–421.

Perl, J., Shin, J., Schuemann, J., Faddegon, B., and Paganetti, H. (2012). TOPAS:

An innovative proton Monte Carlo platform for research and clinical applications. *Medical Physics*, 39(11):6818–20.

Rancati, T., Wennberg, B., Lind, P., Svane, G., and Gagliardi, G. (2007). Early clinical and radiological pulmonary complications following breast cancer radiation therapy: NTCP fit with four different models. *Radiotherapy and Oncology*, 82(3):308–316.

Rørvik, E., Fjæra, L. F., Dahle, T. J., Dale, J. E., Engeseth, G. M., Stokkevåg, C. H., Thörnqvist, S., and Ytre-Hauge, K. S. (2018). Exploration and application of phenomenological RBE models for proton therapy. *Physics in Medicine and Biology*, 63(18):185013.

Sachs, R. K., Hahnfeld, P., and Brenner, D. J. (1997). The link between low-LET dose-response relations and the underlying kinetics of damage production/repair/misrepair. *International journal of radiation biology*, 72(4):351–374.

Schaffner, B., Pedroni, E., and Lomax, A. (1999). Dose calculation models for proton treatment planning using a dynamic beam delivery system: an attempt to include density heterogeneity effects in the analytical dose calculation. *Physics in Medicine and Biology*, 44(1):27–41.

Schuemann, J., Giantsoudi, D., Grassberger, C., Moteabbed, M., Min, C. H., and Paganetti, H. (2015). Assessing the Clinical Impact of Approximations in Analytical Dose Calculations for Proton Therapy. *Radiation Oncology Biology*, 92(5):1157–1164.

Schultheiss, T., Orton, C. G., and Peck, R. A. (1983). Models in radiotherapy: volume effects. *Medical Physics*, 10(4):410–415.

Semenenko, V. A. and Stewart, R. D. (2004). A fast Monte Carlo algorithm to simulate the spectrum of DNA damages formed by ionizing radiation. *Radiation Research*, 161(4):451–457.

Semenenko, V. A. and Stewart, R. D. (2006). Fast Monte Carlo simulation of DNA damage formed by electrons and light ions. *Physics in Medicine and Biology*, 51(7):1693–1706.

Stewart, R. D., Streitmatter, S. W., Argento, D. C., Kirkby, C., Goorley, J. T., Moffitt, G., Jevremovic, T., and Sandison, G. A. (2015). Rapid MCNP simulation of DNA double strand break (DSB) relative biological effectiveness (RBE) for photons, neutrons, and light ions. *Physics in Medicine and Biology*, 60(21):8249–8274.

Stewart, R. D., Yu, V. K., Georgakilas, A. G., Koumenis, C., Park, J. H., and Carlson, D. J. (2011). Effects of Radiation Quality and Oxygen on Clustered DNA Lesions and Cell Death. *Radiation Research*, 176(5):587–602.

Thames, H. D. and Suit, H. D. (1986). Tumor radioresponsiveness versus fractionation sensitivity. *Radiation Oncology Biology*, 12(4):687–691.

van Leeuwen, C. M., Oei, A. L., Crezee, J., Bel, A., Franken, N. A. P., Stalpers, L. J. A., and Kok, H. P. (2018). The alfa and beta of tumours: a review of parameters of the linear-quadratic model, derived from clinical radiotherapy studies. *Radiation Oncology*, 13(1):96–11.

Verburg, J. M., Grassberger, C., Dowdell, S. J., Schuemann, J., Seco, J., and Paganetti, H. (2016). Automated Monte Carlo Simulation of Proton Therapy Treatment Plans. *Technology in cancer research & treatment*, 15(6):NP35–NP46.

Wedenberg, M., Lind, B. K., and Hårdemark, B. (2013). A model for the relative biological effectiveness of protons: The tissue specific parameter α/β of photons is

a predictor for the sensitivity to LET changes. *Acta Oncologica*, 52(3):580–588.

Williams, M. V., Denekamp, J., and Fowler, J. F. (1985). A review of alpha/beta ratios for experimental tumors: implications for clinical studies of altered fractionation. *Radiation Oncology Biology*, 11(1):87–96.

Withers, H. R., Taylor, J. M., and Maciejewski, B. (1988). Treatment volume and tissue tolerance. *Radiation Oncology Biology*, 14(4):751–759.

Zhu, J., Simon, A., Haigron, P., Lafond, C., Acosta, O., Shu, H., Castelli, J., Li, B., and de Crevoisier, R. (2016). The benefit of using bladder sub-volume equivalent uniform dose constraints in prostate intensity-modulated radiotherapy planning. *OncoTargets and therapy*, 9:7537–7544.